DEVELOPMENT OF ADVANCED CROSS CONJUGATED SYSTEMS AND APPLICATIONS IN RATIOMETRIC SENSING: ALTERING THE ELECTRONIC PROPERTIES OF CRUCIFORMS AND POLY(PARA-PHENYLENEETHYNYLENE)S TO ELICIT DIFFERING REACTIVITY AND RESPONSE

A Dissertation
Presented to
The Academic Faculty

by

Evan Andrew Davey

In Partial Fulfillment
of the Requirements for the Degree
Doctor of Philosophy in Chemistry
in the School of Chemistry and Biochemistry

Georgia Institute of Technology

August, 2012

DEVELOPMENT OF ADVANCED CROSS CONJUGATED SYSTEMS AND APPLICATIONS IN RATIOMETRIC SENSING: ALTERING THE ELECTRONIC PROPERTIES OF CRUCIFORMS AND POLY(PARA-PHENYLENEETHYNYLENE)S TO ELICIT DIFFERING REACTIVITY AND RESPONSE

Approved by:

Dr. Uwe H.F. Bunz, Advisor
School of Chemistry and Biochemistry
Georgia Institute of Technology

Dr. David Collard
School of Chemistry and Biochemistry
Georgia Institute of Technology

Dr. Laren M. Tolbert
School of Chemistry and Biochemistry
Georgia Institute of Technology

Dr. Anselm Griffin
School of Materials Science
Georgia Institute of Technology

Dr. Stefan France
School of Chemistry and Biochemistry
Georgia Institute of Technology

Date Approved: February 24 2012

This document is dedicated to my parents, Michael and Maria. Thank you for all of your love and support throughout the years.

ACKNOWLEDGEMENTS

First and foremost, I must thank the two gentlemen who made this entire endeavor possible for me: my friend, mentor, and advisor, Uwe Bunz, and the man who stood in his place when the fatherland called, Laren Tolbert. Without the both of you, I don't know how I would have gotten through this journey in one piece.

Secondly, I cannot continue without thanking the most important people in my life, my family. To my parents, Michael and Maria, thank you for raising me to be the person I am today. Everything that I am and everything I have done is a direct reflectance of the influence you've been in my life; I love both of you more than I could ever describe. To my brothers, Michael and Griffin, thank you for being two of the best brothers a person could ask for. From playing video games in the basement to the many Frisbee games we've played together over the years, I will never forget the times we've spent together.

In addition to Uwe and Laren, there are two other individuals who have made an everlasting impact on my growth as a scientist. I worked for and was advised by Dr. Joel Ressner and Dr. Felix Goodson during my time at West Chester, and owe the entirety of my scientific background to these two men. Outside of the lab, I have shared many meals, beers, and stories and with both. Thank you for the drive and inspiration you instilled in me, if not for both of your encouragement, I never would have made it to this point in my career.

A special thank you goes out to the past members of the Bunz group: Scott Brombosz, Anthony Appleton, Yexiang Zhang, Psaras McGrier, Ronnie Phillips, Juan Tolosa, Chris Kub, Drew Zappas, and Eric Gharakhanian, I'll never forget the good times

we had: hanging out getting pizza late nights in lab, partying at Uwe's apartment, eating steak, drinking wine, and listening to Uwe's stories that made us all laugh (and even cringe just a little).

To the present members of the Bunz group at Heidelberg University in Germany, specifically, Jonny Bryant, Ben Coombs and Ben Lindner, you guys have made me feel so welcome during my trips to Europe, and I hope we continue to share the good times we've had over the past two years.

There are two people who I must thank individually for their help during my graduate career. Dr. AJ Zucchero, the impact of your guidance upon my career has been unparalleled. Beginning with my introduction into the group, you were always there providing "elder-statesman" advice, and I took it all to heart. Apart from work, I with always value your friendship and look back fondly on the many late-night documentaries and games of Civilization IV in the lab. I'll always remember Uwe saying at one point: "Evan...AJ...when you two are actually working and putting your brains together, you can be as competent as one normal graduate student." Coming from Uwe, I'll take that as a perfectly acceptable compliment.

When I think of Anthony Baldridge, there is one word that comes to mind: whiskey. The porch sitting at Main Street, whiskey drinking, Mad Men watching evenings were some of the best times I had in graduate school. You are the sole reason I did not go completely insane at work after my lab was moved. I hope your time at Berkeley is filled with many new bourbons to try and I’m looking forward to having you come back to the East Coast so we can continue right where left off: somewhere around ¼ of the bottle left.

To all of the friends I have in Atlanta, all I can say is thank you. And to all of the animals that we all share and take care of for each other: Russe, Mano, Chloe, Maggie, Kelvin, Stella, Peety, Chip! The memories that we've made together at 1709, Chip's house, tailgating at school, going to hockey games, it will all live with me for the rest of my life. Adam and Gaelle Offenbacher, Chip and Jess Humpheries, Nick Haase, Carley Shulman, Kyle Flack, thanks for being there for me when I needed you. Even though we're all beginning to spread around the country, you are all people with who I fully intend on keeping in contact with.

Stadium Grille (RIP), West Chester, Pennsylvania. In that small sports grille, the biggest ruse in the life of Michael J. Lutz took place; a year-long endeavor that shaped the face of our company as we know it today and ended with one word: WOOOO! To Tommy Jack, Mike Lutz, Steve Ferraioli, Matt Taylor, Paul Mejia, Frank Lemmo, and The Coug, a famous man once said "they're the boys I been down the road with". There's no better way that I could describe all of you. And to Jim Tocyloski: you're still the furthest thing from my mind.

I also have to send a special thank you to two individuals who somehow managed to put up with me over the years as a roommate, Alex Irvine and John Bustamante. I know I can't be the easiest person in the world to live with, but somehow you guys dealt with me. Some of the funniest moments in my life have been spent with you guys. Even though no one else understands, you both know that I get upgrades before units, cannon my own base instead of the choke point, 4-gate for defense, 9-pool for defense, and 4-racks for defense, yet you're both still willing to play computer games with me. You guys are my best friends, there's no other way for me to put it.

Last, and certainly not least, I must thank a person who arrived in my life very late in my graduate career, but has provided nothing but unconditional love and support during the writing of this document, my starting a new job, all while living halfway across the country. To Theresa McNerney, thank you for being everything that you are. I am constantly reminded of how lucky I am to have someone as awesome as you in my life. I love you with all of my heart; you are a shining light in my life that I will always cherish.

TABLE OF CONTENTS

LIST OF TABLES

LIST OF FIGURES

LIST OF EQUATIONS

LIST OF SYMBOLS AND ABBREVIATIONS

DCM	Dichloromethane
EtOAc	Ethyl Acetate
MeCN	Acetonitrile
THF	Tetrahydrofuran
DMF	Dimethylformamide
DMSO	Dimethylsulfoxide
iPrOH	Isopropanol
EtOH	Ethanol
MeOH	Methanol
H_2O	Water
Ether	Diethyl Ether
XF	Cruciform
PPE	Poly(*para*-phenyleneethynylene)
TMS	Trimethylsilane
OTf	Triflate
TFA	Trifluoroacetic Acid
TEA	Triethylamine
NBS	N-Bromosuccinimide
TBAF	Tetrabutylammonium fluoride
mmol	millimole
K	Kelvin
C	Celcius
Pd-Cat	$Pd(PPh_3)Cl_2$

Ar	Aryl Group
HB	Hyperbranced
OSw	Swallowtail Unit
UV	Ultra Violet
FMO	Frontier Molecular Orbital
HOMO	Highest Occupied Molecular Orbital
LUMO	Lowest Unoccupied Molecular Orbital
M^+	Metal Cation
PPV	Poly(*para*-phenylenevinylene)
λ_{abs}	Absorbance Wavelength
λ_{em}	Emission Wavelength
Φ_f	Fluorescence Quantum Yield
τ_{fl}	Fluorescence Lifetime
^{1}H NMR	Proton Nuclear Magnetic Resonance Spectroscopy
^{13}C NMR	Carbon Nuclear Magnetic Resonance Spectroscopy
ppm	Parts per Million
MHz	Megahertz
IR	Infrared Spectroscopy
FTIR	Fourier Transform Infrared Spectroscopy
MS	Mass Spectrometry
EI-MS	Electron Ionization Mass Spectrometry
RT	Room Temperature
Std	Standard
J	Coupling Constant
MP	Melting Point

BP	Boiling Point
RGB	Red, Green, and Blue Colors
σ	Standard Deviation
σ_i	Relative Standard Deviation
σ_i^{3D} *(R,G,B)*	Relative Standard Deviation in Three Dimensions
MANOVA	Multivariate Analysis of Variance
GFP	Green Fluorescent Protein
PPAR-γ	Peroxisome Proliferator-Activated Receptor Gamma
φ	Single Bond Aryl Twisting
AMI	Arylidenemethylimidazolinone
HSA	Human Serum Albumin
HBDI	Hydroxybenzylideneimidazolidinone
Da	Dalton

SUMMARY

With conjugated materials being used in the development of new sensory devices for detection of metals, bacteria, and chemical warfare agents, the field of organic sensing is growing faster than ever. The purpose of this dissertation is to provide a precedence for the synthesis of new cross-conjugated compounds and outline potential applications of these materials as chemical sensors and molecular probes.

This dissertation is broken into two main sections: Chapters 1-4 primarily outline the synthesis of new compounds, wherein the principal goals were to design new cross-conjugated architectures based on known molecules and to compare the spectroscopic properties with well-defined systems. The central theme of chapter 5-6 is the application of cross-conjugated materials in fluorescence sensing. In both chapters, the development of a three-molecule fluorophore array is discussed along with the ability to identify and discriminate between analytes using only digital photographs of fluorescence and statistical analysis.

This research serves as a meticulous examination into cross-conjugated materials and how alterations of the frontier molecular orbitals can be utilized for applications in "chemical tongue" organic sensing devices.

CHAPTER 1

INTRODUCTION AND OVERVIEW

Motivation and Dissertation Overview

The field of organic electronics has blossomed into an area of highly competitive research resulting in many of the evolutionary leaps in modern technology that we have undergone in the past thirty years. With sub-topics including the development of organic solar cells, light emitting diodes, molecular probes and sensors, and molecular transistors for use in device fabrication, organic electronics have come to the forefront of modern chemical research. As recent literature has shown, there is interest in the development and modification of molecular sensors for a vast array of applications. In the mid-1990s, poly(*para*-phenyleneethynylene)s (PPEs), began to gain prominence in the world of chemistry through the works of Bunz,[1] Swagger,[2] and Müllen.[3] Over the past decade, structural modifications in PPEs have yielded polymeric sensors capable of analyte detection in both organic and most importantly, aqueous solutions, a property that introduced PPEs as viable sensors in biological assays.[4]

First developed as a small molecule derivatives of PPEs, 1,4-distyryl-2,5-arylethynylbenzenes (cruciforms, XFs) were found to exhibit a separation in the frontier molecular orbitals (FMOs), allowing for the highest occupied molecular orbital (HOMO) and the lowest unoccupied molecular orbital (LUMO) to be independently modified and stabilized (or destabilized) in disproportionate amounts, leading to an observable and measurable shift in emission wavelength. This unique electronic characteristic has led to many advances in utilizing XFs as molecular sensors, and has provided the primary motivation for this dissertation.

The initial concept of this work revolved around the synthesis of water soluble polymeric materials for use as sensors in biological assays. From the start, the principle purpose of this research has been the development of new conjugated architectures with a specific focus on how the inclusion of various functionalities would affect not only the solubility in organic and aqueous solutions, but most importantly, the electronic properties and response upon reaction. Over time, the scope of this research narrowed from linear polymeric systems to specifically working with cross-conjugated structures and sought to bridge a gap between the knowledge of PPE and cruciform electronics. From this work, an explicit question arose that this dissertation has strived to answer: Can changes in the electronic properties of polymeric and molecular systems be tuned such that a desired change or resulting spectroscopic goal is achieved? It has been shown that functionalized materials can react to give a recordable response, but how can we better engineer new molecules to maximize specific response while also applying these responses into either a device or sensor to be used for practical purposes?

Overview

With the knowledge base presented in this section, a vast array of questions and challenges arise regarding the manipulation of cross-conjugated organic materials. Systematic analysis and investigation of these problems through a variety of projects is discussed herein along with additional related work presented as appendices:

Chapter 2

Chapter 2 details the successful synthesis of a new family of cruciforms: "T"-shaped materials; these compounds were developed in two classes of compounds,

stilbene and distyrylbenzene, with each class mimicking different features of an analogous parent 1,4-distyryl-2,5-arylethynylbenzene "X"-shaped cruciform (XF).

Chapter 3

Chapter 3 reports the synthesis and characterization of a new poly(*para*-phenyleneethynylene) functionalized with reactive substituents upon the polymer backbone for the purposes of carrying out further reactions upon the material. The development of polymers for the use of "post-functionalization" reactions is highly desirable. Once polymerization is completed, a pure material can be reacted with any number of appropriate reagents to generate a new polymer with the desired spectroscopic properties (i.e. bathochromically shifted emissions) while also retaining the chain length and backbone integrity of the original material.

Chapter 4

Chapter 4 highlights new poly(*para*-phenyleneethynylene)s for the purposes of biosensory applications. Specifically, this chapter focuses on the development of cross-conjugated PPEs that exhibit bathochromically shifted emissions in aqueous solution. Additionally, it was found that these materials can also extract metal-ions from an aqueous phase into an organic phase, a quality that is unique among materials of this type.

Chapter 5

Chapter 5 reports the development of a fluorophore sensor based on a three molecule array and a six solvent system. This sensor was designed for, and successfully tested for, the purpose of discrimination and detection of various organic acids. Using digital photography and computer software to record color changes in the fluorescent

array, a library of known color changes was created, each representing a "finger print" for a specific analyte. A blind study of the known library reported 100% accuracy in discriminating the compounds (Copyright of the American Chemical Society).

Chapter 6

Chapter 6 reports further refinements of the fluorophore sensor discussed in chapter 5. Variations in the molecular array and solvent system were made in the effort to discriminate and detect over-the-counter pharmaceuticals. Initial results have shown high levels of selectivity between many different types of drugs.

Chapter 7

Chapter 7 focuses on the general conclusions of this dissertation and also provides a direction for the future of work in this field of study.

Appendix A

Appendix A details the synthetic development of green fluorescent protein (GPF) chromophore derivatives for use as molecular probes. Specifically, these chromophores were synthesized (using rational design) as binding ligands for the nuclear receptor peroxisome proliferator-activated receptor gamma (PPAR-γ). Initial results are reported herein.

Appendix B

Appendix B contains all of the raw numerical values used in the MANOVA analysis detailed in Chapter 5. Data was collected in triplicate to best represent the average emission color of each photograph.

Appendix C

Appendix C contains all of the raw numerical values used in the blind test of unknown analytes that is detailed in Chapter 5. Data was collected in triplicate to best represent the average emission color of each photograph.

Overview of PPEs and Ratiometric Sensing

For a fluorophore to exhibit a ratiometric response, there must be an incongruent stabilization/destabilization of the HOMO and LUMO upon reaction of the fluorophore with an analyte. The affect on FMOs must also be *incongruent* - resulting in a net change in the band-gap - to produce a color change. This effect is not observed in most organic dyes as changes in HOMO/LUMO are often congruent due to similar orbital coefficients.

Research in the Bunz group has always had a solid foundation in the investigation of poly(*para*-phenyleneethynylene)s. Linear PPEs are rigid-rod polymers that generally fluoresce in the range of 350-600 nm and have found biosensory applications as fluorescent sensors in the detection of protons/metals[5], proteins[6], and bacteria[7] (Figure 1.1).

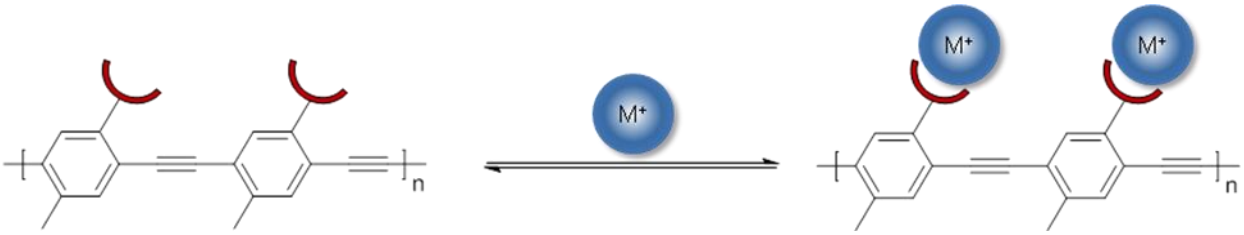

Figure 1.1. PPE binding event.

In 2002, Wilson and Bunz reported a new derivation of PPEs: cross-conjugated 'hybrid' polymers that incorporated a PPE backbone and poly(*para*-phenylenevinylene) (PPV) units on the perpendicular axis (Figure 1.2).[8] With these materials, it was found that the electron-donating strength of the PPV units *exclusively* affected the HOMO. This

vital discovery was the beginning of a decade of high-impact research in the Bunz group into cross-conjugated materials with disproportionally affected FMOs and also provided the original motivation that has led to this dissertation.

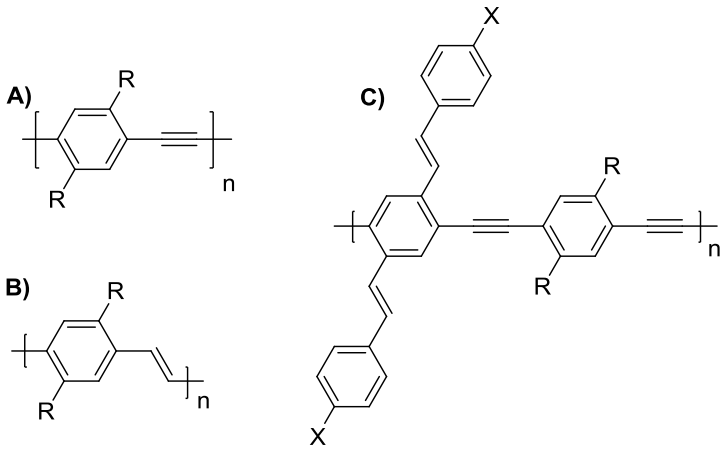

Figure 1.2. A) Linear PPE; **B)** Linear PPV; **C)** Cross-conjugated hybrid PPV-PPE.

From Polymers to Oligomers: Cruciforms

Paralleling our investigation of polymeric systems has been the study of small molecule analogs for the PPV-PPE hybrids. The development of 1,4-distyryl-2,5-bis(arylethynyl)benzenes (cruciforms, XFs) originally began as an endeavor to synthesize small molecule analogs of cross-conjugated PPEs.[9] It was quickly determined that donor- and/or acceptor substitution of the XF arms induced a spatial separation of the frontier molecular orbitals (FMOs) of these molecules. This unique effect allowed for the tuning of electronic properties based on the relative positions of the HOMO and LUMO and generated incongruent effects on both FMOs upon reaction, producing a ratiometric fluorescence response (Figure 1.3).

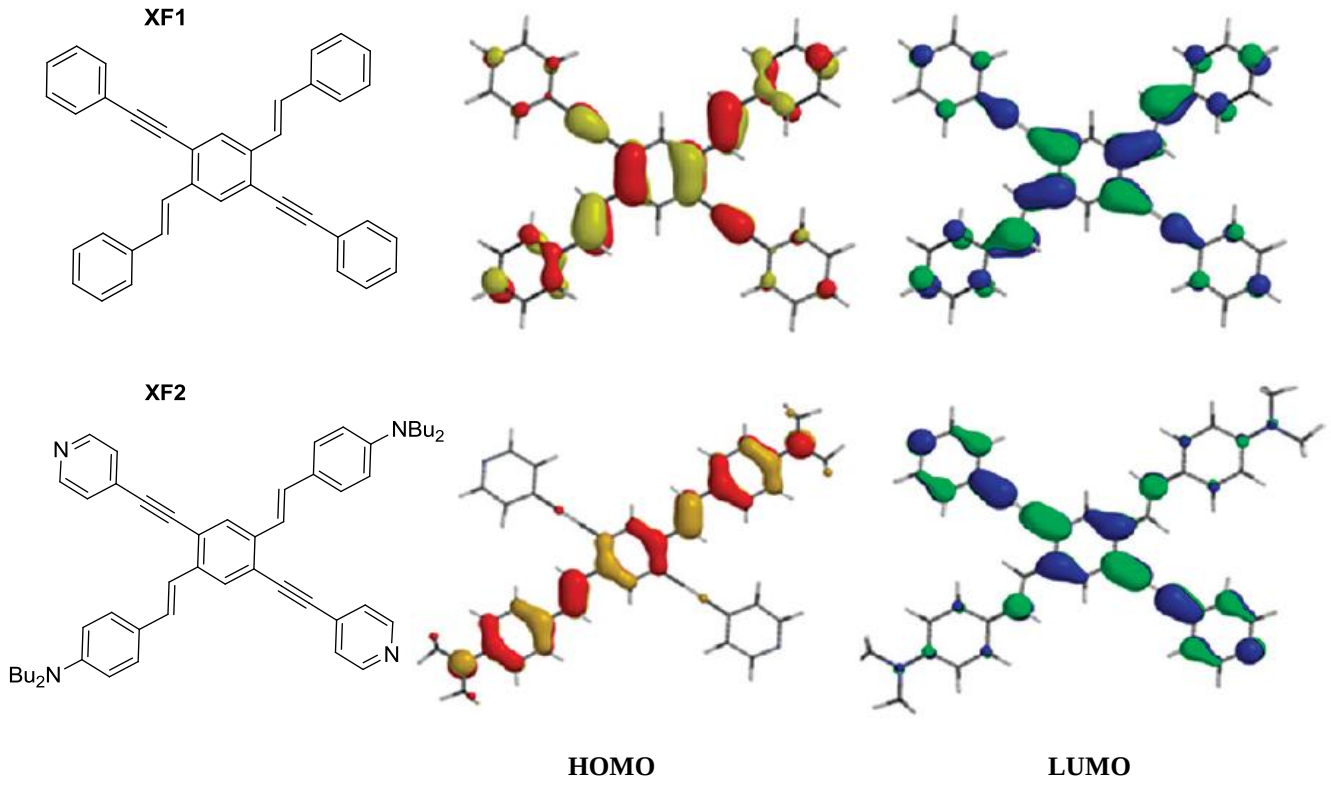

Figure 1.3. Spatially separated frontier molecular orbitals in functionalized cruciforms.[10]

Furthermore, it was found that functionalization of both the alkynyl and styryl axes permitted the construction of dyes exhibiting a two-stage response.[11] The example shown in figure 1.4 illustrates two distinct binding events upon the addition of increasing amounts of zinc (II) triflate to **XF2**: first, the metal cation binds to the dibutylamino groups positioned on the electron rich styryl axis. This binding causes a significant stabilization of the HOMO and has little effect on the LUMO, thus generating a net increase in the band gap, and a resulting hypsochromic shift in emission from yellow to blue. Further addition of the metal cation induces binding to the electron poor pyridyl units located on the arylethynyl axis, which stabilizes the LUMO to a much greater extent

than the HOMO, resulting in a net decrease in the band gap and a bathochromic shift in the emission from blue to green.

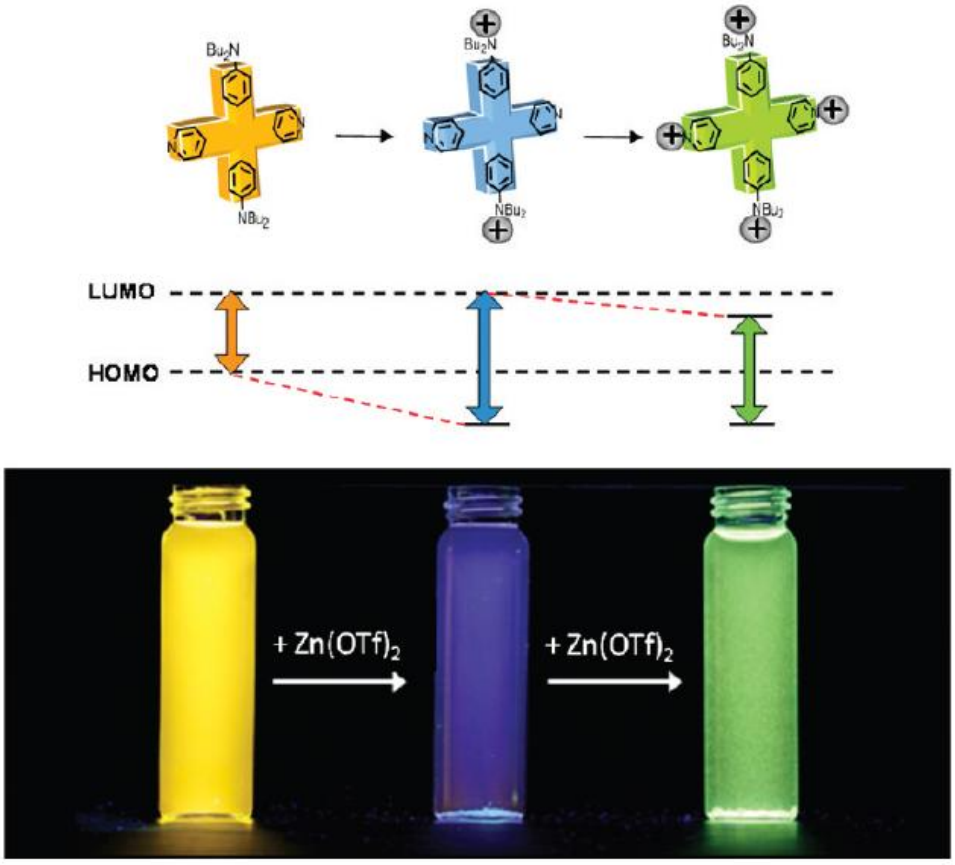

Figure 1.4. Two-stage fluorescence response upon binding with increasing amounts of zinc (II) triflate.[10]

Having clearly defined the electronic properties of both PPE/PPV hybrids and cruciforms, this dissertation seeks to take our current knowledge of these materials and apply it in a rational manner for two purposes: 1) synthesizing new materials where we can tune the spectroscopic properties for a desired purpose and 2) exploiting the ratiometric sensing potential of known materials to design a "chemical nose" sensor capable of analyte discrimination.

References

[1] Bunz, U.H.F. *Chem. Rev.* **2000**, *100*, 1605-1644.

[2] Yang, J.S.; Swager, T.M.; *J. Am. Chem. Soc.* **1998**, *120*, 11864.

[3] Mangel, T.; Eberhardt, A.; Scherf, U.; Bunz, U.H.F.; Mullen, K. *Macromol. Rapid Commun.* **1995**, *16*, 571.

[4] (a) You, C.C.; Miranda, O.R.; Gider, B.; Ghosh, P.S.; Kim, I.-B.; Erdogan, B.; Krovi, S.A.; Bunz, U.H.F.; Rotello, V.M. *Nat. Nanotechnol.* **2007**, *2*, 318-323. (b) Phillips, R.L.; Miranda, O.R.; You, C.C.; Rotello, V.M.; Bunz, U.H.F. *Angew. Chem. Int. Ed.* **2008**, *47*, 2590-2594. (c) Bajaj, A.; Miranda, O.R.; Kim, I.-B.; Phillips, R.; Jerry, D.J.; Bunz, U.H.F.; Rotello, V.M. *Proc. Natl. Acad. Sci. U.S.A.* **2009**, *106*, 10912-10916. (d) Bajaj, A.; Rana, S.; Miranda, O.R.; Yawe, J.C.; Jerry, D.J.; Bunz, U.H.F.; Rotello, V.M. *Chem. Sci.* **2010**, *1*, 134-138. (e) Moyano, D.F.; Rana, S.; Bunz, U.H.F.; Rotello, V.M. *Faraday Discussions* **2011**, *33*, 33-42.

[5] Kim, I.-B.; Phillips, R.; Bunz, U.H.F. *Macromolecules* **2007**, *40*, 5290-5293.

[6] (a) Kim, I.-B.; Dunkhorst, A.; Bunz, U.H.F. *Langmuir* **2005**, *21*, 7985-7989. (b) Miranda, O.R.; You, C.-C.; Phillips, R.; Kim, I.-B.; Gosh, P.S.; Bunz, U.H.F.; Rotello, V.M. *J. Am. Chem. Soc.* **2007**, *129*, 9856-9857.

[7] Duarte, A.; Chworos, A.; Flagan, S.F.; Hanrahan, G.; Bazan, G.C. *J. Am. Chem. Soc.* **2010**, *132*, 12562-12564.

[8] Wilson, J.N.; Windscheif, P.M.; Evans, U.; Myrick, M.L.; Bunz, U.H.F. *Macromolecules* **2002**, *35*, 8681-8683.

[9] Wilson, J.N.; Josowicz, M.; Wang, Y.; Bunz, U.H.F. *Chem. Commun.* **2003**, 2962-2963.

[10] Zucchero, A.J.; McGrier, P.L.; Bunz, U.H.F. *Acc. Chem. Res.* **2010**, *43*, 397-408.

[11] Wilson, J.N.; Bunz, U.H.F. *J. Am. Chem. Soc.* **2005**, *127*, 4124-4125.

CHAPTER 2

T-SHAPED FLUOROPHORES: CUTTING THE CRUCIFORMS

Introduction

Cruciform[1-2] fluorophores are molecules that are X-shaped[3] and typically (but not always) display a central aromatic hub to which conjugated arms consisting of different π-systems are added.[4-7] Derivatives of this concept lead to molecules of similar shapes and topologies that have been termed H-shapes and Z-shapes.[8] The presence of two axes in XFs has dramatic effects on their electronic structure if the axes are donor and acceptor-substituted respectively. In such a case, a locally disjoint frontier molecular orbital picture emerges. The HOMO is almost completely localized on the more electron rich axis of the XF, while the LUMO is localized on the traverse with the electron accepting groups. As a consequence, the effect of attachment of electron donors or electron accepting substituents to the proper axes of the XF has an amplifying effect on their HOMO-LUMO gap and therefore on their absorption and emission maxima. Working with dialkylamino and pyridine groups the emission color of the XFs can be tuned from blue to orange. Both pyridine and dialkylamino groups display free electron pairs, therefore XFs equipped with such structural elements are also metallochromic and acidochromic, and display distinct changes in fluorescence upon protonation or metalation. A hitherto not investigated aspect of XFs is the study of the influence of the single arms on the overall electronic properties of the XF systems. To generate insight into this topic we have created a series of T-shaped fluorophores **1S-5S** and **1T-5T** and investigated their optical and electronic properties and compared them with those of their corresponding XFs **1X-5X**. The S-series is derived from the X-series by "snipping" off a

styryl arm, while the T-series is obtained from the X-series by stripping away an aryleneethynylene unit. Doing this improves the understanding the fundamental properties of the XFs and might give insight into principles that guide the construction of novel fluorophores and chromophores.

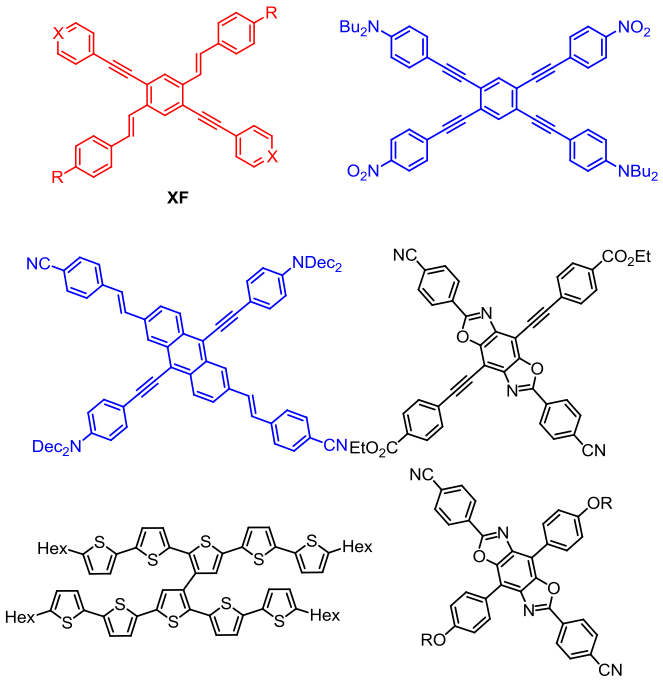

Figure 2.1. Examples of cruciform molecules.

Results and Discussion

Synthesis of T and S Molecules

Figure 2.1 shows the structures in the **T** and **S**-series that have been prepared and compared herein. The synthesis is straightforward and shown in Scheme 1. For the **S**-series we start from **6**, which upon partial radical bromination followed by an Arbuzov reaction with triethylphosphite gives rise to the isolation of **7**. A Horner reaction with any of the aldehydes **8a-d** furnishes the styrene derivatives **9a-d** in yields from X-Y %. A subsequent Sonogashira coupling finishes the sequence to give **1S-5S**. The preparation of the T-series proceeds analogously. Starting from iodoxylene **11,** bromination with

NBS furnishes phosphonate **12** after Arbuzov-reaction of the intermediate with triethylphosphite. Sonogashira alkynylation **10a-c** then furnishes the desired targets **1T-5T** in good-to excellent yields. We did not encounter any difficulties in this synthetic scheme of **T** and **D** which is slightly modified from that of the synthesis of the published compounds **1X-5X**.

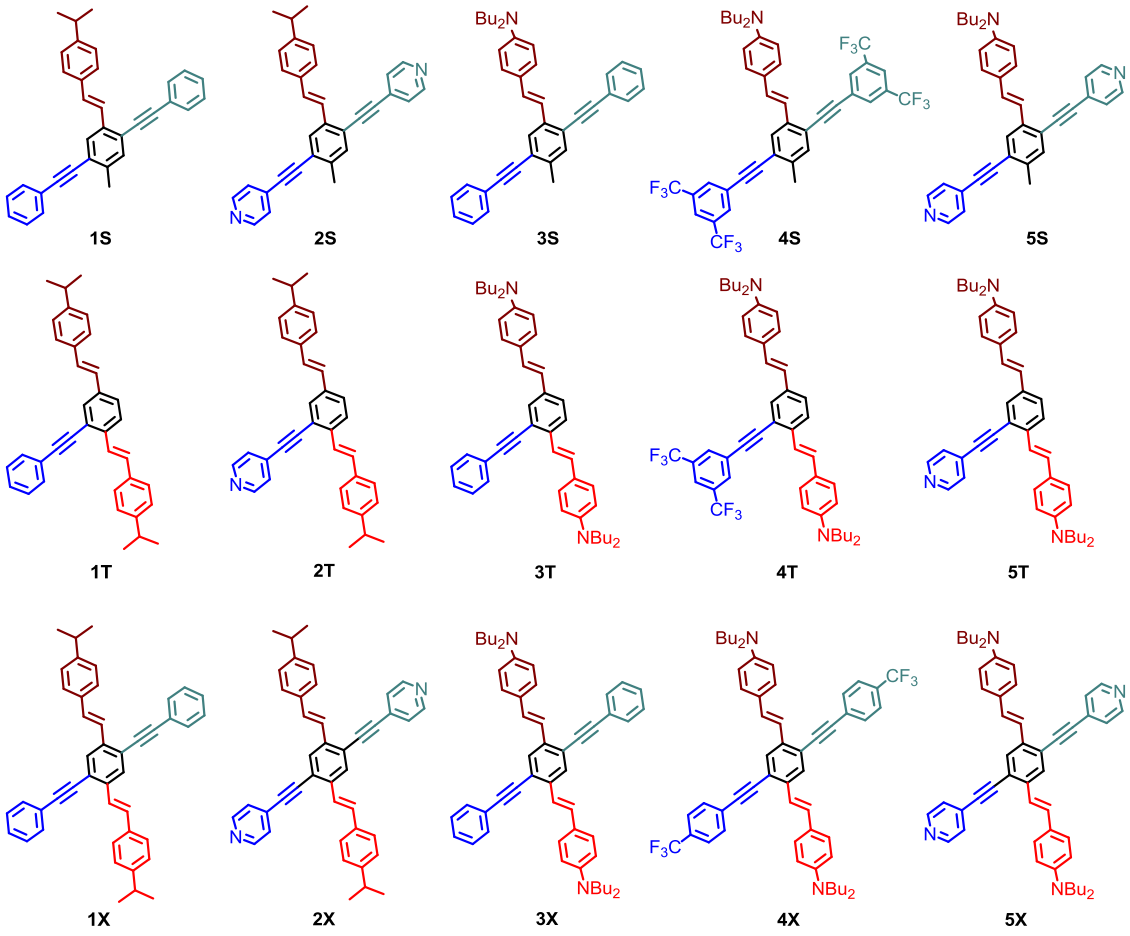

Figure 2.2. Prepared **T** and **S** series T-shapes and comparison to structurally related cruciform **X** series.

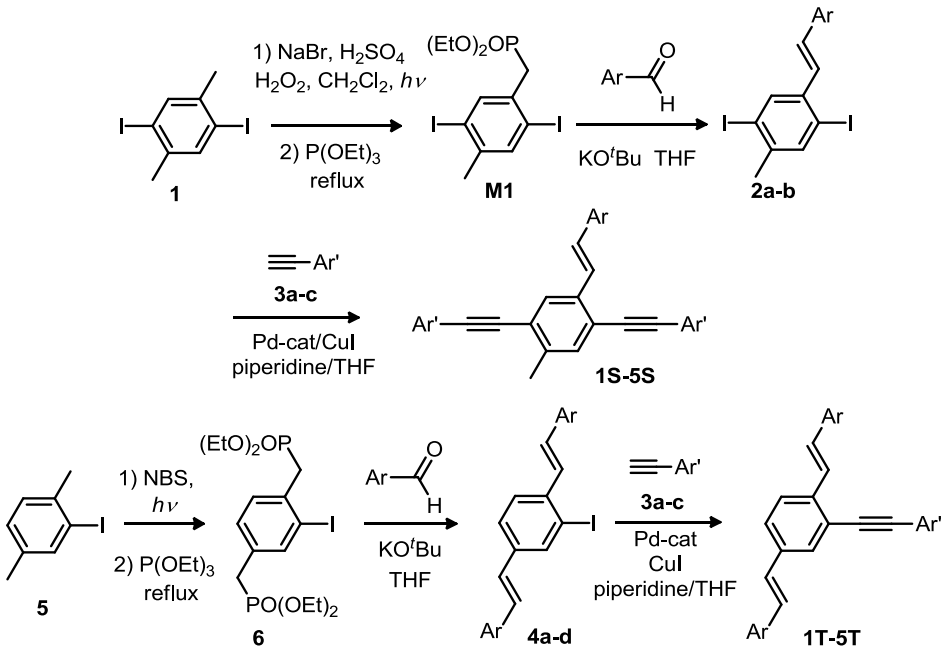

Figure 2.3. Synthesis of **S** and **T** series T-shapes.

Optical and Electronic Properties

The main purpose in the development of these compounds was to serve as a comparison to known 1,4-distyryl-2,5-arylethynylbenzenes, hopefully be able to draw conclusions on how variations in the conjugated system (i.e., removing an arm or part of the electronic system) affected the photophysical properties, and perhaps most importantly, the disjointed FMO structure observed in substituted cruciforms.

As expected from our previous studies with 1,4-distyryl-2,5-arylethynylbenzenes, many of the T-shapes exhibited significant solvatochromism over a wide range of non-polar and polar solvents. In particular, compounds with highly electron donating dibutylamino groups generated emissions ranging the gamut of the visible spectrum, while neutral and electron-accepting substituted compounds retained similar fluorescence in a variety of solvents (figure 2.4). Tables 2.1 and 2.2 detail the optical properties of the stilbene (table 2.1) and distyrylbenzene (table 2.2) compounds in hexanes.

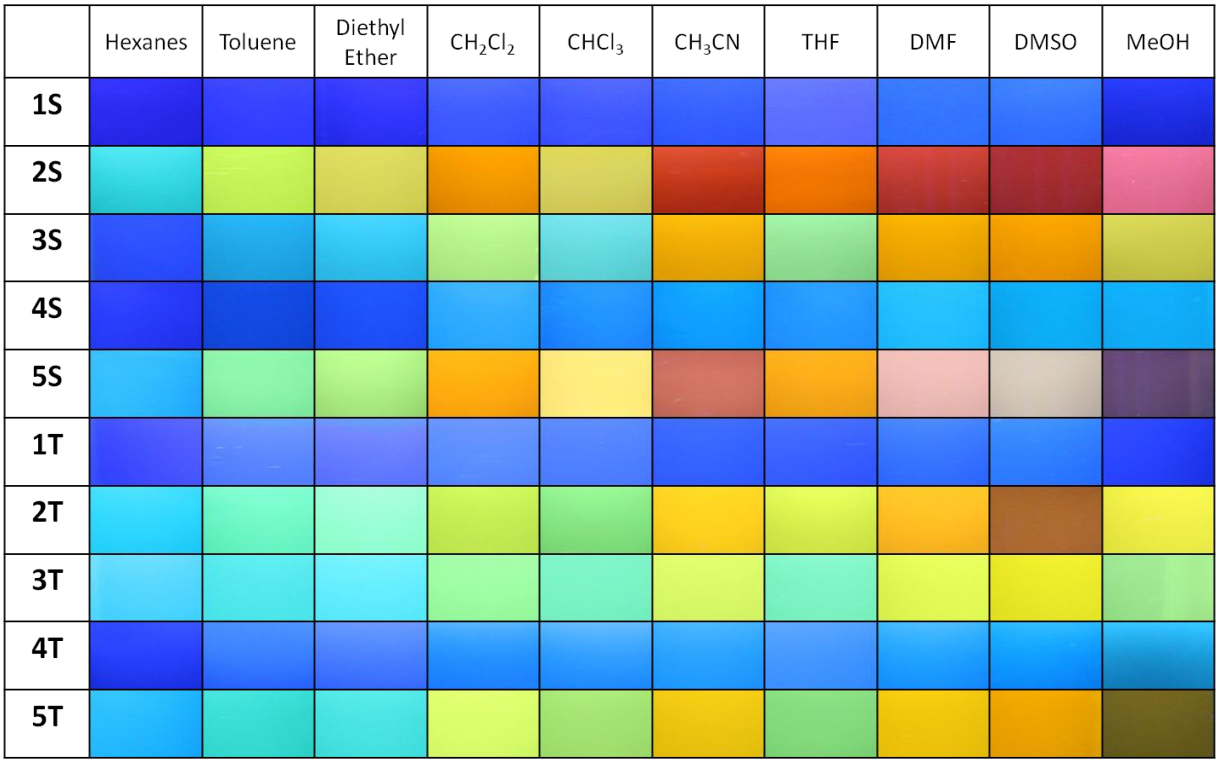

Figure 2.4. Digital photographs of T-shape emission in 10 different solvents. Photographs were taken under a handheld UV light (λ_{max} ex = 365 nm) using a Canon EOS 30D digital camera equipped with a Canon EFS 18-55mm zoom lens.

Table 2.1. Absorption and emission of **1S**-**5S** in a representative solvent. Quantum yield and fluoroescence lifetimes were not recorded for these compounds due to issues with photostability of the compounds.

	Optical Property*	**1S**	**2S**	**3S**	**4S**	**5S**
Hexanes	**λ_{max} Abs (nm)**	**305**	**323**	**323, 364**	**305**	**319**
	λ_{max} Em (nm)	**385, 402**	**493**	**441, 453**	**401, 421**	**493**
	Stokes Shift (cm^{-1})	**6813**	**10676**	**8284**	**5849**	**11064**

Table 2.2. Optical properties of **1T-5T** in hexanes.

	Optical Property	1T	2T	3T	4T	5T
Hexanes	λ_{max} Abs (nm)	300, 362	273, 419	268, 412	297, 359	269, 415
	λ_{max} Em (nm)	401, 424	479	455, 485	404, 426	466
	Quantum Yield (Φ)	0.98	0.38	0.44	0.98	0.5
	Fl. Lifetime (τ, ns)	1.26	1.75	1.02	1.46	1.20
	Stokes Shift (cm^{-1})	8395	15753	15335	8918	15716

Photostability of Stilbene T-Shapes

While collecting fluorescence data, it was discovered that the stilbenoid compounds exhibited variations in emission upon exposure to ambient light. To investigate this problem, a time dependent study was conducted in which the emission of a representative stilbene (**3S**) was recorded over a one hour time period upon exposure to various amounts of ultraviolet light (figure 2.5). The initial sample was prepared in dichloromethane in a dark room and produced a broad emission at 533 nm with a small peak visible at 332 nm. Even after short exposure to light (2 min), the relative intensities of the two peaks were nearly equivalent and a new peak at 349 nm was clearly evident. The growth of the higher energy peaks drastically increased in intensity as the molecule was continually exposed to light over a one hour time frame.

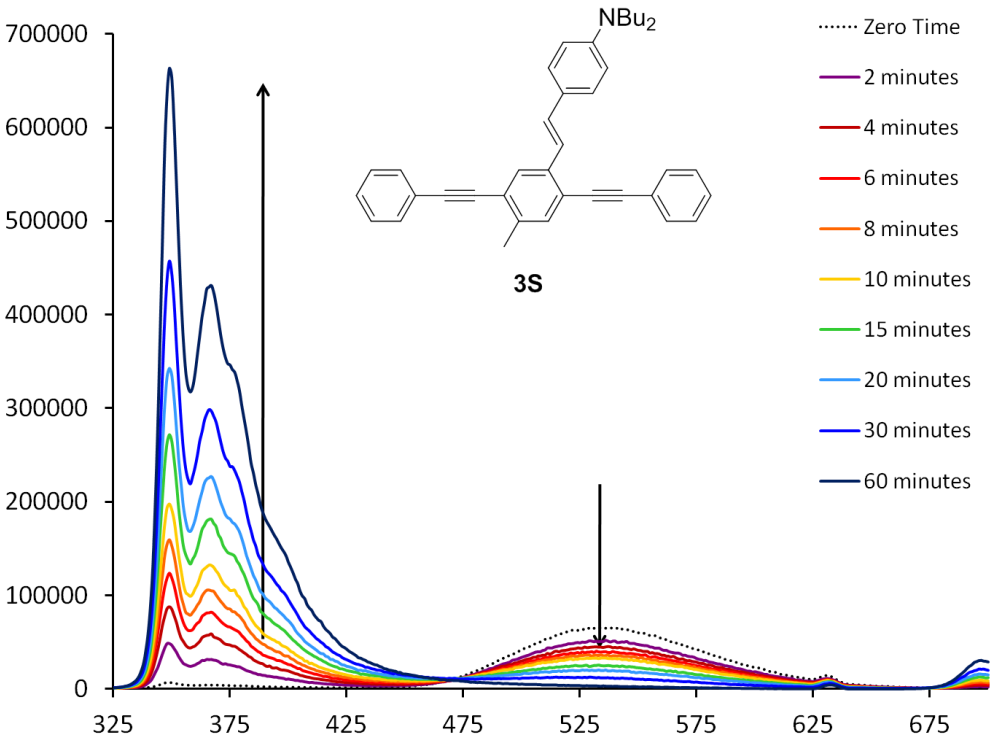

Figure 2.5. Emission of **3S** upon continual exposure to UV-light (λ_{max} = 365 nm).

Since compounds **1S-5S** exhibit these variable emissions in solution, application in sensing assays become severely limited and impractical for widespread use. The mechanism for this transition is currently unknown; ^{1}H NMR data was inconclusive in determining the possibility of a 'hula-twist' around the double bond, a characteristic previously observed with stilbenes.[9-11] we chose to withhold further investigations into the stilbene compounds as the purposes of our studies were to develop new compounds for use as proton and metal detection probes. Conversely, none of the distyryl T-shapes demonstrated instability to light, and therefore became a much more attractive structure for further examination. This knowledge will also aid in the development of future molecular architectures as we begin to gain insight into the stability of different types of cross-conjugated materials.

Proton and Metal Sensing

Alterations in spectroscopic properties were investigated in compounds with reactive functionalities (Figure 2.6). As expected, no changes in emission were observed upon addition of Na^+ or K^+ to any of the compounds. Additionally, **3T-5T** bound Li^+ while **2T** did not, which was also analogous to previously reported data on 1,4-distyryl-2,5-arylethynylbenzene models.[12] The most unexpected results were found in the lack of binding of **2T** with Mg^{2+} along with the quenching associated with zinc, manganese, copper, and trifluoroacetic acid. Reaction of Mg^{2+} to the corresponding pyridyl substituted XF had been found to elicit a significant bathochromic shift in the emission,[12] whereas the T-shape model exhibited no alterations in fluorescence. Upon reaction with the transition metals, the emission was highly red-shifted, but more importantly, the relative fluorescence of the bound material was reduced to the point that it appeared completely quenched to the naked eye, lending this molecule towards use as a very effective turn-off sensor.

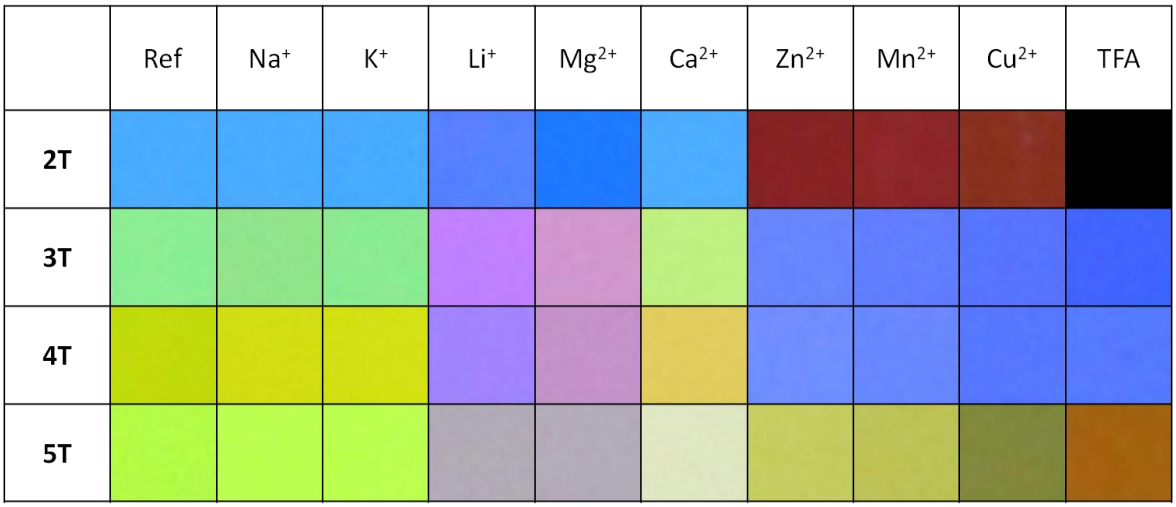

Figure 2.6. Reaction of **2T**-**5T** with metal triflates and trifluoroacetic acid. All sensing studies were performed in dichloromethane at a concentration equivalent to the solubility of each metal salt in the solvent. Photographs were taken under a handheld UV light (λ_{max} ex = 365 nm) using a Canon EOS 30D digital camera equipped with a Canon EFS 18-55mm zoom lens.

Conclusions

We have synthesized a new series of cross-conjugated distyryl-arylethynylbenzene derivatives based on a "T-shape" motif. Incorporation of various reactive functionalities impart binding capabilities of various metals in solution, allowing for the ratiometric detection of these analytes. It was found that the stilbenoid analogues degraded over time upon exposure to ambient light while the distyryl compounds were photostable, knowledge that provides a solid foundation for future synthesis of new cross-conjugated architectures. Additionally, an effective turn-off sensor was developed using the pyridyl-substituted compound upon reaction with Zn^{2+}, Mn^{2+}, Cu^{2+}, and H^{+}. Work is currently underway to build new libraries of cruciforms with much larger conjugated systems containing multiple axes.

Experimental Procedures

Materials and Methods

All chemicals and solvents were purchased from commercial sources and were used without further purification unless otherwise specified. All IR spectra were obtained using a Shimadzu FTIR-8400s spectrometer. ^{1}H NMR spectra were recorded at 298 K on a 300 MHz spectrometer. Chemical shifts are reported in parts per million (ppm), using residual solvent (chloroform-*d*) as an internal standard. The data is reported as follows: chemical shift, multiplicity (s = singlet, d = doublet, t = triplet, q = quartet, m = multiplet, br = broad), and integration. ^{13}C HMR spectra were recorded at 400 MHz, and ^{13}C chemical shifts (δ) are referenced to residual $CHCl_3$ at 77.23 ppm or residual DMSO at 39.5 ppm. All absorption spectra were collected using a Shimadzu UV-2401PC spectrophotometer. All emission spectra were acquired using a Shimadzu RF-5301PC

spectrofluorophotometer. Quantum yields for the polymer was measured using standard procedures.[13] In all cases, quinine sulfate and 2-aminopyridine were used as standards and all solutions were purged with nitrogen prior to measurement.

Synthesis and Characterization Data

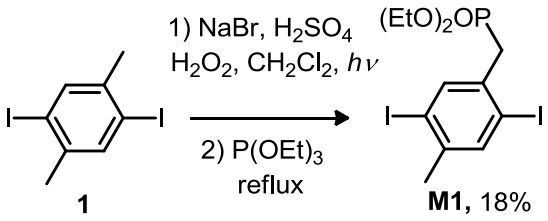

Figure 2.7. Synthesis of monomer **M1**.

A stirred suspension of **1** (35.8 g, 100 mmol), NaBr (11.3 g, 110 mmol) and 30% H_2O_2 (15 mL, 150 mmol) in CH_2Cl_2 (200 mL) was cooled on an ice bath. Conc. H_2SO_4 (10 mL, 180 mmol) was added dropwise over 5 min. The ice bath was removed and the reaction was irradiated by a tungsten incandescent bulb, whilst vigorous stirring was maintained. After 24 h, irradiation was stopped and the mixture was allowed to cool to room temperature. The solution was washed with dilute Na_2SO_3 (aq) followed by H_2O. The organic fraction was dried over $MgSO_4$ and the solvent was evaporated in vacuo. The residue after evaporation consisted chiefly of an equimolar mixture of **13** and the mono-brominated product. To this mixture of products, $P(OEt)_3$ (10 g, 60 mmol) was added and the suspension was refluxed with stirring for 6h. After cooling to RT, the resulting solid was purified by column chromatography (hexanes to CH_2Cl_2) followed by recrystallization from hexanes, providing **M1** (9.02 g, 18% yield) as a colorless solid. Mp: 80-81^{o}C. ^{1}H-NMR, $CDCl_3$ (δ, 300MHz): 1.26 (t, 6H, J = 6 Hz); 2.31 (d, 3H, J = 3 Hz); 3.26 (d, 2H, J = 27 Hz); 4.04 (p, 4H, J = 6 Hz); 7.64 (s, 1H); 7.79 (d, 1H, J = 3 Hz). ^{13}C-NMR, $CDCl_3$ (δ, 75MHz): 16.7, 27.2, 37.0, 62.6, 100.9, 101.0, 135.0, 140.1, 140.3,

142.3. IR (cm^{-1}): 2979.2, 2928.0, 2388.0, 1468.8, 1241.2, 1043.5, 1018.5, 598.0, 526.6, 509.22.

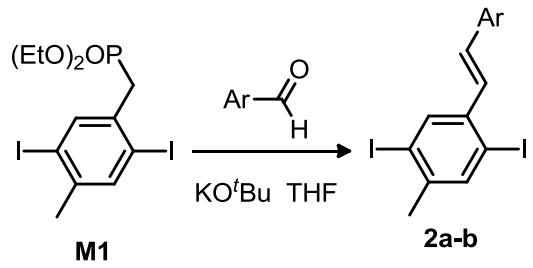

Figure 2.8. General reaction for the synthesis of diiodostilbene precursors for **1S-5S**.

Synthesis of **2a**.

A solution of **M1** (3.90g, 7.89 mmol) in dry THF (30 mL) was stirred under N_2. To this solution, KO^{t}Bu (1.40g, 12.5 mmol) was added followed by 4-(1-methylethyl)benzaldehyde (1.11g, 7.49 mmol). The solution was stirred for 2h and subsequently quenched with MeOH (5 mL). The solvent was removed in vacuo and the residue purified by column chromatography (hexanes). Stilbene **2a** (2.72g, 70% yield) was obtained as a colorless solid. Mp: 74-76^{o}C (decomp.). ^{1}H-NMR, $CDCl_3$ (δ, 300MHz): 1.27 (d, 6H, *J* = 7 Hz); 2.36 (s, 3H); 2.92 (m, 1H, *J* = 7 Hz); 6.89 (d, 1H, *J* = 16 Hz); 7.11 (d, 1H, *J* = 16 Hz); 7.23 (d, 2H, *J* = 6 Hz); 7.46 (d, 2H, *J* = 8 Hz); 7.69 (s, 1H); 7.99 (s, 1H). ^{13}C-NMR, $CDCl_3$ (δ, 75MHz): 24.0, 27.2, 34.0, 99.8, 101.2, 122.2, 126.9, 126.9, 129.7, 131.8, 134.3, 135.7, 139.8, 139.9, 142.1, 149.2. IR (cm^{-1}): 3035.1, 3001.3, 2967.6, 2956.0, 2934.8, 2348.4, 1898.0, 1347.3, 1051.2, 854.5.

Synthesis of **2b**.

A solution of **M1** (2.6g, 5.26 mmol) in dry THF (20 mL) was stirred under N_2. To this, KO^{t}Bu (0.71g, 6.33 mmol) was added followed by 4-dibutylaminobenzaldehyde (1.18g, 5.06 mmol). The solution was stirred for 2 hours and quenched with H_2O. The

mixture was extracted with Et_2O, and dried over $MgSO_4$. An excess of dry HCl in Et_2O was added; the precipitated solid was recovered via vacuum filtration and recrystallized from $CHCl_3/Et_2O$. Compound **2b** (1.53g, 48% yield) was obtained as a colorless crystalline solid. Mp: 196-198^oC (decomp.). ^{1}H-NMR, $CDCl_3$ (δ, 300MHz): 0.85 (m, 6H); 1.27 (m, 6H); 2.01 (m, 2H); 2.37 (s, 3H); 3.33 (m, 4H); 6.90 (d, 1H, *J* = 16 Hz); 7.21 (d, 1H, *J* = 16 Hz); 7.69 (m, 5H), 7.98 (s, 1H); 13.95 (s, 1H). ^{13}C-NMR, $CDCl_3$ (δ, 75MHz): 13.5, 19.9, 26.6, 27.3, 58.8, 100.0, 101.2, 122.2, 123.1, 128.4, 129.5, 133.2, 136.0, 137.5, 138.5, 138.8, 139.9, 143.1. IR (cm^{-1}): 3035.1, 2961.8, 2872.1, 2398.6, 2348.4, 1514.2, 1041.6, 671.3, 602.8. MS (EI): (M^+) 573.0386 (found); 573.0390 (calc'd for $C_{23}H_{29}I_2N$).

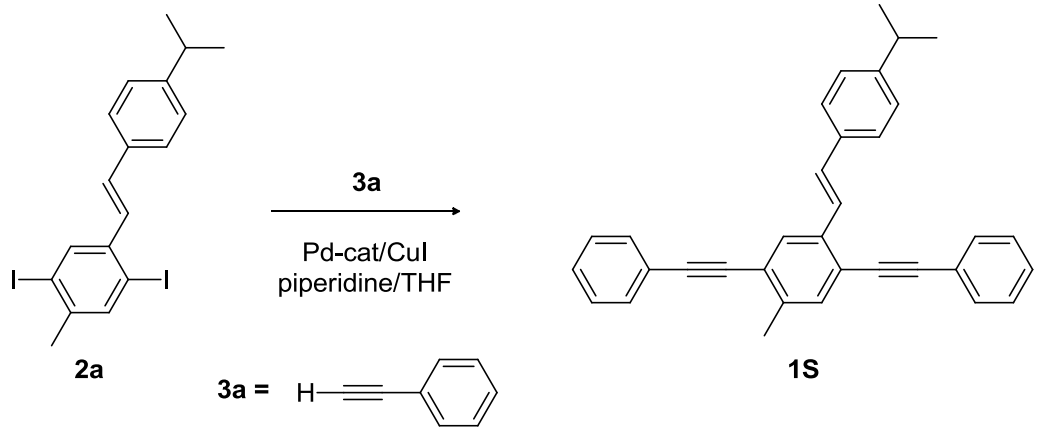

Figure 2.9. Synthesis of **1S**.

Synthesis of **1S**.

To a degassed solution of **M1** (0.30 g, 0.62 mmol) in 30% piperidine/THF (4 mL), **3a** (0.31 g, 3.1 mmol) was added followed by CuI (1 mg, 0.006 mmol) and $Pd(PPh_3)_2Cl_2$ (7 mg, 0.009 mmol). The solution was allowed to stir overnight under N_2. The mixture was diluted with H_2O, neutralized with AcOH and extracted with hexanes. The solvent was evaporated *in vacuo*, and the residue was purified via column

chromatography (hexanes to 8% CH_2Cl_2/Hexanes) followed by recrystallization from EtOAc/MeOH at -10°C. Compound **1S** (0.20g, 75% yield) was obtained as a colorless crystalline powder. Mp: 123-124°C. ^{1}H-NMR, $CDCl_3$ (δ, 300MHz): 1.27 (d, 6H, *J* = 7 Hz); 2.51 (s, 3H); 2.93 (m, 1H, *J* = 7 Hz); 7.24 (m, 3H); 7.39 (m, 7H); 7.51 (m, 2H, *J* = 8 Hz); 7.59 (m, 5H); 7.86 (s, 1H). ^{13}C-NMR, $CDCl_3$ (δ, 75MHz): 14.7, 20.3, 24.0, 34.0, 88.0, 88.1, 94.7, 95.4, 121.8, 122.2, 123.3, 123.5, 124.9, 126.7, 126.9, 128.0, 128.4, 128.5, 130.0, 131.5, 131.6, 133.4, 135.0, 136.5, 138.7, 148.8. IR (cm^{-1}): 3051.5, 2955.0, 2863.4, 2357.1, 1504.5, 1439.9, 959.6, 751.3, 690.5. MS (EI): (M^+) 436.2194 (found); 436.2191 (calc'd for $C_{34}H_{28}$). Anal. Found (calc'd for $C_{34}H_{28}$): C 93.41% (93.54%), H 6.49% (6.46%).

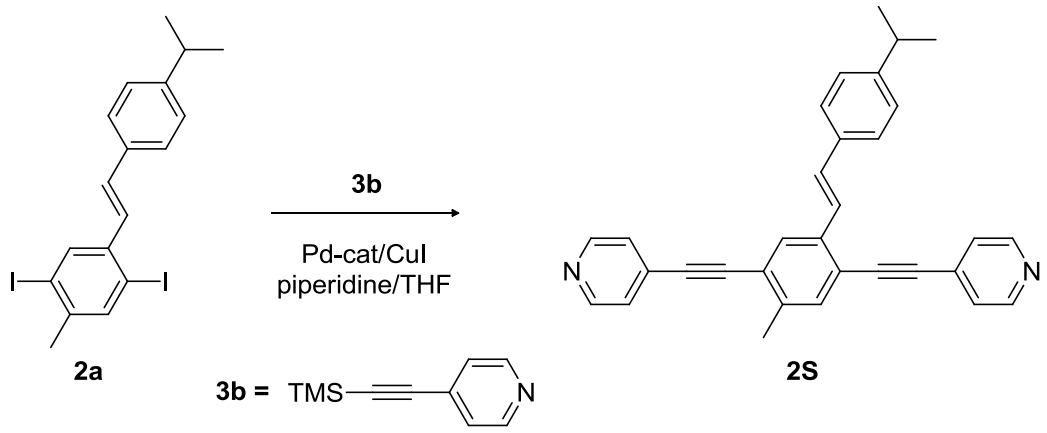

Figure 2.10. Synthesis of **2S**.

Synthesis of **2S.**

To a solution of **3b** (0.62 g, 1.3 mmol) in 30% piperidine/THF (3.5 mL), TBAF•3H_2O (1.60 g, 5.08 mmol) was added. The solution was allowed to stir under N_2 for 5 min and **2a** (0.82 g, 3.17 mmol) was added followed by CuI (3 mg, 0.01 mmol) and $Pd(PPh_3)_2Cl_2$ (14 mg, 0.020 mmol). The mixture was allowed to stir overnight under N_2, H_2O was added and the mixture was extracted with Et_2O. The extracts were dried over

NaOH pellets and evaporated in vacuo. The residue was purified via column chromatography (hexanes to 25% EtOAc/hexanes) followed by recrystallization from pet. ether (-78°C). Compound **4** (0.13 g, 23% yield) was obtained as a dark yellow crystalline solid. Mp: 150-151°C (decomp.). ^{1}H-NMR, $CDCl_3$ (δ, 300MHz): 1.47 (d, 6H, *J* = 8 Hz); 2.51 (s, 1H); 2.94 (m, 1H, *J* = 8 Hz); 7.25 (m, 3H); 7.48 (m, 8H); 7.87 (s, 1H); 8.64 (m, 4H). ^{13}C-NMR, $CDCl_3$ (δ, 75MHz): 20.2, 23.9, 34.0, 92.1, 92.2, 92.3, 92.8, 121.3, 123.2, 124.2, 125.4, 125.5, 126.7, 127.0, 128.5, 131.0, 131.2, 133.8, 134.6, 137.1, 139.1, 149.3, 149.9. IR (cm^{-1}): 3040.9, 3023.5, 2966.6, 2865.4, 2385.1, 2223.0, 2206.6, 1537.3, 1514.2, 1496.8, 1406.2, 819.8. MS (EI): (M^+) 438.2099 (found); 438.2096 (calc'd for $C_{32}H_{26}N_2$).

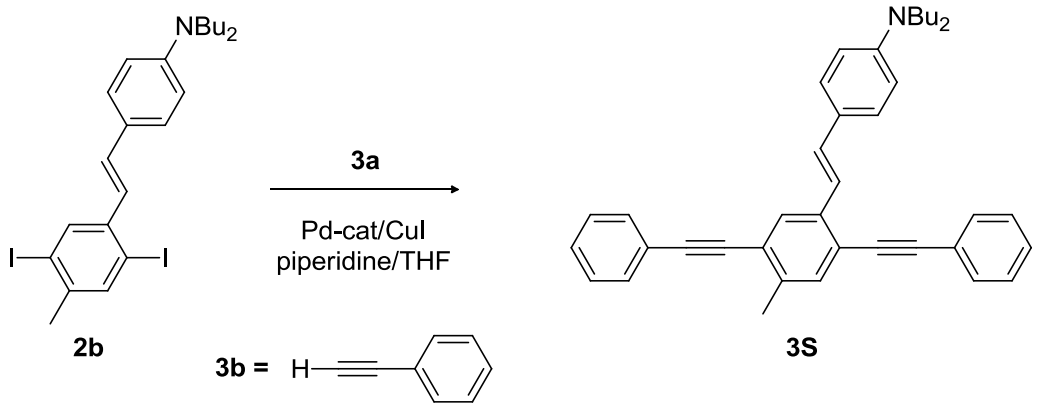

Figure 2.11. Synthesis of **3S**.

Synthesis of **3S**

A degassed solution of **2b** (0.45 g, 0.74 mmol) in 50% piperidine/THF (5 mL) was stirred under N_2. To this solution, CuI (2 mg, 0.008 mmol) and $Pd(PPh_3)_2Cl_2$ (8 mg, 0.01 mmol) were added, followed by **3a** (0.40 g, 3.9 mmol). The solution was stirred overnight, and water was added. The mixture was extracted with Et_2O, dried over NaOH pellets, and the solvent was evaporated *in vacuo*. The residue was purified via column chromatography (hexanes to 1:5:94 TEA/CH_2Cl_2/Hexanes) providing an oil. The oil was

crystallized from petroleum ether at -78°C to provide **3S** (0.22 g, 49% yield) as a yellow solid. Mp: 40-42°C (decomp.). ^{1}H-NMR, $CDCl_3$ (δ, 300MHz): 0.95 (t, 6H, *J* = 7 Hz); 1.43 (m, 4H, *J* = 7 Hz); 1.56 (m, 4H, *J* = 7 Hz); 2.48 (s, 3H); 3.28 (t, 4H, *J* = 7 Hz); 6.62 (d, 2H, *J* = 9 Hz); 7.14 (d, 1H, *J* = 16 Hz); 7.37 (m, 10H); 7.57 (m, 4H); 7.82 (s, 1H). ^{13}C-NMR, $CDCl_3$ (δ, 75MHz): 14.1, 14.7, 20.4, 29.5, 50.8, 88.4, 88.5, 94.4, 95.1, 111.6, 120.6, 121.1, 122.2, 123.3, 123.4, 123.5, 124.5, 127.5, 128.1, 128.3, 128.4, 128.5, 130.4, 131.5, 131.6, 133.3, 137.4, 137.7, 148.0. IR (cm^{-1}): 3031.2, 2954.1, 2869.2, 2201.8, 1605.8, 1597.1, 1515.1, 1366.6, 1183.4, 958.7, 688.6. MS (EI): (M^+) 521.3085 (found); 521.3083 (calc'd for $C_{39}H_{39}N$).

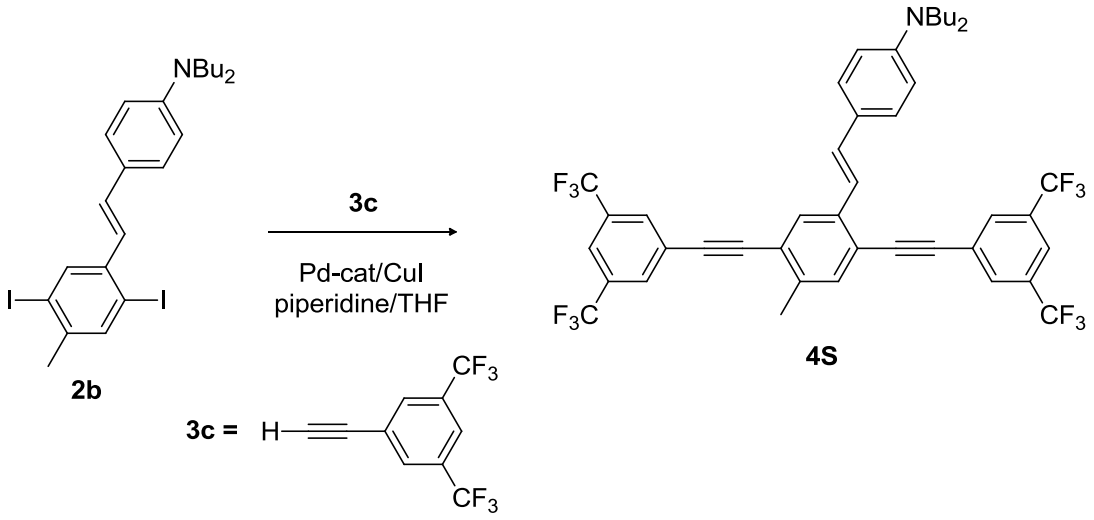

Figure 2.12. Synthesis of **4S**.

Synthesis of **4S**

A 20% (m/v) KOH/MeOH solution (3 mL) was cooled on an ice bath and **2b** (0.50 g, 0.82 mmol) was added followed by **3c** (0.56 g, 2.5 mmol). The solution was cooled for 5 min with periodic shaking and then added to a solution of 50% piperidine/THF (10 mL). The mixture was allowed to stir for 3 minutes under N_2 at

which point, CuI (2 mg, 0.008 mmol) and $Pd(PPh_3)_2Cl_2$ (8 mg, 0.01 mmol) were added. The mixture was stirred overnight under N_2 at 40°C. Next, dilute NH_3 (aq) was added and the mixture was extracted with Et_2O. The extract was dried over Na_2SO_4 and the solvent removed under reduced pressure. The residue was purified by column chromatography (30% CH_2Cl_2/hexanes) followed by recrystallization from pet. ether at -78°C which provided **4S** (0.43g, 66% yield) as an orange solid. Mp: 155-157°C (decomp.). ^{1}H-NMR, $CDCl_3$ (δ, 300MHz): 0.97 (t, 6H, *J* = 7 Hz); 1.38 (m, 4H, *J* = 7 Hz); 1.59 (m, 4H, *J* = 7 Hz); 2.51 (s, 3H); 3.31 (t, 4H, *J* = 7 Hz); 6.65 (d, 2H, *J* = 9 Hz); 7.15 (d, 1H, *J* = 16 Hz); 7.35 (d, 1H, *J* = 16 Hz); 7.43 (m, 3H); 7.82 (m, 3H); 7.99 (m, 4H, *J* = 4 Hz). ^{13}C-NMR, $CDCl_3$ (δ, 75MHz): 14.0, 14.7, 20.3, 29.4, 50.8, 91.5, 91.7, 92.4, 111.6, 119.6, 120.5, 121.2, 121.7, 122.2, 122.3 123.0, 123.9, 124.8, 125.6, 125.7, 128.0, 128.1, 131.3, 131.8, 132.3, 132.7, 133.5, 137.9, 138.2, 148.3. IR (cm^{-1}): 2962.8, 2936.7, 2931.9, 2876.0, 2207.6, 1604.8, 1523.8, 1370.5, 1275.0, 1171.8, 1106.2. MS (EI): (M^+) 793.2571 (found); 793.2578 (calc'd for $C_{43}H_{35}F_{12}N$).

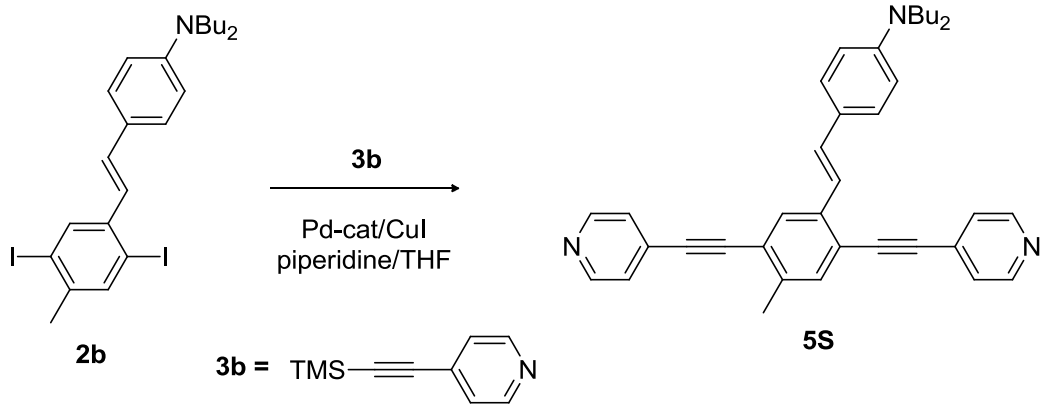

Figure 2.13. Synthesis of **5S**.

Synthesis of **5S**.

A solution of **2b** (0.45 g, 0.74 mmol) in 50% piperidine/THF (3.5 mL) was stirred under N_2 and TBAF•$3H_2O$ (2.5 g, 7.9 mmol) was added. The solution was heated to 40^oC and **3b** (0.48 g, 1.85 mmol) was added, followed by CuI (2 mg, 0.008 mmol) and $Pd(PPh_3)_2Cl_2$ (8 mg, 0.01 mmol). The mixture was stirred under nitrogen for 2 days at 40^oC, after which, brine was added. The mixture was extracted with Et_2O and washed with dilute $NH_{3(aq)}$. The organic phase was dried over NaOH pellets and the solvent was removed under reduced pressure. The residue was purified by column chromatography (1:49:50 TEA/EtOAc/Hexanes) which provided **5S** (0.17 g, 44% yield) as a red/orange waxy solid. ^{1}H-NMR, $CDCl_3$ (δ, 300MHz): 0.95 (t, 6H, *J* = 6 Hz); 1.35 (m, 4H, *J* = 6 Hz); 1.58 (m, 4H, *J* = 6 Hz); 2.46 (s, 3H); 3.28 (t, 4H, *J* = 6 Hz); 6.62 (d, 2H, *J* = 9 Hz); 7.13 (d, 1H, *J* = 16 Hz); 7.31 (d, 1H, *J* = 16 Hz); 7.40 (m, 7H); 7.83 (s, 1H); 8.62 (m, 4H). ^{13}C-NMR, $CDCl_3$ (δ, 75MHz): 14.0, 20.0, 20.3, 29.5, 50.7, 91.9, 92.6, 92.7, 92.8, 111.8, 119.8, 120.7, 123.1, 124.2, 125.4, 128.1, 131.3, 131.4, 133.7, 137.9 138.1, 148.4, 149.8. IR (cm^{-1}): 3026.4, 2953.1, 2943.5, 2924.2, 2867.3, 2859.6, 2435.2, 2201.8, 1591.3, 1515.1, 817.9. MS (EI): (M^+) 523.2986 (found); 523.2987 (calc'd for $C_{37}H_{37}N_3$).

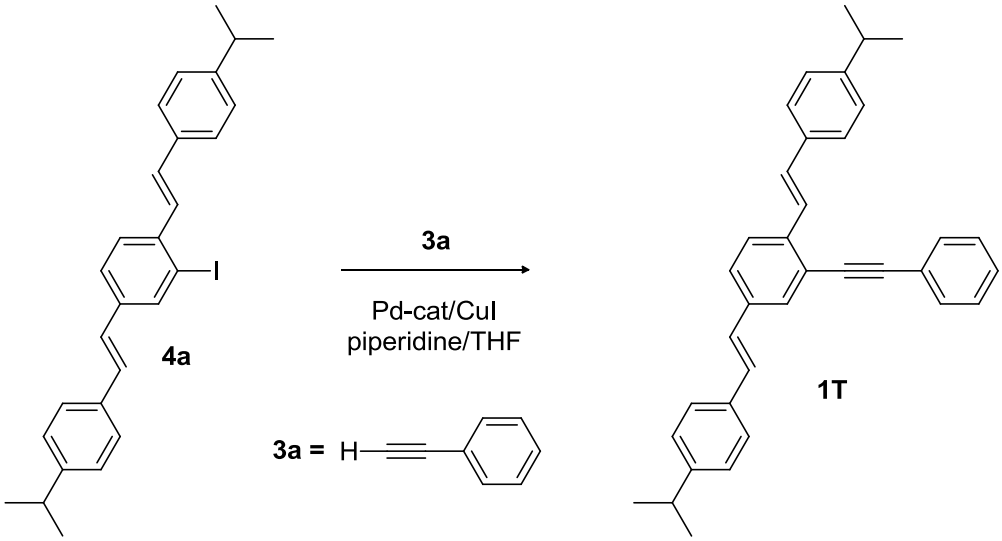

Figure 2.14. Synthesis of **1T**

Synthesis of **1T**.

To a degassed solution of **4a** (0.60 g, 1.2 mmol) in 33% piperidine/THF (7 mL), CuI (5 mg, 0.02 mmol) and $Pd(PPh_3)_2Cl_2$ (30 mg, 0.043 mmol) were added, followed by **3a** (0.25 g, 2.44 mmol). The solution was stirred overnight under N_2 and poured into H_2O. The mixture was extracted with Et_2O and dried over Na_2SO_4. The solvent was evaporated in vacuo and the residue was purified by column chromatography (hexanes to 5% CH_2Cl_2/hexanes), providing **1T** (0.26 g, 45% yield) as a green solid. Mp: 141-142^oC. ^{1}H-NMR, $CDCl_3$ (δ, 300MHz): 1.26 (d, 12H, *J* = 7 Hz); 2.91 (m, 2H, *J* = 7 Hz); 7.02 (d, 1H, *J* = 16 Hz); 7.13 (d, 1H, *J* = 16 Hz); 7.22 (m, 5H); 7.44 (m, 8H); 7.60 (m, 2H); 7.68 (m, 3H). ^{13}C-NMR, $CDCl_3$ (δ, 75MHz): 23.9, 33.9, 88.1, 94.3, 122.4, 123.5, 125.0, 125.7, 126.5, 126.6, 126.7, 126.7, 126.8, 126.8, 128.3, 128.4, 129.2, 130.0, 130.6, 131.6, 134.9, 135.2, 136.5, 137.9, 148.7, 148.8. IR (cm^{-1}): 3047.6, 3022.6, 2956.0, 2361.0, 2331.1, 1513.2, 1492.0, 967.3, 755.2. MS (EI): (M^+) 466.2654 (found); 466.2661 (calc'd for $C_{36}H_{34}$). Anal. Found (calc'd for $C_{36}H_{34}$): C 92.48% (92.66%), H 7.23% (7.34%).

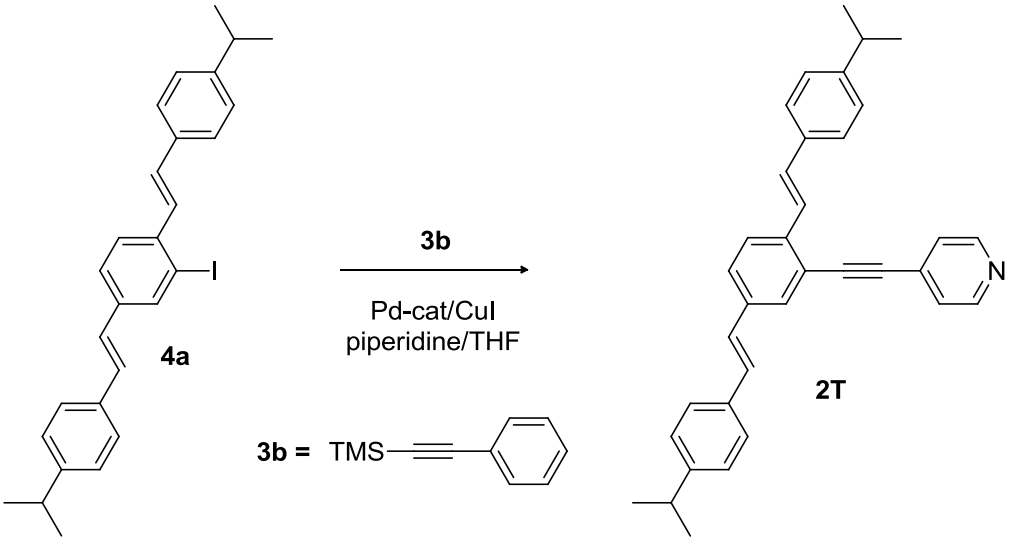

Figure 2.14. Synthesis of **2T**.

Synthesis of **2T**

A degassed solution of **3b** (0.30 g, 1.1 mmol) and TBAF•$3H_2O$ (0.50 g, 1.6 mmol) in 30% piperidine/THF (4 mL) was stirred for 5 min under N_2; **4b** (0.45 g, 0.91 mmol) was added, followed by $Pd(PPh_3)_2Cl_2$ (10 mg, 0.014 mmol) and CuI (2 mg, 0.009 mmol). The solution was stirred overnight at 40°C and poured into dilute NH_3 (aq). The mixture was extracted with Et_2O, and the extracts were dried over NaOH pellets. The solvent was removed in vacuo and the residue was purified column chromatography (30% CH_2Cl_2/Hexanes to CH_2Cl_2) followed recrystallization from pet. ether at -78°C, which provided compound **2T** (0.18 g, 43% yield) as a yellow-green solid. Mp: 154°C (decomp.). ^{1}H-NMR, $CDCl_3$ (δ, 300MHz): 1.28 (d, 12H, *J* = 7 Hz); 2.93 (m, 2H, *J* = 7 Hz); 7.03 (d, 1H, *J* = 17 Hz); 7.15 (d, 1H, *J* = 17 Hz); 7.25 (m, 5H); 7.48 (m, 7H); 7.61 (d, 1H, *J* = 17 Hz); 7.72 (m, 2H); 8.72 (m, 2H). ^{13}C-NMR, $CDCl_3$ (δ, 75MHz): 23.8, 33.9, 34.0, 91.4, 92.7, 121.1, 125.1, 126.3, 126.6, 126.7, 126.8, 126.9, 127.4, 129.5, 130.6, 130.8, 134.7, 134.9, 136.6, 138.3, 148.9, 149.1, 149.8. IR (cm^{-1}): 3022.6, 2957.0,

2869.2, 2348.4, 2209.5, 1592.3, 1513.2, 966.4, 830.4, 815.0. MS (EI): (M^+) 467.2614 (found); 467.2613 (calc'd for $C_{35}H_{33}N$).

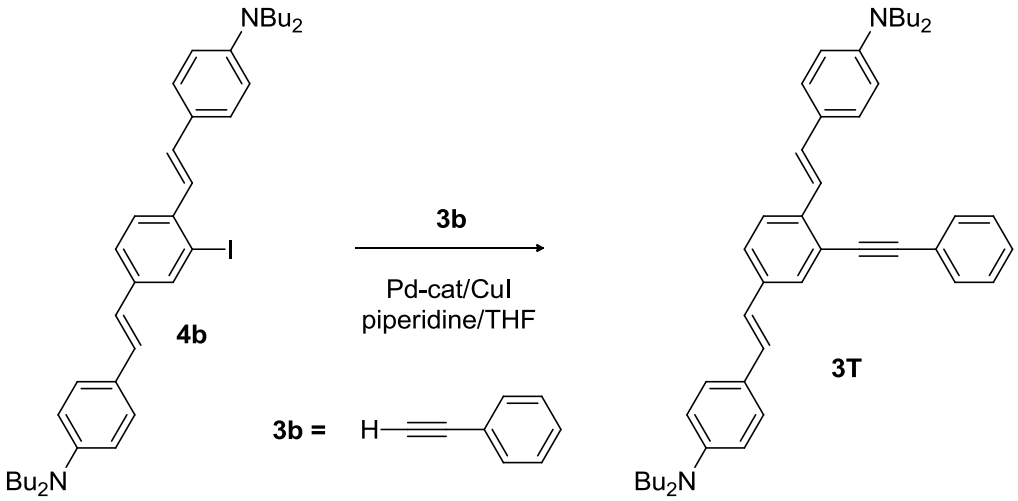

Figure 2.16. Synthesis of **3T**.

Synthesis of **3T**.

To a degassed mixture of **4b** (0.71g, 1.1 mmol) in 50% piperidine/THF (6 mL), **3b** (0.49 g, 4.3 mmol) was added under N_2. Next, CuI (4 mg, 0.02 mmol) and $Pd(PPh_3)_2Cl_2$ (26 mg, 0.037 mmol) were added and the mixture was stirred overnight at 40°C. The mixture was poured into brine and extracted with Et_2O. The extracts were dried over NaOH pellets, and the solvent was evaporated in vacuo. The residue was purified via column chromatography (hexanes to 20% CH_2Cl_2/hexanes), providing **3T** (0.44g, yield 65%) as an orange oil. ^{1}H-NMR, $CDCl_3$ (δ, 300MHz): 0.95 (t, 12H, J = 7 Hz); 1.35 (m, 8H, J = 8 Hz); 1.57 (m, 8H, J_1 = 8 Hz, J_2 = 7 Hz); 3.28 (t, 8H, J = 7 Hz); 6.61 (d, 2H, J = 9 Hz); 6.62 (d, 2H, J = 9 Hz); 6.81 (d, 1H, J = 16 Hz); 7.03 (d, 1H, J = 16 Hz); 7.12 (d, 1H, J = 16 Hz); 7.38 (m, 8H); 7.48 (d, 1H, J = 16 Hz); 7.61 (m, 4H). ^{13}C-NMR, $CDCl_3$ (δ, 75MHz): 14.3, 20.6, 29.7, 51.1, 88.9, 93.9, 111.8, 111.9, 121.6, 121.7, 122.8, 124.0, 124.5, 124.7, 125.0, 126.3, 128.1, 128.2, 128.4, 128.6, 129.1, 130.0,

130.3, 131.8, 136.6, 138.1, 148.1, 148.2. IR (cm^{-1}): 3032.2, 2955.0, 2894.3, 2348.4, 1601.0, 1519.0, 1360.8, 1185.3, 957.7. MS (EI): (M^+) 636.4425 (found); 636.4444 (calcd for $C_{46}H_{56}N_2$).

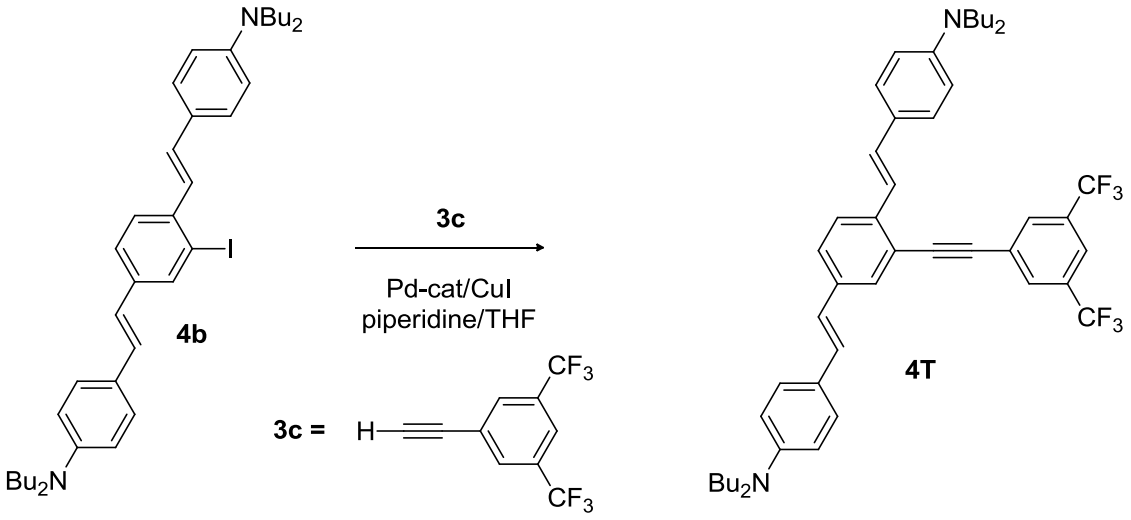

Figure 2.17. Synthesis of **4T**.

Synthesis of **4T**

A solution of **3c** (0.49 g, 1.6 mmol) in 10% KOH/MeOH (5 mL) was shaken periodically over 10 min. This solution was added to a degassed mixture of **4b** (0.75 g, 1.1 mmol) in 50% piperidine/THF (6 mL) under N_2. To this, CuI (2 mg, 0.01 mmol) was added, followed by $Pd(PPh_3)_2Cl_2$ (12 mg, 0.017 mmol), and the mixture was stirred overnight. The mixture was poured into water and extracted with Et_2O. The extracts were dried over Na_2SO_4, and the solvent was evaporated *in vacuo*. The residue was purified by column chromatography (15% CH_2Cl_2 / hexanes) followed by crystallization from $CHCl_3$/MeOH. Compound **4T** (0.50g, yield 57%) was recovered as a yellow-orange solid. MP: 84-86^oC (decomp.). ^1H-NMR, $CDCl_3$ (δ, 300MHz): 0.96 (t, 12H, *J* = 7 Hz); 1.33 (m, 8H, *J* = 7 Hz); 1.58 (m, 8H, *J* = 7 Hz); 3.29 (t, 8H, *J* = 7 Hz); 6.62 (d, 2H, *J* = 9 Hz); 6.64 (d, 2H, *J* = 9 Hz); 6.82 (d, 1H, *J* = 16 Hz); 7.05 (d, 1H, *J* = 16 Hz); 7.13 (d, 1H,

J = 16 Hz); 7.41 (m, 6H); 7.63 (d, 1H, *J* = 8 Hz); 7.64 (d, 1H, *J* = 16 Hz); 7.82 (s, 1H); 8.01 (s, 2H). ^{13}C-NMR, $CDCl_3$ (δ, 75MHz): 13.8, 13.9, 20.3, 20.4, 29.5, 29.6, 50.8, 90.6, 92.6, 111.8, 120.0, 121.0, 121.3, 122.3, 124.4, 124.5, 124.6, 124.9, 126.2, 127.0, 127.9, 128.0, 129.4, 130.0, 130.5, 131.3, 131.4, 131.8, 132.3, 132.7, 136.6, 138.4, 148.1, 148.3. IR (cm^{-1}): 3093.0, 2956.0, 2872.1, 2388.0, 2209.0, 1601.0, 1519.0, 1185.3, 893.1. MS (EI): (M^+) 772.4164 (found); 772.4191 (calc'd for $C_{48}H_{54}F_6N_2$). Anal. Found (calc'd for $C_{48}H_{54}F_6N_2$): C 74.35% (74.59%), H 7.15% (7.04%).

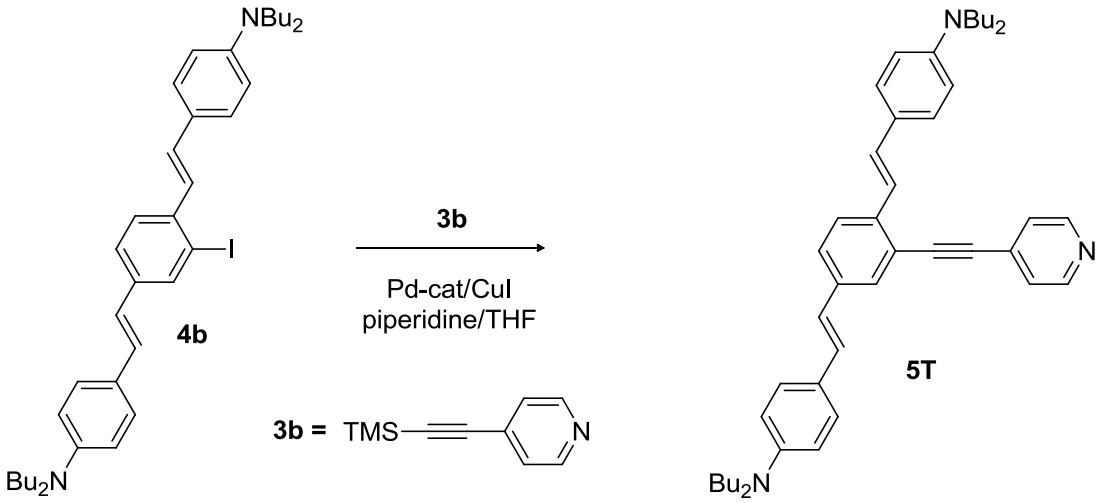

Figure 2.18. Synthesis of **5T**.

Synthesis of **5T**

To a solution of 10% KOH/MeOH (4 mL) at -10°C, **4b** (0.70 g, 4.0 mmol) was added and the solution was cooled in the dark for 20 min. This was added to a degassed solution of **3b** (0.60 g, 1.2 mmol), CuI (7 mg, 0.04 mmol) and $Pd(PPh_3)_2Cl_2$ (16 mg, 0.022 mmol) in of 50% TEA/THF (7 ml) under N_2. The reaction mixture was stirred overnight, and filtered through 50 mL of silica (10% MeOH/EtOAc). The filtrate was concentrated *in vacuo*, dissolved into 50% $Et_2O/CHCl_3$ and titrated with anhy. HCl in Et_2O until salt ceased precipitating. The supernatant was washed with dilute K_2CO_3 (aq)

and concentrated *in vacuo*, providing a red oil. The residue was purified by column chromatography (30% CH_2Cl_2/Hexanes to 2% TEA/CH_2Cl_2) providing **5T** (0.25 g, 38% yield) as an orange oil. ^{1}H-NMR, $CDCl_3$ (δ, 300MHz): 0.95 (t, 12H, *J* = 7 Hz); 1.35 (m, 8H, *J* = 8 Hz); 1.57 (m, 8H, *J* = 8 Hz); 3.28 (t, 8H, *J* = 8 Hz); 6.62 (m, 4H); 6.81 (d, 1H, *J* = 16 Hz); 7.04 (d, 1H, *J* = 16 Hz); 7.12 (d, 1H, *J* = 16 Hz); 7.39 (m, 8H); 7.62 (d, 1H, *J* = 7 Hz); 7.63 (d, 1H, *J* = 16 Hz); 8.62 (d, 2H, *J* = 6 Hz). ^{13}C-NMR, $CDCl_3$ (δ, 75MHz): 14.1, 20.4, 29.5, 50.8, 90.9, 93.5, 111.6, 111.7, 120.2, 120.8, 122.2, 124.3, 124.4, 124.5, 125.5, 127.0, 127.9, 128.1, 129.2, 130.2, 130.4, 131.8, 136.5, 138.3, 148.0, 148.1, 149.9. IR (cm^{-1}): 3033.2, 2955.0, 2868.2, 2384.1, 2204.7, 1601.9, 1519.0, 1185.3, 818.8. MS (EI): (M^+) 637.4373 (found); 637.4396 (calcd for $C_{45}H_{55}N_3$).

References

[1] Zucchero, A.J.; McGrier, P.L.; Bunz, U.H.F. *Acc. Chem. Res.* **2010**, *43*, 397-408.

[2] Klare, J.E.; Tulevski, G.S.; Sugo, K.; de Picciotto, A.; White, K.A.; Nuckolls, C. *J. Am. Chem. Soc.* **2003**, *125*, 6030-6031.

[3] Osowska K, Miljanic OS, *Chem. Commun.* **2010**, *46*, 4276-4278.

[4] (a) Marsden, J.A.; Miller, J.J.; Shirtcliff, L.D.; Haley, M.M.; *J. Am. Chem. Soc.* **2005**, *127*, 2464-2476. (b) Spitler, E.L.; Shirtcliff, L.D.; Haley, M.M. *J. Org. Chem.* **2007**, *72*, 86-96. (c) Spitler, E.L.; Monson, J.M.; Haley, M.M. *J. Org. Chem.* **2008**, *73*, 2211-2223.

[5] Zhang, H.C.; Guo, E.Q.; Zhang, Y.L.; Ren, P.H.; Yang, W.J. *Chem. Mater.* **2009**, *21*, 5125-5135.

[6] Zen, A.; Bilge, A.; Galbrecht, F.; Alle, R.; Meerholz, K.; Grenzer, J.; Neher, D.; Scherf, U.; Farrell, T. *J. Am. Chem. Soc.* **2006**, *128*, 3914-3915.

[7] Hu, K.; Zhu, P.W.; Yu, Y.; Facchetti, A.; Marks, T.J. *J. Am. Chem. Soc.* **2004**, *126*, 15974-15975.

[8] Zhou, N.Z.; Wang, L.; Thompson, D.W.; Zhao, Y.M. *Tetrahedron* **2011**, *67*, 125-143.

[9] Tolbert, L.M.; Baldridge, A.; Kowalik, J.; Solntsev, K.M. *Acc. Chem. Res.* **2011**, *44*, DOI: 10.1021/ar2000925.

[10] Fuβ, W.; Kosmidis, C.; Schmid, W.E.; Trushin, S.A. *Angew. Chem. Int. Ed.* **2004**, *43*, 4178-4182.

[11] Yang, L.-Y.; Harigai, M.; Imamoto, Y.; Kataoka, M.; Ho, T.-I.; Andrioukhina, E.; Federova, O.; Shevyakov, S.; Liu, R.S.H. *Photochem. Photobiol. Sci*. **2006**, *5*, 874-882.

[12] Wilson, J.N.; Josowicz, M.; Wang, Y.; Bunz, U.H.F. *Chem. Commun*. **2003**, *24*, 2962-2963.

[13] "A Guide to Recording Fluorescence Quantum Yields." Horiba Jobin Yvon Ltd. available online: http://www.jobinyvon.co.uk/ukdivisions/Fluorescence/plqy.html

CHAPTER 3

POST-FUNCTIONALIZATION OF PHOSPHONATE-SUBSTITUTED POLY(PARA-PHENYLENEETHYNYLENE)S TO GENERATE BATHOCHROMICALLY SHIFTED CROSS CONJUGATED MATERIALS

Introduction

The concept of post-functionalizing materials is one that many groups have investigated in recent years, with simplification of synthesis being at the forefront of this research.[1-3] Specifically, convergent methodologies, routes leading to the least number of intermediates with minimal purification are vital to combinatorial techniques or the synthesis of multiple targets from a few starting materials. With the classical and modified Sonogashira coupling techniques that have been popularized through the works of Bunz,[4] Swager,[5] and Müllen,[6] convergent methodologies are often difficult to pursue, as many polymers are synthesized from two different starting materials requiring individual synthesis and purification (Figure 3.1).

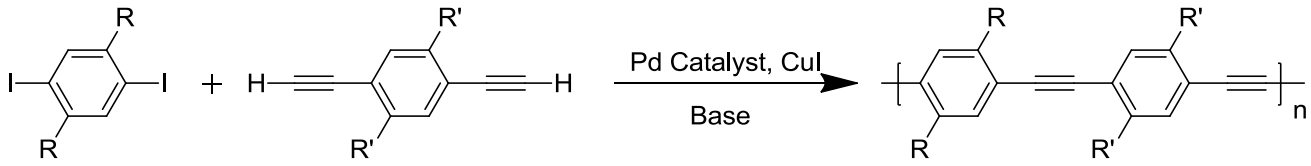

Figure 3.1. General reaction conditions for Sonogashira cross-coupling polymerizations.

Recent developments in the Bunz group have extended the concept of post-functionalization into the world of polymerizations, designing a new methodology for "hyper-branched" (HB) poly(*para*-phenyleneethynylene)s (PPEs) (Figure 3.2).[7]

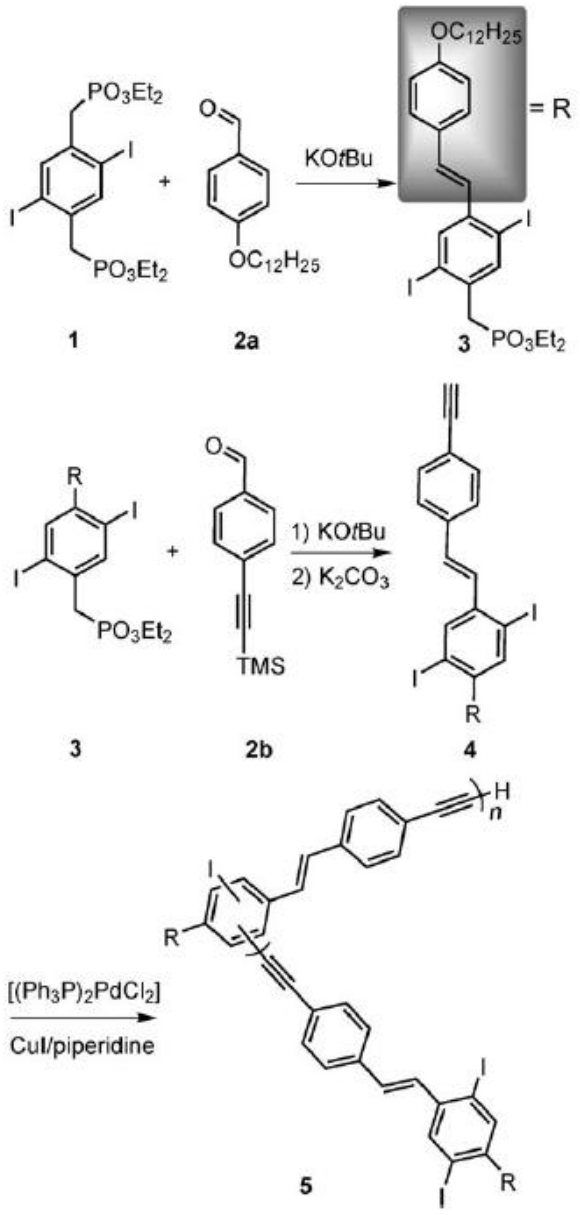

Figure 3.2. Synthesis of hyper-branched poly(*para*-phenyleneethynylene)s.[1]

While similar HB polymers have been reported,[8-9] our group's primary focus has been the manipulation and tuning of electronic properties through post-polymerization reactivity. Having successfully exploited both Horner-Emmons-Wadsworth[10] and Sonogashira cross-coupling reactions[11] to produce a variety of HB PPEs, our focus shifted to applying these techniques to linear materials (Figure 3.3).

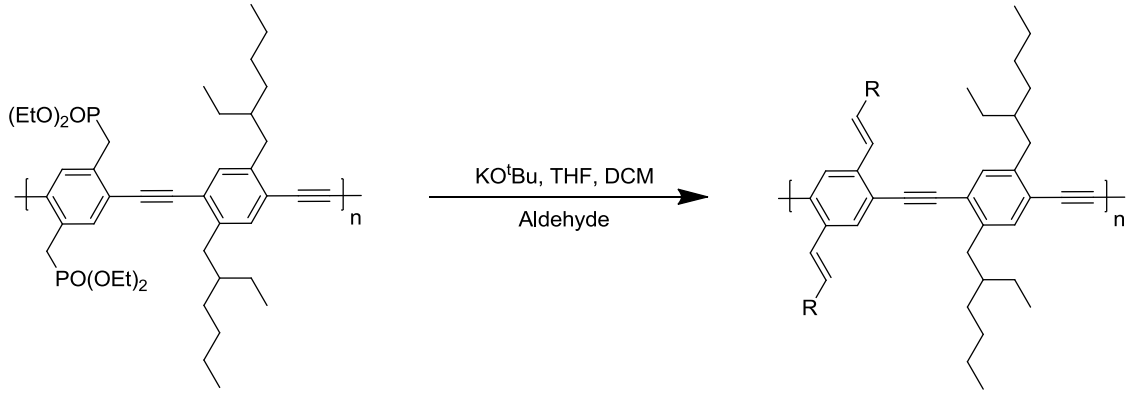

Figure 3.3. Post-functionalization reaction of linear poly(*para*-phenyleneethynylene)s.

Results and Discussion

The overriding purpose of this work was to first prepare a polymer backbone upon which further reactions could be performed to yield a material with desired set of electronic properties, specifically, a particular emission wavelength (Figure 3.4.).

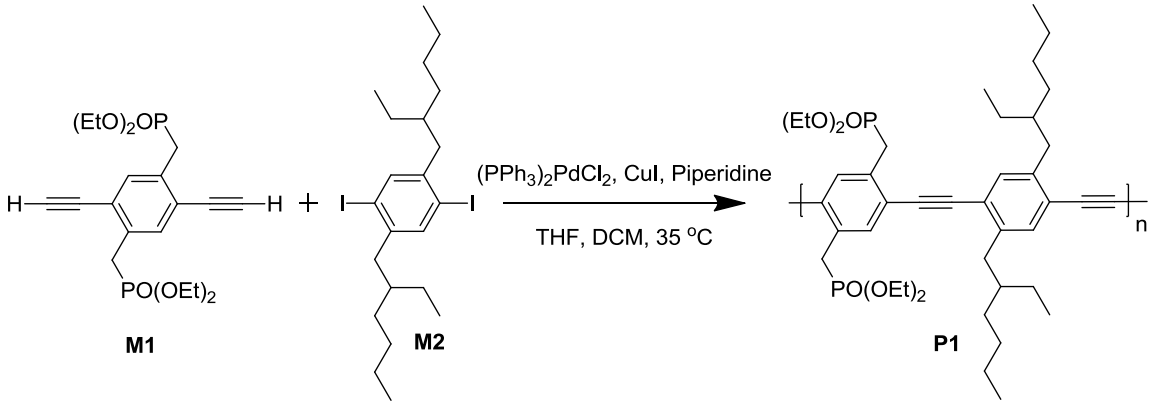

Figure 3.4. Synthesis of PPE **P1**.

Monomer **M1** was synthesized via Sonogashira coupling of TMS-acetylene with the previously reported diiodide analogue,[12] while **M2** was synthesized according to literature procedures.[13] Synthesis of material **P1** provided a basic polymer core from which hybrid PPE-poly(*para*-phenylenevinylene) (PPV) materials could be subsequently prepared via Horner-Emmons-Wadsworth reaction of the phosphonate moieties with any

convenient aromatic aldehyde. Prior to any post-functionalization, **P1** exhibited bright blue fluorescence in the solid state, dichloromethane (DCM), and tetrahydrofuran (THF). We have previously reported the practicality of preparing cross-conjugated PPE-PPV materials, as the inclusion of styryl units on a PPE backbone, especially those substituted with highly electron donating/electron accepting units, leads to a bathochromic shift in emission wavelength.[12] To this end, one could envision easily preparing a PPE-PPV with a specific emission wavelength by simply taking a pre-made polymer, adding a known aldehyde, and subsequently precipitating the material upon coupling. The Horner reaction has no effect upon the backbone of the material, a facet of these reactions that drastically simplifies any purification techniques; theoretically, the reaction progress could be simply monitored by recording the emission at time intervals, and noting when the initial fluorescence peak has completely disappeared.

For the initial experiments, this project was approached from the standpoint of preparing an identical material using two methodologies and comparing the resultant emissions: 1) Post-functionalization of a precursor polymer and 2) classical cross-coupling polymerization (Figure 3.5.).

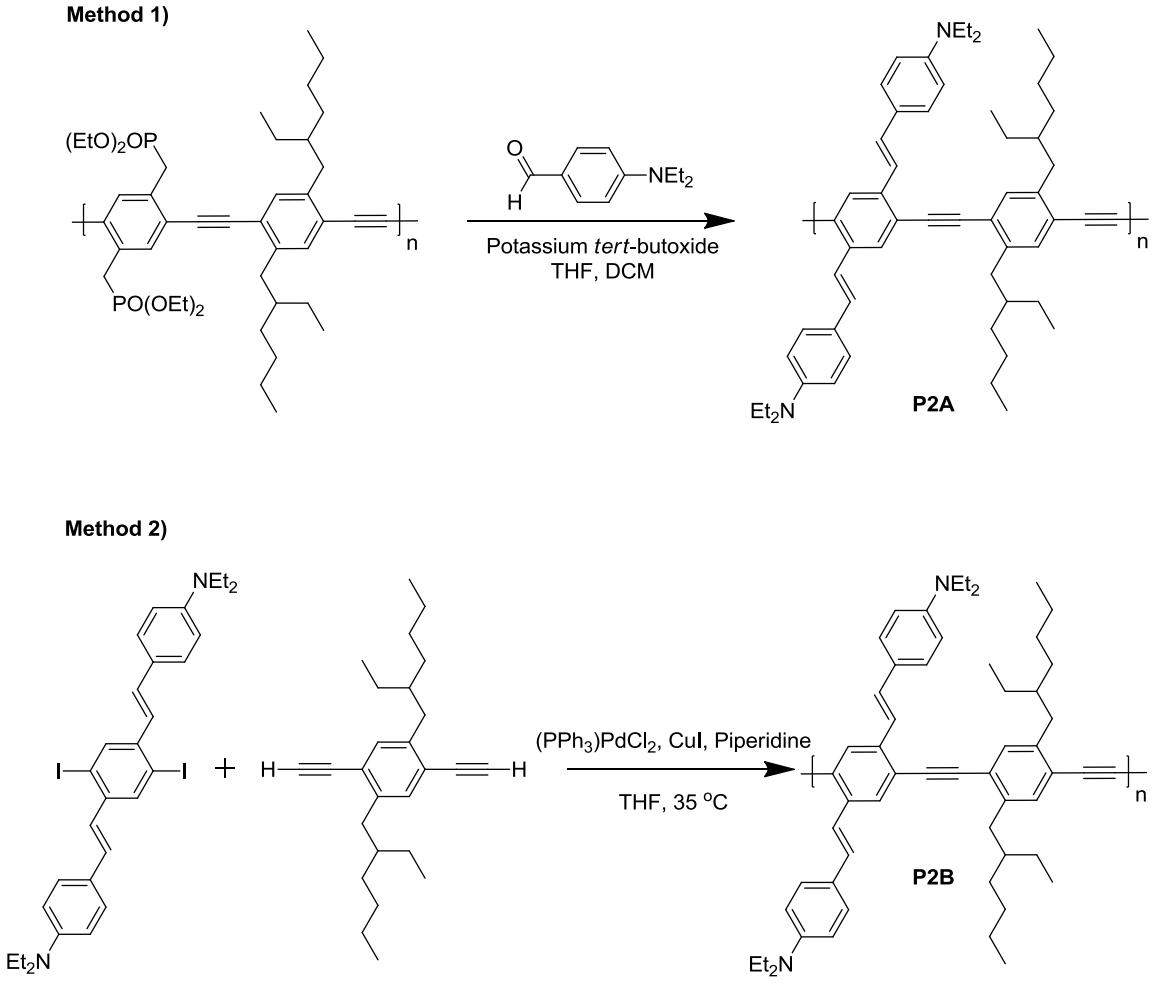

Figure 3.5. Two synthetic approaches: Method 1) Post-functionalization of **P1** to yield **P2A**; Method 2) Preparation of **P2B** under modified Sonogashira cross-coupling conditions.

The resulting data qualitatively illustrated that is was feasible to post-functionalize the backbone of a PPE to achieve results similar to the classical synthetic approach. As seen in Table 3.1, photographs of the fluorescence recorded under blacklight, there is a significant bathochromic shift upon reaction of **P1** with diethylaminobenzaldehyde (**P2A**), indicating that a reaction has taken place, and additionally, the emission is nearly identical to that of the classically prepared polymer (**P2B**). After precipitation of **P2A** into hexanes and subsequent dissolution into DCM,

addition of trifluoroacetic acid afforded a hypsochromic shift in emission that is characteristic of amine protonation in similar systems.[13]

Table 3.1. Emission of **P1**, **P2A**, **P2B**, and **P2A + TFA** in dichloromethane. Photographs were recorded under a handheld UV light (λ_{max} ex = 365 nm) using a Canon EOS 30D digital camera equipped with a Canon EFS 18-55mm zoom lens. Photograph exposure times were held constant for all pictures.

Having qualitatively shown a proof-of-concept, we sought to manually tune the emission by reacting aldehydes with neutral, electron donating, and electronic accepting properties (Figure 3.6). For these studies, it was imperative to record the spectroscopic data (Figure 3.7) in addition to qualitatively examining the emission color via photographs (Table 3.2) for the purposes of building a library where a specific aldehyde can be associated with a known emission wavelength.

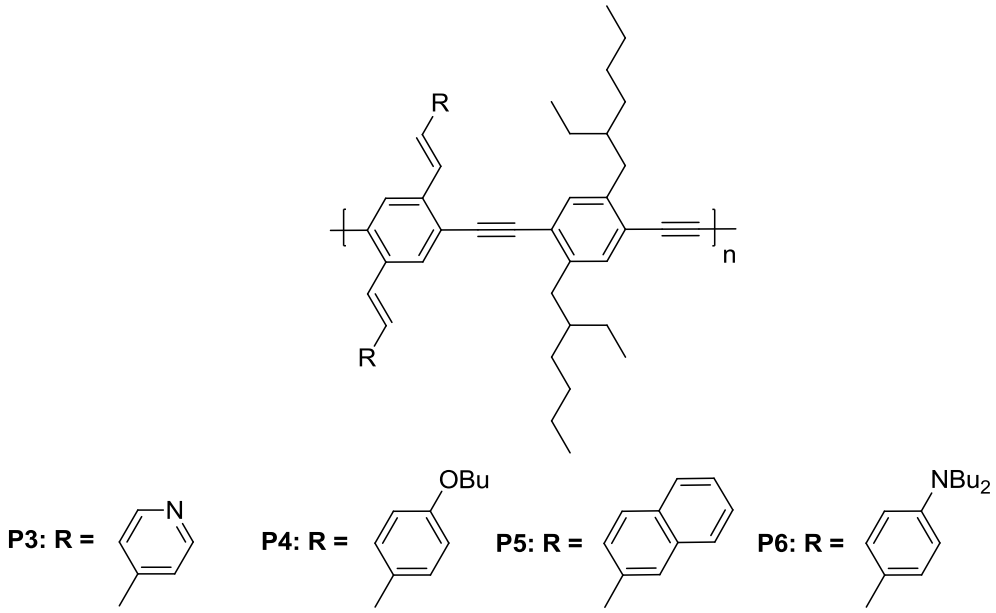

Figure 3.6. Synthesis of **P3**, **P4**, **P5**, and **P6**.

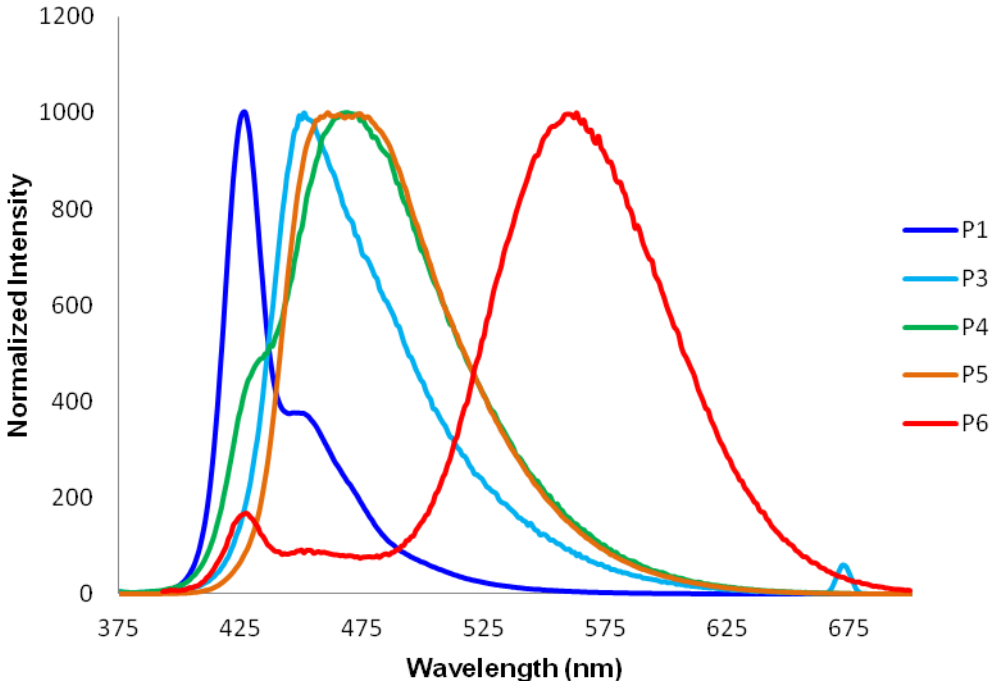

Figure 3.7. Normalized emission spectra of precursor polymer **P1** and post-functionalized products **P3**-**P6**.

Table 3.2. Emission of **P1**, **P3**, **P4**, **P5**, and **P6** in tetrahydrofuran. Photographs were recorded under a handheld UV light (λ_{max} ex = 365 nm) using a Canon EOS 30D digital camera equipped with a Canon EFS 18-55mm zoom lens. Photograph exposure times were held constant for all pictures.

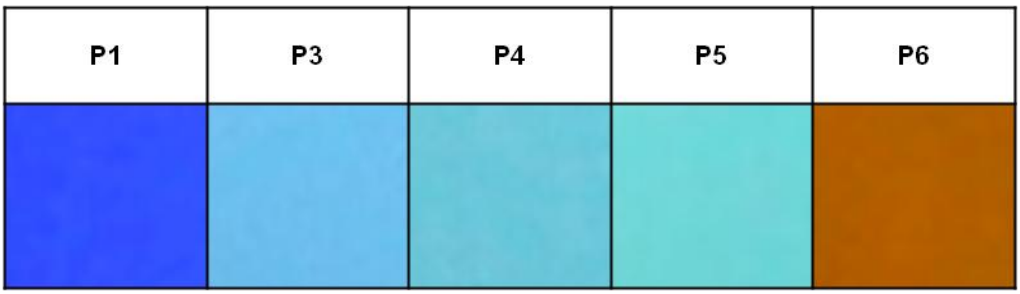

In all cases, clear distinction in the spectroscopic data was made between unreacted **P1** and the post-functionalized materials **P3**-**P6**, with **P6** exhibiting a bathochromic shift of over 130 nm upon inclusion of the highly donating dibutylamino functionality on the bis-styryl axis. In reference to reaction progression, it was noted that in the formation of **P6** had not progressed to completion based on characteristic peak at

425 nm that is associated with the phosphonate substituted PPE. For the purposes of these experiments, further reaction was not undertaken, as the goal of achieving significant red-shifted emissions were obtained.

Conclusions and Future Work

This chapter has described the successful synthesis of a linear polymer and subsequent post-functionalization of the polymer backbone to induce significant bathochromic shifts in the emission. Reaction of the pre-cursor PPE with dibutylamino benzaldehyde generated a material exhibiting orange fluorescence, with an overall red-shift of 136 nm; all other aldehydes used in these experiments yielded smaller red-shifts in the emission maxima, ranging from 25-42 nm. While we have demonstrated the viability of utilizing post-functionalization reactions with polymers, we have yet to achieve post-functionalized emission maxima that span the entire visible spectrum. Based on the results of **P6**, the goal of filling in the "missing" colors will likely be dependent on the electron donating strength of the corresponding aldehyde; our group is currently pursuing these reactions in the hopes of presenting a system where any desired color can be achieved through the convenient methodology described in this work.

Experimental Procedures

Materials and Methods

All chemicals and solvents were purchased from commercial sources and were used without further purification unless otherwise specified. ^{1}H NMR spectra were recorded at 298 K on a 300 MHz spectrometer. Chemical shifts are reported in parts per million (ppm), using residual solvent (chloroform-*d*) as an internal standard. The data is reported as follows: chemical shift, multiplicity (s = singlet, d = doublet, t = triplet, q =

quartet, m = multiplet, br = broad), and integration. All emission spectra were acquired using a Shimadzu RF-5301PC spectrofluorophotometer.

Synthesis and Characterization Data

Monomer **M1** has been previously prepared within our lab[14] and **M2** was synthesized according to previously reported literature.[12]

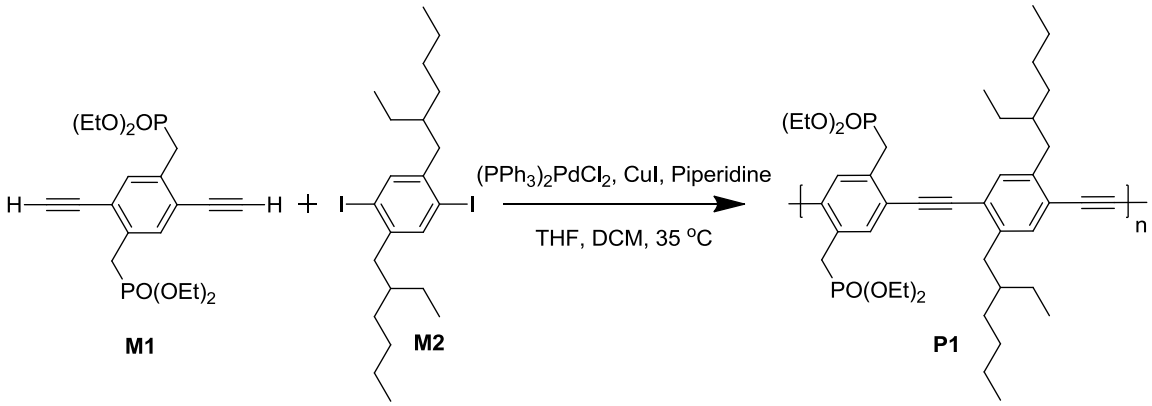

Figure 3.8. Synthesis of pre-cursor polymer **P1**.

Synthesis of **P1**

Monomer **M1** (300 mg, 7.04 x 10^{-4} mol) was combined with monomer **M2** (390 mg, 7.04 x 10^{-4} mol) in a 25 mL Schlenk tube with 2 mL THF, 1 mL DCM and 1.5 mL piperidine. The solution was freeze-pump-thawed three times, followed by addition of $(PPh_3)_2PdCl_2$ (0.49 mg, 0.1 mol %) and CuI (0.27 mg, 0.2 mol %) under a nitrogen atmosphere. The reaction was allowed to stir at 35 ^oC for 48 hrs, at which time the material was precipitated into a large volume of hexanes. Three subsequent dissolutions and precipitations yielded a green solid material in 29.4% yield (150 mg). ^1H NMR (300 MHz, $CDCl_3$): δ 7.63 (s, 2H), δ 7.38 (s, 2H), δ 4.10 (t, 8H), δ 3.45 (br-m, 2H), δ 2.74 (br-m, 2H), δ 1.75 (s, 2H), δ 1.22 (m, 32H), δ 0.82 (m, 12H).

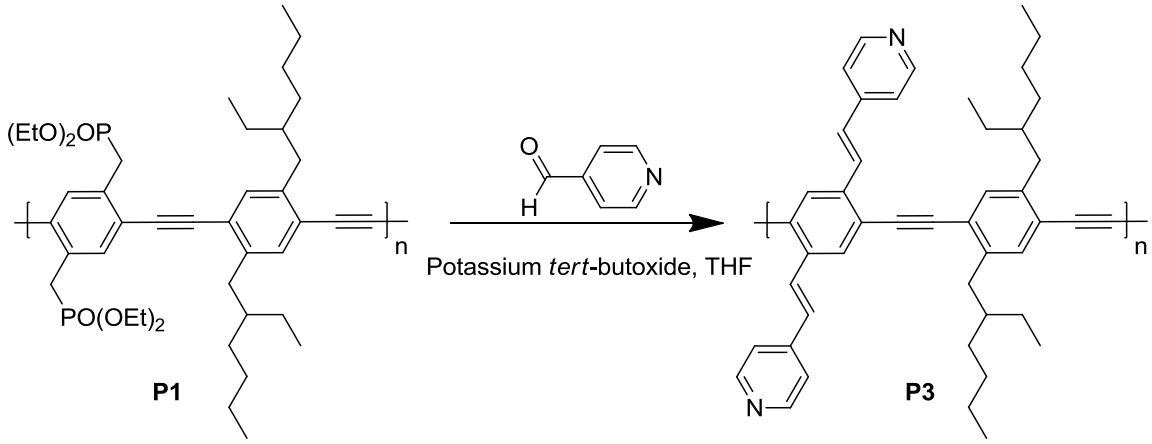

Figure 3.9. Synthesis of **P3**.

Synthesis of **P3**

Compound **P1** (10 mg, 1.34 x 10^{-5} mol) and 4-pyridinecarboxaldehyde (0.033 mL, 26 mol eq) were dissolved in 2 mL THF under nitrogen. Once dissolved, potassium *tert*-butoxide (39 mg, 26 mol eq.) was added to the mixture, which was allowed to stir for 24 hours, at which time the resulting material was precipitated in methanol, yielding a yellow solid exhibiting $\lambda_{max\ em}$ = 451 nm.

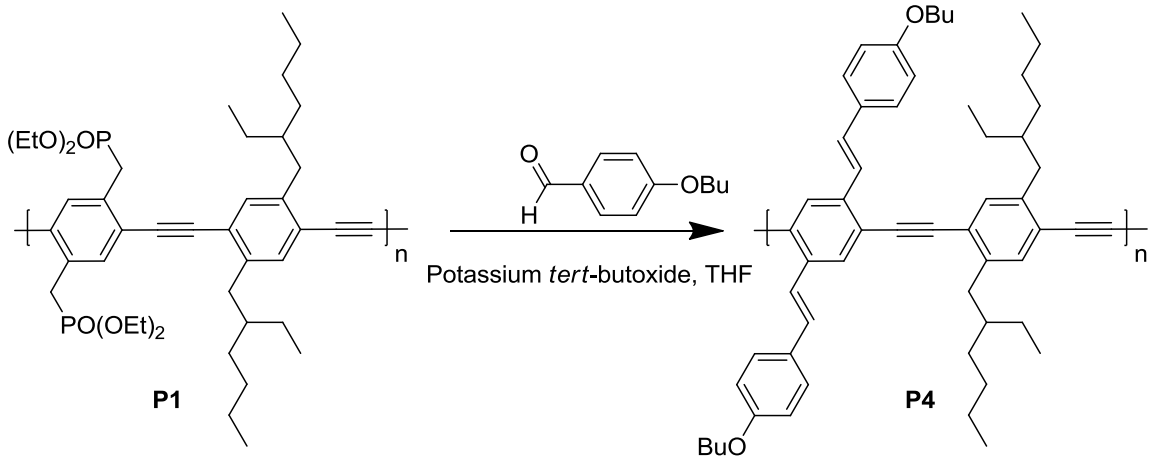

Figure 3.10. Synthesis of **P4**.

Synthesis of **P4**

Compound **P1** (10 mg, 1.34 x 10^{-5} mol) and 4-butoxybenaldehyde (0.056 mL, 26 mol eq) was dissolved in 2 mL THF under nitrogen. Once dissolved, potassium *tert*-butoxide (39 mg, 26 mol eq.) was added to the mixture, which was allowed to stir for 24 hours, at which time the resulting material was precipitated in methanol, yielding a green solid exhibiting $\lambda_{max\ em}$ = 469 nm.

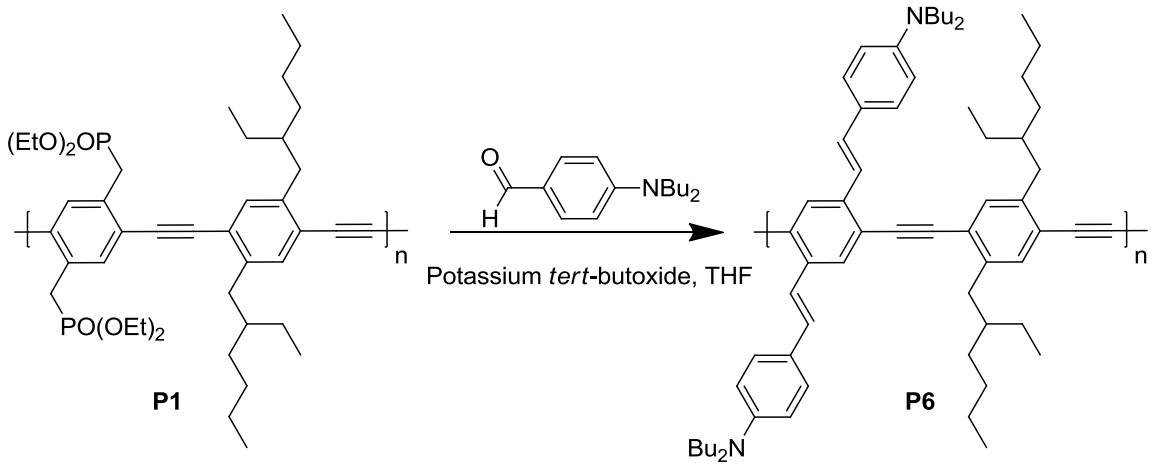

Figure 3.11. Synthesis of **P5**

Synthesis of **P5**

Compound **P1** (10 mg, 1.34 x 10^{-5} mol) and 1-naphthylcarboxaldehyde (55 mg, 26 mol eq) were dissolved in 2 mL THF under nitrogen. Once dissolved, potassium *tert*-butoxide (39 mg, 26 mol eq.) was added to the mixture, which was allowed to stir for 24 hours, at which time the resulting material was precipitated in methanol, yielding a green solid exhibiting $\lambda_{max\ em}$ = 461 nm.

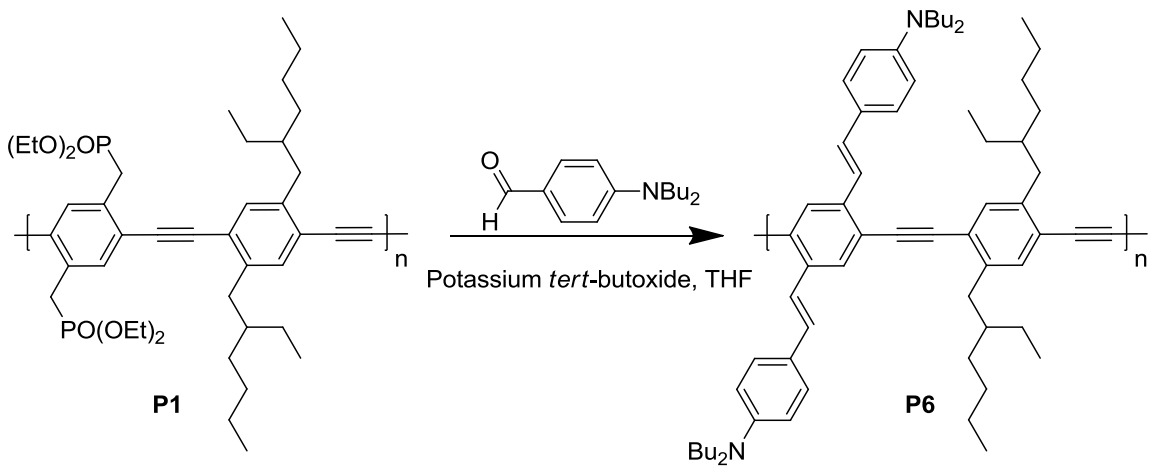

Figure 3.12. Synthesis of **P6**.

Synthesis of **P6**

Compound **P1** (10 mg, 1.34 x 10^{-5} mol) and 4-(N,N dibutyl)aminobenzaldehyde (81 mg, 26 mol eq) was dissolved in 2 mL THF under nitrogen. Once dissolved, potassium *tert*-butoxide (39 mg, 26 mol eq.) was added to the mixture, which was allowed to stir for 24 hours, at which time the resulting material was precipitated in methanol, yielding a green solid exhibiting $\lambda_{max\ em}$ = 563 nm.

References

[1] Tolosa, J.; Kub, C.; Bunz, U.H.F. *Angew. Chem. Int. Ed.* **2009**, *48*, 4610-4612.

[2] (a) Stubbs, L.P.; Weck, M. *Chem. Eur. J.* **2003**, *9*, 992-999. (b) Pollino, J.M.; Weck, M. *Chem. Soc. Rev.* **2005**, *34*, 193-207.

[3] (a) Huisgen, R. *Angew. Chem. Int. Ed. Engl.* **1963**, *2*, 565-598. (b) Huisgen, R.; Szeimies, G.; Möbius, L. *Chem. Ber.* **1967**, *100*, 2494-2501. (c) Helms, B.; Mynar, J.L.; Hawker, C.J.; Frechet, J.M.J. *J. Am. Chem. Soc.* **2004**, *126*, 15020-15021. (d) Englert, B.C.; Bakbak, S.; Bunz, U.H.F. *Macromolecules*, **2005**, *38*, 5868-5877. (e) Thibault, R.J.; Takizawa, K.; Lowenheilm, P.; Helms, B.; Mynar, J.L.; Frechet, J.M.J.; Hawker, C.J. *J. Am. Chem. Soc.* **2006**, *128*, 12084-12085. (f) Bock, V.D.; Hiemstra, H.; van Maarseveen, J.H. *Eur. J. Org. Chem.* **2006**, 51-68. (g) Binder, W.H.; Sachsenhofer, R. *Macromol. Rapid Commun.* **2007**, *28*, 15-54. (h) Lutz, J.F. *Angew. Chem. Int. Ed.* **2007**, *46*, 1018-1025.

[4] (a) Bunz, U.H.F. *Chem. Rev.* **2000**, *100*, 1605-1644. (b) Kim, I.-B.; Dunkhorst, A.; Bunz, U.H.F. *Langmuir*, **2005**, *21*, 7985-7989. (c) Kim, I.-B.; Phillips, R.; Bunz, U.H.F. *Macromolecules*, **2007**, *40*, 5290-5293.

[5] (a) Kim, J.; McQuade, T.; McHugh, S.K.; Swager, T.M. *Angew. Chem. Int. Ed.* **2000**, *39*, 3868-3872. (b) Zhu, Z.; Swager, T.M. *J. Am. Chem. Soc.* **2002**, *124*, 9670-9671. (c) Kim, Y.; Bouffard, J.; Kooi, S.E.; Swager, T.M. *J. Am. Chem. Soc.* **2005**, *127*, 13726-13731. (d) Ishow, E.; Bouffard, J.; Kim, Y.; Swager, T.M. *Macromolecules* **2006**, *39*, 7854-7858. (e) Moslin, R.M.; Espino, C.G.; Swager, T.M. *Macromolecules* **2009**, *42*, 452-454. (f) Chan, J.M.W.; Kooi, S.E.; Swager, T.M. *Macromolecules* **2010**, *43*, 2789-2793.

[6] (a) Mangel, T.; Eberhardt, A.; Scherf, U.; Bunz, U. H. F.; Müllen,K. *Macromol. Rapid Commun.* **1995**, *16*, 571. (b) Wu, J.; Watson, M.D.; Zhang, L.; Wang, Z.; Müllen, K. *J. Am. Chem. Soc.* **2004**, *126*, 177-186. (c) Ma, C.-Q.; Pisula, W.; Weber, C.; Feng, X.-L.; Müllen, K.; Bäuerle *Chem. Eur. J.* **2011**, *17*, 1507-1518.

[7] Kub, C.; Tolosa, J.; Zucchero, A.J.; McGrier, P.L.; Subramani, C.; Khorasani, A.; Rotello, V.M.; Bunz, U.H.F. *Macromolecules,* **2010**, *43*, 2124-2129.

[8] (a) Hittinger, E.; Kokil, A.; Weder, C.; *Angew. Chem. Int. Ed.* **2004**, *43*, 1808-1811. (b) Mendez, J.D.; Schroeter, M.; Weder, C. *Macromol. Chem. Phys.* **2007**, *208*, 1625-1636.

[9] (a) Bejan, A. *Shape and Structure, from Engineering to Nature*, Cambridge University Press, Cambridge, **2000**. (b) Bray, D. *Science*, **2003**, *301*, 1864-1865.

[10] (a) Horner, L.; Hoffmann, H.; Wippel, H.G. *Chem. Ber.* **1958**, *91*, 61. (b) Horner, L; Klink, W. *Tetrahedron Lett.* **1964**, *36*, 2467.

[11] Sonogashira, K. *J. Organomet. Chem.* **2002**, *653*, 46-49.

[12] Wilson, J.N.; Windscheif, P.M.; Evans, U.; Myrick, M.L.; Bunz, U.H.F. *Macromolecules*, **2002**, *35*, 8681-8683.

[13] (a) Wilson, J.N.; Bunz, U.H.F. *J. Am. Chem. Soc.* **2005**, *127*, 4124-4125. (b) Zucchero, A.J.; McGrier, P.L.; Bunz, U.H.F. *Acc. Chem. Res.* **2010**, *43*, 397-408.

[14] The author of this report gratefully acknowledges Dr. Juan Tolosa for his synthesis and characterization of monomer **M1**. For the purposes of full acknowledgement in future publications, the synthetic procedure will not be included in this dissertation.

CHAPTER 4

RESPONSIVE POLY(PARA-PHENYLENEETHYNYLENE)S WITH BATHOCHROMICALLY-SHIFTED EMISSION IN AQUEOUS SOLUTION

Introduction

Poly(*para*-phenyleneethynylene)s (PPEs)[1] are stable and display attractive optical properties. PPEs have been used to detect metal cations,[2] explosives,[3] cancer cells,[4-5] and proteins.[6] Ionically-functionalized PPEs selectively can associate with cellular structures via multivalent interactions, making them potentially useful as stains/dyes for microscopy.[7] The utility of PPEs in fluorescence detection can be expanded if PPEs are interfaced with a recognition element to form a functional construct. Here, the fluorescence of the PPE serves as a transducer while the other construct component functions as a recognition element. Examples include the use of PPE-gold nanoparticle[8] and PPE-protein[9] constructs to identify and quantify inorganic and biological analytes including bacteria and proteins.[10]

PPEs typically possess vibrant blue/blue-green emissions in solution not ideal for use in biosensing; the background fluorescence of biological samples limits the efficacy of PPEs in these applications. The performance of PPEs in biosensory applications could be improved by designing PPEs with lower energy emissions in solution. Though potential useful, few examples water soluble PPEs emitting at longer wavelengths have been reported; to date, all such materials possess vanishingly small quantum yields in water.[11]

The introduction of cross-conjugated motifs into PPEs provides an opportunity to engineer the bandgap of PPEs.[12] In the case of PPE-PPV hybrid polymers such as **1**, the electronic substitution of the styryl axis exclusively affects either the level of the HOMO or LUMO. Introduction of electron donors on the styryl axis results in PPEs exhibiting longer wavelength emissions through lifting, i.e. destabilization of the HOMO. The incorporation of swallowtail (e.g. branched oligoethylene glycols) side chains in PPEs conveys omniphilic solubility (including water) and helps preserve functional quantum yields in highly polar solvents (Figure 4.1).[13]

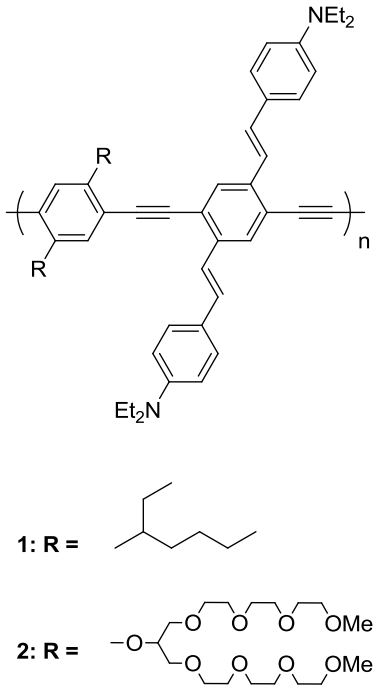

Figure 4.1. Cross conjugated PPEs.

Results and Discussion

To examine the potential of this approach we synthesized PPE **2**, an alternating copolymer containing swallowtail chains as well as donor-functionalized styryl sidechains (Figure 4.2).

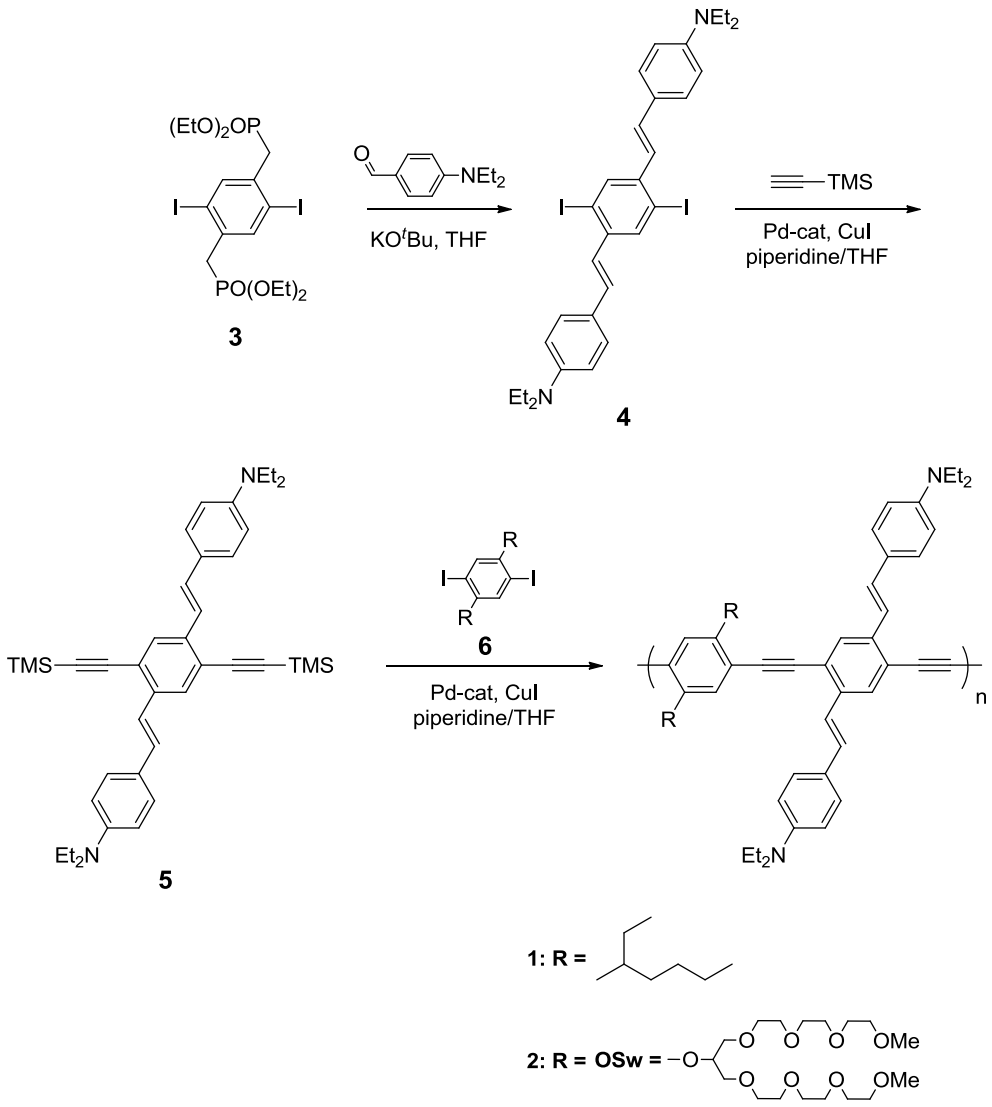

Figure 4.2. Synthesis of PPEs **1** and **2**.

The requisite distyryl monomer **5** was prepared from bisphosphonate **3**.[14] A Horner olefination[15] with *para*-(diethylamino)benzaldehyde yields **4**; subsequent Sonogashira coupling[16] furnishes the TMS-protected monomer **5** as a brilliant orange solid, which was deprotected *in situ* using KOH and polymerized with swallowtail monomer **6** using a modified Sonogashira protocol, yielding PPE **2** in 69 % yield (M_n = 1.7 x 10^4, M_w/M_n = 1.5). The fluoresence of **2** in six different solvents (with and without

the inclusion of acid) is represented in figure 4.3, while the full set of photophysical properties are outlined in table 4.1 for PPEs **1** and **2**.

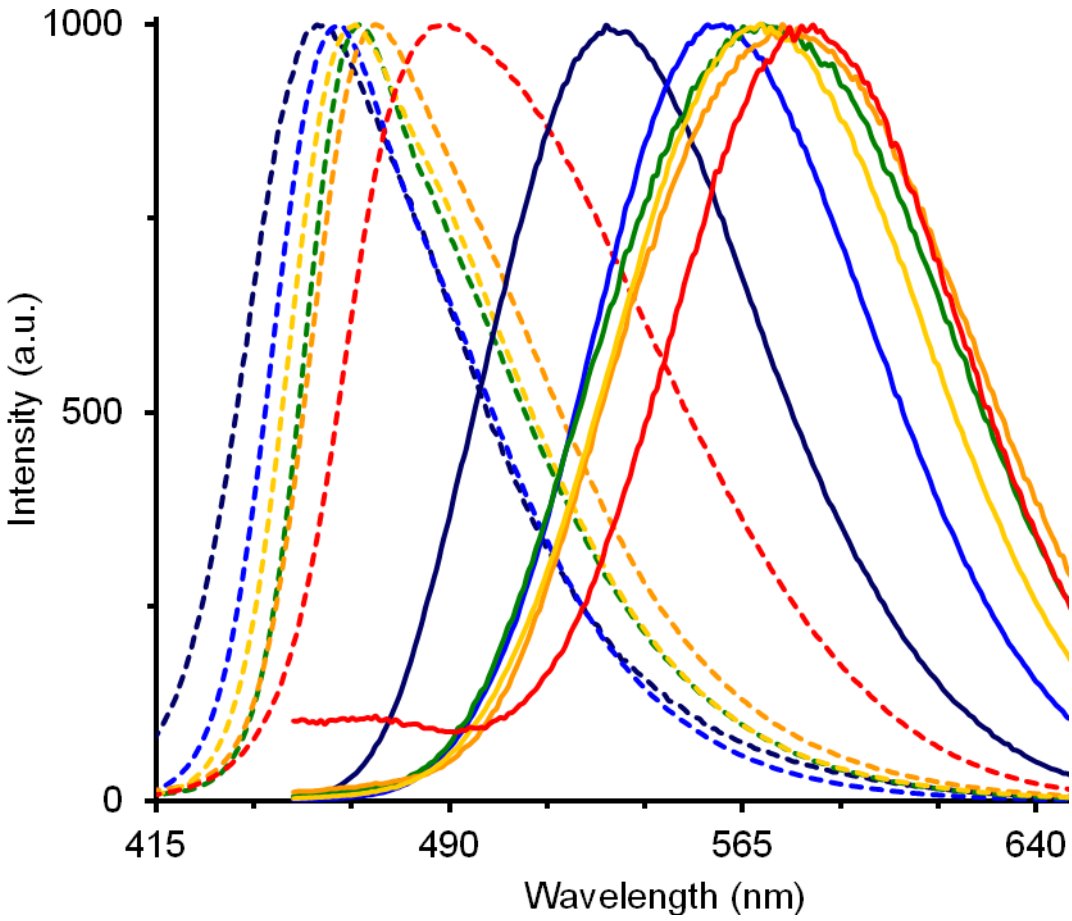

Figure 4.3. Emission of **2** (solid traces) and $\mathbf{2H^+}$ (dotted traces) in diethyl ether (dark blue trace), $CHCl_3$ (blue trace), CH_3CN (green trace), MeOH (yellow trace), DMSO (orange trace), and H_2O (red trace).

Table 4.1. Photophysical properties of **1**, **1H**$^+$, **2**, and **2H**$^+$.

		1	**1H**$^+$	**2**	**2H**$^+$
Ether	λ_{max} Abs (nm)	395	344	404	346
	λ_{max} Em (nm)	524	444	530	456
	Quantum Yield (Φ)	0.22	0.14	0.17	-[a]
	Fluorescence Lifetime (τ, ns)	3.0	1.2	2.7	1.0
$CHCl_3$	λ_{max} Abs (nm)	385	343	408	357
	λ_{max} Em (nm)	538	445	556	462
	Quantum Yield (Φ)	0.20	0.35	0.08	0.30
	Fluorescence Lifetime (τ, ns)	3.2	1.4	2.4	1.0
CH_3CN	λ_{max} Abs (nm)	402	352	411	356
	λ_{max} Em (nm)	569	441	570	467
	Quantum Yield (Φ)	6.3×10^{-4}	0.34	0.004	0.26
	Fluorescence Lifetime (τ, ns)	3.6	1.3	1.2	1.7
DMSO	λ_{max} Abs (nm)	387	351	419	363
	λ_{max} Em (nm)	567	442	575	471
	Quantum Yield (Φ)	-[b]	-[b]	0.003	0.005
	Fluorescence Lifetime (τ, ns)	-	-	1.0	1.8
MeOH	λ_{max} Abs (nm)	417	352	410	351
	λ_{max} Em (nm)	566	431	570	466
	Quantum Yield (Φ)	-[b]	0.024	0.017	0.045
	Fluorescence Lifetime (τ, ns)	0.3	1.3	2.6	1.8
H_2O	λ_{max} Abs (nm)	-	-	417	351
	λ_{max} Em (nm)	-	-	583	489
	Quantum Yield (Φ)	-	-	0.001	0.05
	Fluorescence Lifetime (τ, ns)	-	-	0.5	2.4

a) could not be recorded due to solubility problems. b) quantum yield too low to be measured.

PPE **1** is moderately soluble in ether, chloroform, and acetonitrile but precipitates from methanol (Figure 4.4). Incorporation of swallowtail side-chains allows for dissolution of **2** in solvents ranging from ether to methanol.

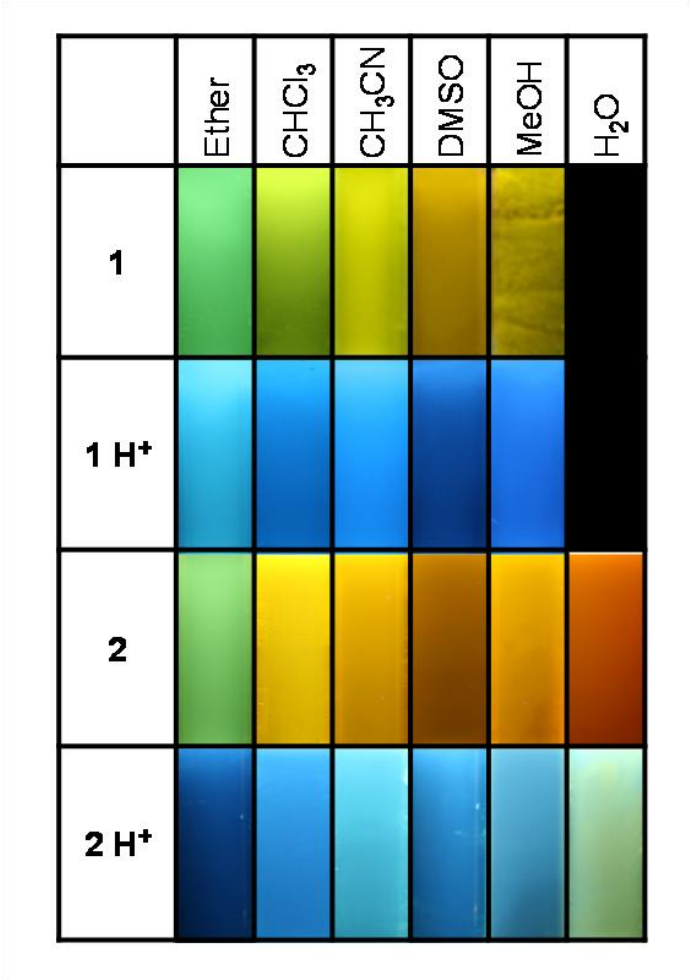

Figure 4.4. Emission of **1**, **1H**$^+$, **2**, and **2H**$^+$ in a range of solvents. Vials were photographed under a handheld UV light (λ_{max} ex = 365 nm) using a Canon EOS 30D digital camera equipped with a Canon EFS 18-55mm zoom lens. Photograph exposure times were varied for each solution to produce images reflecting the color of emission.

In diethyl ether, **1** exhibits a broad absorption (λ_{max} = 395 nm) and broad green emission (λ_{max} = 524 nm). Significant positive solvatochromism is observed in the emission of **1** (from 524 nm in ether to 566 nm in methanol); however, the effect is less pronounced in the absorption (395 nm → 417 nm). Upon moving to $CHCl_3$, we observe a small blue shift in absorption to 385 nm and a redshift in emission to 538 nm. As solvent polarity increases further, both absorption and emission become more bathochromically shifted; in methanol, **1** possesses a broad absorption centered at 417 nm and a broad yellow emission at 566 nm.

The absorption and emission of **2** are redshifted relative to **1**, which can be attributed to the electron donating character of the alkyoxy-substitution in **2** compared to the alkyl-substituted **1**. In ether, **2** exhibits a broad emission at 404 nm and a featureless green emission at 530 nm. As in **1**, significant positive solvatochromism is observed in the emission of **2** (from 530 nm in ether to 583 nm in water); similarly, the effect in absorption is minimal (404 nm → 417 nm). This trend remains constant when transitioning into more polar solvents.

As predicted, addition of TFA to **1** and **2** leads to shifts in both absorption and emission in all solvents, with no evidence of significant solvatochromism. Substitution of the styryl axis exclusively affects the level of the HOMO, suggesting localization of the PPE's HOMO on the styryl sidechains. As a result, protonation of the alkylanilines in **1** and **2** disproportionately stabilizes the HOMO relative to the LUMO, increasing the FMO gap and eliciting a spectroscopic blueshift.

We also determined the fluorescence quantum yields of **1**, $\mathbf{1H^+}$, **2**, and $\mathbf{2H^+}$ in a range of solvents. Generally, as the polarity of the solvent increases, the quantum yield decreases, in qualitative accordance with the energy gap law.[17] Similarly, the spectral blueshifts induced by protonation of **1** and **2** are generally accompanied by considerable increase in quantum yield. In less polar solvents including diethyl ether and $CHCl_3$, **1** possesses a higher quantum yield than **2**. This trend is reversed in more polar solvents such as CH_3CN, DMSO, and MeOH. In these cases, **2** displays a higher quantum yield than **1**.

The monoexponential fluorescence lifetimes of **1** and **2** are 3.0 and 2.7 ns respectively, significantly longer that typical alkyl-functionalized PPEs (generally ≈ 300-

700 ps).[18] The lifetimes of **1H**$^+$ and **2H**$^+$ in ether are shorter (1.2 and 1.0 ns). The lifetime of **1** in methanol is substantially decreased (300 ps). Alkyl PPEs typically exhibit lifetimes of 300-700 ps in solution; their lifetimes in the solid state decrease considerably to around 70 ps due to planarization and aggregate/excimer formation.[19] Aggregation is visible upon addition of **1** to methanol and is the likely cause for the dramatic decrease in fluorescence lifetime (Figure 4.5).

Figure 4.5. Tyndall effect observed by passing a laser through **1** in MeOH (left) and **2** in H_2O (right).

Upon dissolution of **2** to water, changes in photophysical properties are observed. When compared to **2** in methanol, both absorption and emission are redshifted with the quantum yield and fluorescence lifetime being significantly reduced. The fluorescence lifetime of **2** in water (500 ps) suggests that aggregation occurs; tyndall scattering is observed even in the most dilute aqueous solutions.

To further investigate this phenomenon, samples of an aqueous "suspension" of **2** were investigated using TEM (Figure 4.6). We observe the formation of fairly monodisperse polymer nanospheres ranging from 50-100 nm. While interesting, this aggregate formation modulates the photophysical properties of **2**, a potential problem for inclusion in biosensory applications.

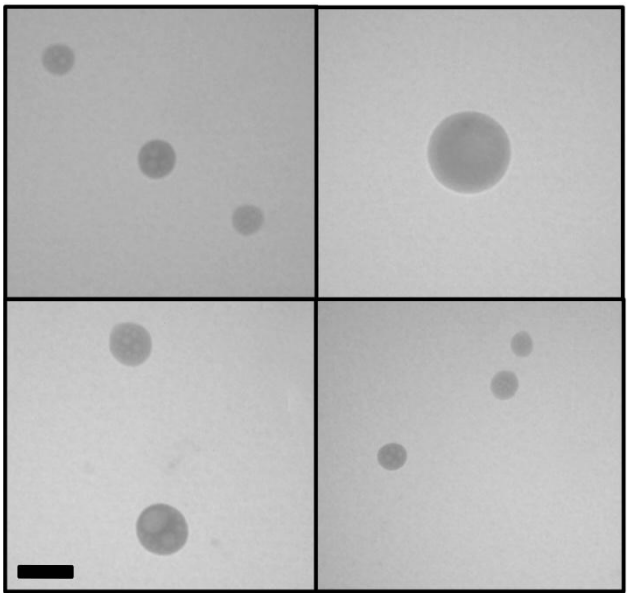

Figure 4.6. TEM images of aggregates of **2** in water. Aggregates were formed upon addition of a small amount of **2** in DMSO to a large volume of water. Scale bar = 100 nm.

Upon addition of TFA to **2** in water, we observe a significant blueshift in absorption (417 nm → 351 nm) and emission (583 nm → 489 nm); this is accompanied by a fiftyfold increase in quantum yield, from 0.001 to 0.05. The fluorescence lifetime also increases from 500 ps to 2.4 ns, and the Tyndall effect disappears, suggesting that $\mathbf{2H}^{+}$ does not aggregate in water.

Additionally, PPE **2** exhibits a particularly interesting quality that has never been observed with the small molecule cruciform analogues: the ability to extract metal ions from aqueous solution into the organic phase (Figure 4.7). For each metal tested, 100 mg of the corresponding triflate salt was dissolved in 10 mL H_2O (10 mg/mL), to which an aliquot of **2** (dissolved in DCM) was added to the vial and shaken thoroughly. As seen in Figure 3.7, the emission was completely quenched upon binding with Hg^{2+}, likely due to heavy atom effects.

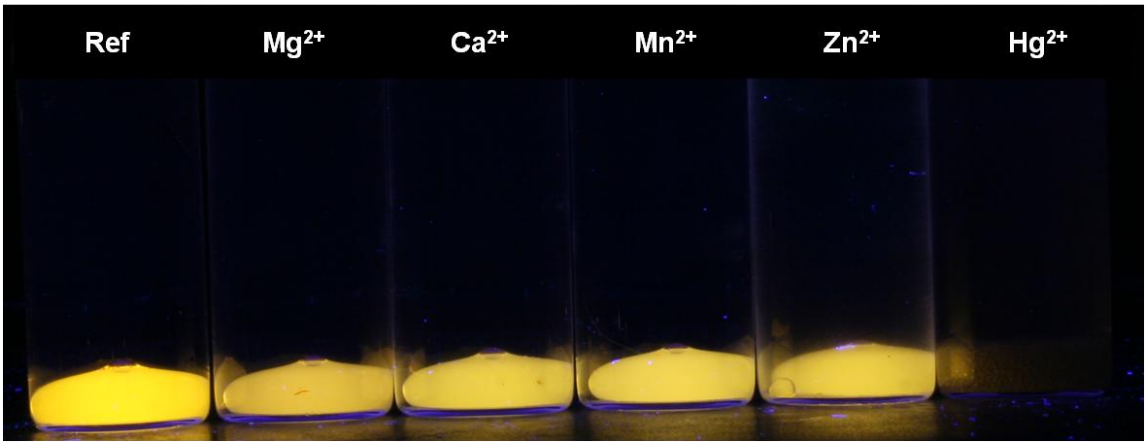

Figure 4.7. Extraction of metals (PPE **2**) from H_2O into organic solution (DCM). Metal triflate salts were used in all examples.

Conclusions

PPE-PPV hybrid polymers offer a novel opportunity to construct longer wavelength emitting systems. Herein, we report our first efforts to incorporate both donor-functionalized styryl sidechains and branched polyethylene glycol swallowtail sidechains into the PPEs. The extraction of metal ions from aqueous to organic phases is an effect that is wholly unique among materials of this type; a full panel of metal extraction studies are currently in progress along with work towards developing new water-soluble PPEs with increased quantum yield and even further bathochromically shifted emissions.

Experimental Procedures

Materials and Methods

All chemicals and solvents were purchased from commercial sources and were used without further purification unless otherwise specified. All IR spectra were obtained using a Shimadzu FTIR-8400s spectrometer. ^{1}H NMR spectra were recorded at 298 K on a 300 or 500 MHz spectrometer. Chemical shifts are reported in parts per million (ppm),

using residual solvent (chloroform-*d* or dimethylsulfoxide-*d*6) as an internal standard. The data is reported as follows: chemical shift, multiplicity (s = singlet, d = doublet, t = triplet, q = quartet, m = multiplet, br = broad), and integration. ^{13}C HMR spectra were recorded at 400 MHz, and ^{13}C chemical shifts (δ) are referenced to residual $CHCl_3$ at 77.23 ppm or residual DMSO at 39.5 ppm. All absorption spectra were collected using a Shimadzu UV-2401PC spectrophotometer. All emission spectra were acquired using a Shimadzu RF-5301PC spectrofluorophotometer. Quantum yields for the polymer was measured using standard procedures.[20] In all cases, quinine sulfate and 2-aminopyridine were used as standards and all solutions were purged with nitrogen prior to measurement.

Synthesis and Characterization Data

Compounds **S1**[21] and **M3**[22] were synthesized according to previous reported literature procedures.

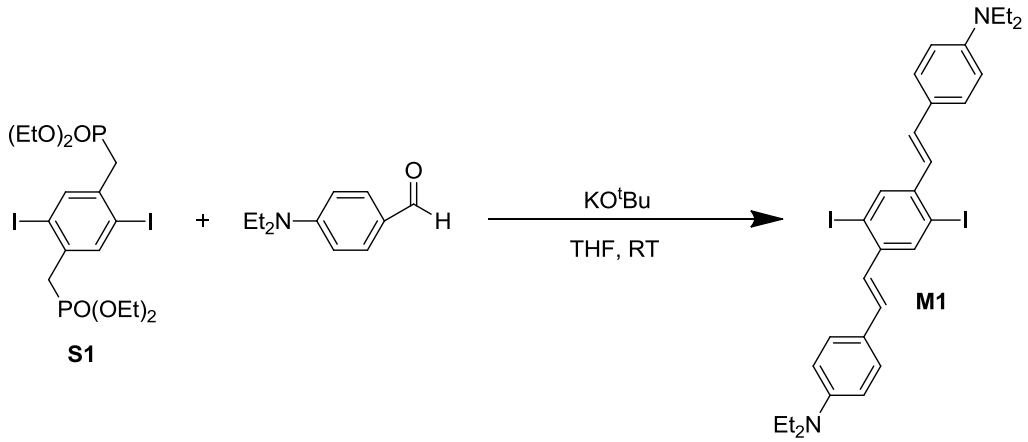

Figure 4.8. Synthesis of monomer **M1**.

Synthesis of **M1**

Compound **S1** (2.55 g, 4.05 mmol) was placed in 50 mL THF followed by addition of potassium *tert*-butoxide (1.14 g, 10.13 mmol) and *p*-(N,N-diethylamino)benzaldehyde and allowed to stir overnight at room temperature. The mixture was poured into 800 mL methanol and the resulting precipitate was collected via

vacuum filtration. The collected solid was purified by silica gel chromatography using dichloromethane as the eluent. The product was collected as an orange crystalline solid in 62% yield. ^{1}H NMR (300 MHz, $CDCl_3$): δ 8.01 (s, 2H), 7.41 (d, 4H, $J_{3,\ H,H}$ = 8.7 Hz), 6.94 (2d, 2H, $J_{3\ H,H}$ = 15.9 Hz), 6.86 (d, 2H, $J_{3\ H,H}$ =15.6 Hz), 6.66 (d, 4H, $J_{3\ H,H}$ = 9 Hz), 3.38 (q, 8H, $J_{3\ H,H}$ = 6.9 Hz), 1.18 (t, 12H, $J_{3\ H,H}$ = 6.9 Hz). ^{13}C NMR (300 MHz, $CDCl_3$): δ 147.77, 140.44, 135.44, 131.91, 128.35, 125.48, 123.98, 111.53, 100.15, 44.40, 12.63. IR (cm^{-1}): 3417.63, 3195.83, 3068.53, 3028.03, 2960.53, 2931.60, 2597.94, 1872.75, 1785.96, 1554.52, 1519.80, 1265.22, 1151.42, 1039.56, 952.77. MP: 211 °C.

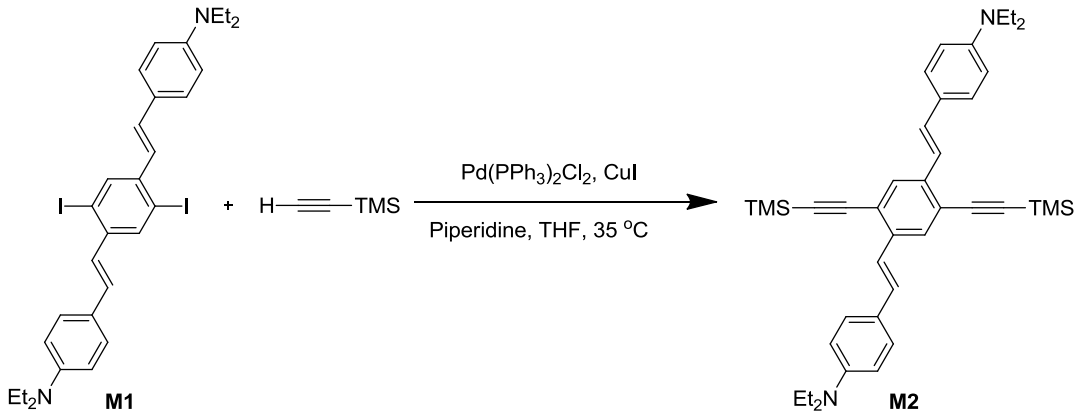

Figure 4.9. Synthesis of monomer **M2**.

Synthesis of **M2**

Monomer **M1** (2.00 g, 2.95 mmol) was dissolved in THF (10 mL), dichloromethane (3 mL), and piperidine (2 mL) in a Schlenk flask under nitrogen purge. The flask was freeze-pump-thawed three times, after which $(Ph_3P)_2PdCl_2$ (10 mg, 14.2 μmol) and CuI (5.6 mg, 29.5 μmol) were added. The mixture was allowed to stir at room temperature for 24 h. The solution was diluted with dichloromethane and extracted with water four times. The organic layer was collected and the solvent removed under reduced pressure. The resulting solid was purified by silica gel chromatography using

dichloromethane as the eluent. The product was collected as a pale orange solid in 73% yield (1.33 g). ^{1}H NMR (300 MHz, $CDCl_3$): δ 7.73 (s, 2H,), 7.36 (m, 6H), 7.09 (d, 2H, $J_{3\ H,H}$ = 16.5 Hz), 6.64 (d, 2H, $J_{3\ H,H}$ = 8.7 Hz), 3.37 (q, 8H, $J_{3\ H,H}$ = 6.9 Hz), 1,171 (t, 12H, $J_{3\ H,H}$ = 6.9 Hz), 0.31 (s, 18H). ^{13}C NMR (300 MHz, $CDCl_3$): δ 147.53, 137.48, 130.17, 128.08, 128.00, 124.67, 121.38, 120.52, 111.57, 103.87, 100.03, 44.36, 12.65, 0.09. IR (cm^{-1}): 3419.56, 3178.47, 3089.75, 3033.82, 2966.31, 2927.74, 2150.48, 1872.75, 1801.39, 1600.81, 1519.80, 1149.50, 956.63, 806.19. MP: 216 °C.

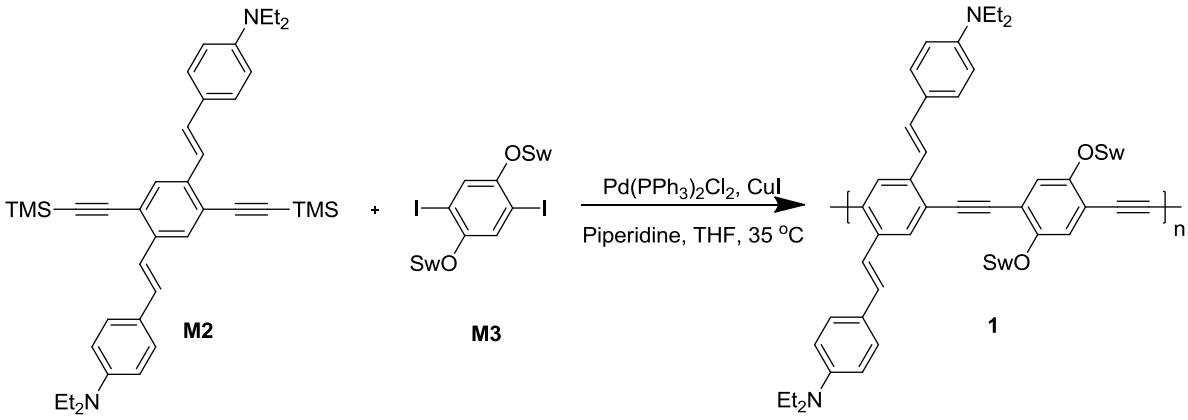

Figure 4.10. Synthesis of PPE **1**.

Synthesis of **1**

Monomer **M2** (0.753 g, 1.22 mmol) was combined with 2 mL THF and 1 g of potassium hydroxide in a Schlenk flask under nitrogen purge. After 10 minutes, monomer **M3** (1.33 g, 1.22 mmol) and 4 mL THF were added to the flask, which was then frozen and purged three times, after which $(Ph_3P)_2PdCl_2$ (4.28 mg, 6.1 µmol) and CuI (2.32 mg, 12.2 µmol) were added. The mixture was allowed to stir at 35 °C for 48 h. The solution was poured into hexanes and the solid precipitate collected via vacuum filtration in 69% yield (1.11 g). The weight averaged molecular weight (M_w) was estimated to be 25.8 kDa with a polydispersity (M_w/M_n) of 1.5. Synthesis of $\mathbf{1H^+}$ was performed by addition of

trifluoroacetic acid to pure **1**. ^{1}H NMR (300 MHz, DMSO-*d*6), δ 7.81 (m, 4H), 7.42 (m, 8H), 7.2 (m, 4H), 6.6 (2H), 4.6 (m, 2H), 3.45 (m, 76H), 1.18 (m, 12H) Compound was not sufficiently soluble to obtain ^{13}C NMR. IR (cm^{-1}): 3427.27, 3033.82, 2966.31, 2873.74, 2819.73, 1598.88, 1519.80, 1269.07, 1190.00, 1108.99, 854.41, 811.98.

References

[1] (a) Bunz, U.H.F. *Chem. Rev.* **2000**, *100*, 1605-1644. (b) Bunz, U.H.F. *Adv. Polym. Sci.* **2005**, *177*, 1-52. (c) Bunz, U.H.F. *Macromol. Rapid Commun.* **2009**, *30*, 772-805.

[2] (a) Wilson, J.N.; Bunz, U.H.F. *J. Am. Chem. Soc.* **2005**, *127*, 4124-4125. (b) Zucchero, A.J.; McGrier, P.L.; Bunz, U.H.F. *Acc. Chem. Res.* **2010**, *43*, 397-408.

[3] Swager, T.M. *Acc. Chem. Res.* **2008**, *41*, 1181-1189.

[4] Miranda, O.R.; You, C.C.; Phillips, R.L.; Kim, I.-B.; Ghosh, P.S.; Bunz, U.H.F.; Rotello, V.M. *J. Am. Chem. Soc.* **2007**, *129*, 9856-9857.

[5] Kim, I.-B.; Shin, H.; Garcia, A.J.; Bunz, U.H.F. *Bioconjugate Chem.* **2007**, *18*, 815-820.

[6] McRae, R.L.; Phillips, R.L.; Kim, I.-B.; Bunz, U.H.F.; Fahrni, C.J. *J. Am. Chem. Soc.* **2008**, *130*, 7851-7853.

[7] Phillips, R.L.; Miranda, O.R.; You, C.-C.; Rotello, V.M.; Bunz, U.H.F. *Angew. Chem. Int. Ed.* **2008**, *47*, 2590-2594.

[8] Bunz, U.H.F.; Rotello, V.M. *Angew. Chem. Int. Ed.* **2010**, *49*, 3268-3279.

[9] Kim, I.-B.; Bunz, U.H.F. *J. Am. Chem. Soc.* **2006**, *128*, 2818-2819.

[10] (a) Pinto, M.R.; Kristal, B.M.; Schanze, K.S. *Langmuir* **2003**, *19*, 6523-6533. (b) Jiang, H.; Taranekar, P.; Reynolds, J.R.; Schanze, K.S. *Angew. Chem. Int. Ed.* **2009**, *48*, 4300-4316.

[11] Wilson, J.N.; Windscheif, P.M.; Evans, U.; Myrick, M.L.; Bunz, U.H.F. *Macromolecules* **2002**, *35*, 8681-8683.

[12] Kim, I.-B.; Phillips, R.L.; Bunz, U.H.F. *Macromolecules* **2007**, *40*, 5290-5293.

[13] Horner, L.; Hoffmann, H.; Wippel, H.G. *Chem. Ber.* **1958**, *91*, 61.

[14] Horner, L.; Klink, W. *Tetrahedron Lett.* **1964**, *36*, 2467.

[15] (a) Sonogashira, K. *J. Organomet. Chem.* **2002**, *653*, 46-49. (b) Negishi, E.; Anatasia, L. *Chem. Rev.* **2003**, *103*, 1979-2017.

[16] (a) Zucchero, A.J.; Wilson, J.N.; Bunz, U.H.F. *J. Am. Chem. Soc.* **2006**, *128*, 11872-11881. (b) Hauck, M.; Schönhaber, J.; Zucchero, A.J.; Hardcastle, K.I.; Müller, T.J.J.; Bunz, U.H.F. *J. Org. Chem.* **2007**, *72*, 6714-6725.

[17] Tolbert, L.M.; Solntsev, K.M. *Acc. Chem. Res.* **2002**, *35*, 19-27.

[18] Sluch, M.I.; Godt, A.; Bunz, U.H.F.; Berg, M.A. *J. Am. Chem. Soc.* **2001**, *123*, 6447-6448.

[19] Bunz, U.H.F.; Imhof, J.M.; Bly, R.K.; Bangcuyo, C.G.; Rozanski, L.; Vanden Bout, D.A. *Macromolecules* **2005**, *38*, 5892-5896.

[20] "A Guide to Recording Fluorescence Quantum Yields." Horiba Jobin Yvon Ltd. available online: http://www.jobinyvon.co.uk/ukdivisions/Fluorescence/plqy.html

[21] Wilson, J.M.; Josowicz, M.; Wang, Y.; Bunz, U.H.F. *Chem. Commun.* **2003**, *39*, 2962-2963.

[22] Khan, A.; Müller, S.; Hecht, S. *Chem. Commun.* **2005**, *5*, 584-586.

CHAPTER 5

DISCRIMINATION OF ORGANIC ACIDS USING A THREE MOLECULE ARRAY BASED UPON CRUCIFORM FLUOROPHORES

Introduction

Tuning and enhancing the discriminatory sensory responses of fluorophores or chromophores towards classes of compounds emerges as an important topic at the interface of analytical, biological, organic, materials and supramolecular chemistry.[1] Application of array-based sensing concepts by Suslick *et al.*,[2] Lavigne *et al.*,[3] and by Anslyn *et al.*[4] provides material systems that discern, with surprising selectivity, even complex mixtures of similar compounds. Attention-grabbing examples are the discrimination of different whiskey brands[5] or the identification of a selection of coffee grounds (Starbucks vs. Folgers)[6] by small arrays of chromophores immobilized on suitable substrates. The concept is known as chemical "tongue" or chemical "nose" and works also for example to discriminate amines.[7] Are there generalized conditions for chemical tongues to be particularly successfully applied? They work best when reporting the departure of the analyte from a defined composition, identifying (undesired) changes in an otherwise regulated/defined environment. For that reason, even complex mixtures, such as alcoholic spirits, coffee grounds, beers, etc. can be “fingerprinted” and compared to each other by a specific set of sensory compounds or arrays. Chemical tongues are therefore particularly good for sophisticated quality control.

The detection of adulterated or counterfeit drugs is critically important as one wants to avoid ingestion of poisonous substances, or the use of (for example) malaria medications that contain the wrong or adulterated ingredients or are just expired.[8] A significant number of prescription drugs display either free amines (often as their ammonium salts) or free carboxylic acids (occasionally in their salt form). Examples for the latter class are aspirin, ibuprofen, Artesunate®, Lipitor®, Crestor®, Cellcept® and Sector®. A simple fluorescence-based test discerning organic acids might therefore be of great interest and potential to perform quality control in drug samples of questionable origin (internet pharmacies, gray market). Such a tool would be useful for public health applications. In this communication we describe the identification of ten structurally related acids **B**-**K** derived from benzoic and phenylacetic acids by a small fluorophore array of 1,4-distyryl-2,5-bisarylethynylbenzenes (**XF1**- **XF3**) in different solvents.

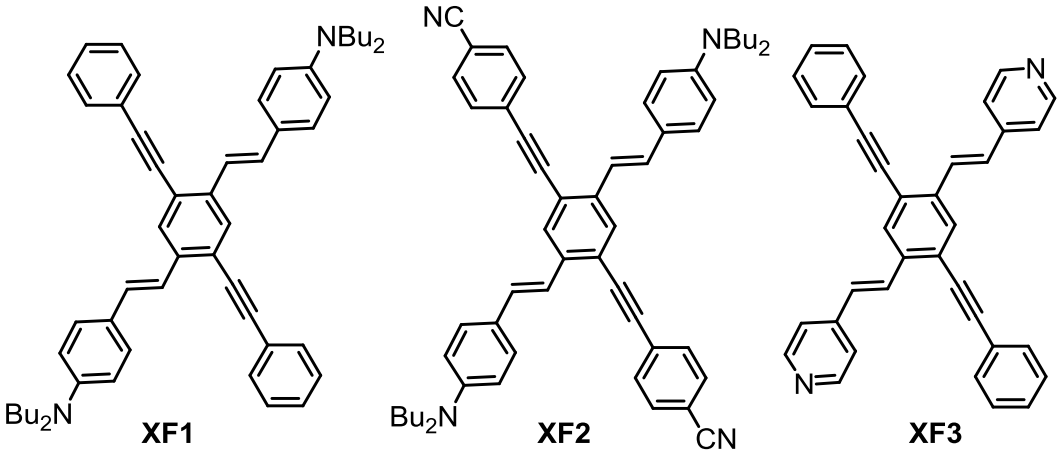

Figure 5.1. Reactive 1,4-distyryl-2,5-bisarylethynylbenzenes.

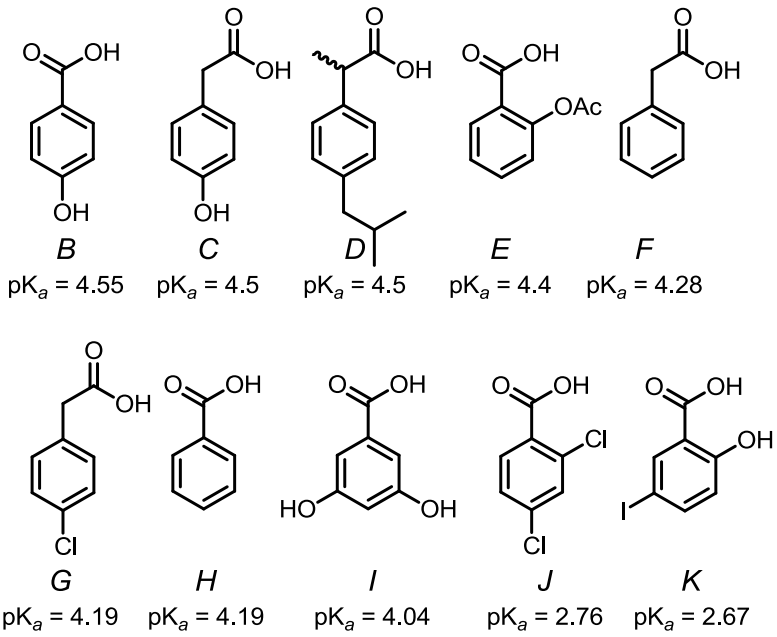

Figure 5.2. Benzoic and phenylacetic acid derivatives analyzed.

Results and Discussion

In a first experiment we investigated the interaction of phenylacetic acid (**F**) with **XF1**[9] to obtain the concentration dependence of the response of the XF to the acid.[10] At concentrations above 500 mg of C in a 20 mL vial (25 gL^{-1}) the fluorescence starts to shift from green to blue due to the protonation of the aniline nitrogens (Figure 5.3). This experiment demonstrates that weak acids elicit a response under these conditions.

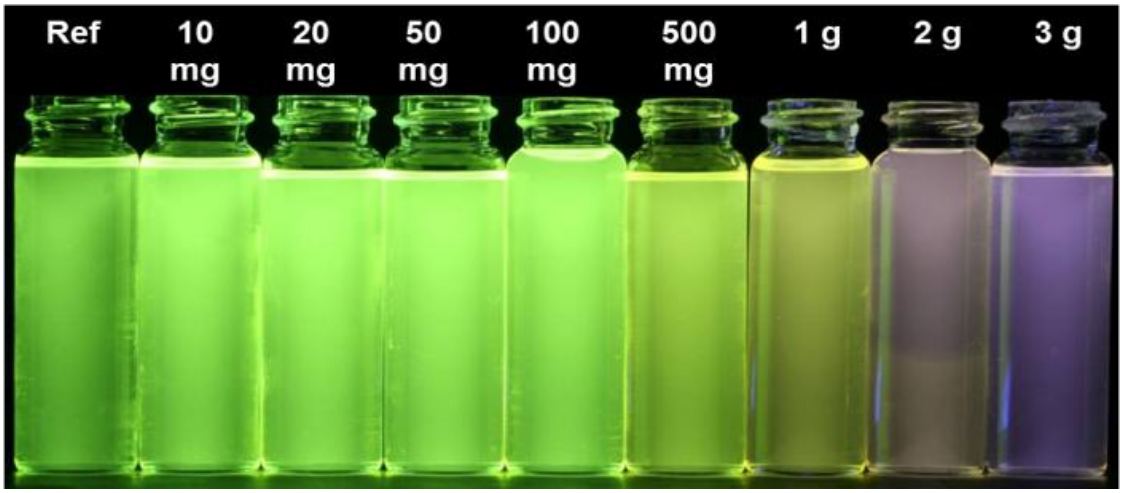

Figure 5.3. Digital photograph of **XF1** with increasing amounts of phenylacetic acid in dichloromethane.

To determine if different weak acids are differentially recognized, we exposed the acids **B**-**K** towards a small cruciform array (18 members: 3 cruciforms in 6 solvents each) at an acid concentration of $25gL^{-1}$ (Figure 5.4). The results are striking, as all carboxylic acids can be discerned, even though the pKa differences are small in some cases. Not unsurprisingly, the most acidic analytes (dichlorobenzoic acid **J**, iodosalicylic acid **K**) show the largest changes in the response patterns, as could be expected. Extraction of the RGB values from a photograph of the array using Color Contrast Analyzer[11], a downloadable freeware program, is followed by statistical evaluation of the response patterns.

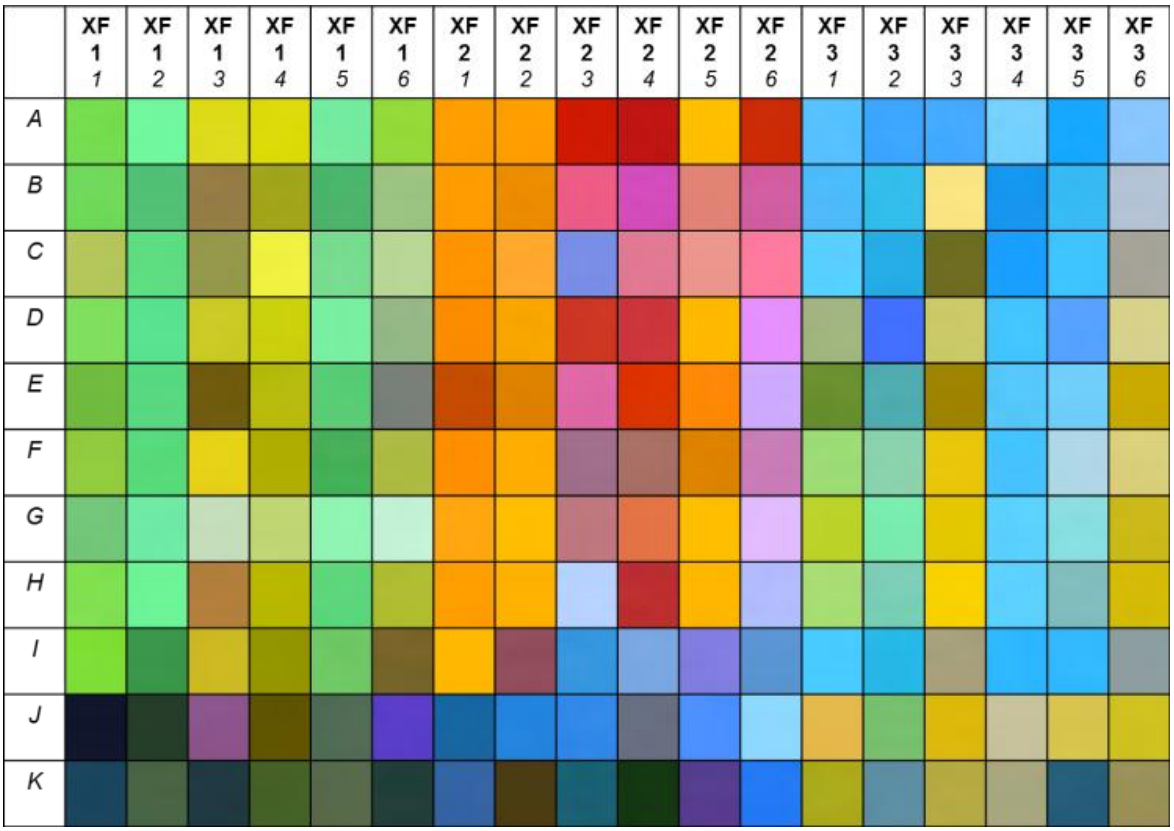

Figure 5.4. Photograph of three XFs (**1-3**) in six different solvents (*1* = DCM, *2* = EtOAc, *3* = MeCN, *4* = DMF, *5* = iPrOH, *6* = MeOH) and exposed to ten different carboxylic acids (**A** = XF reference emission, **B** = 4-Hydroxybenzoic acid pKa = 4.55; **C** = 4-Hydroxyphenylacetic acid pKa = 4.5; **D** = Ibuprofen pKa = 4.5; **E** = Aspirin pKa = 4.4; **F** = Phenylacetic acid, pKa = 4.28; **G** = 4-Chlorophenylacetic acid pKa = 4.19; **H** = Benzoic acid, pKa = 4.19; **I** = 3,5-Dihydroxybenzoic acid, pKa = 4.04; **J** = 2,4-Dichlorobenzoic acid pKa = 2.76; **K** = 5-Iodosalicylic acid pKa = 2.67). All photographs were taken under blacklight at an excitation wavelength of 366 nm.

A differential fluorescence correlation plot obtained by multivariate analysis of variance (MANOVA) identifies unknowns by their fluorescence signature (Figure 5.5) and demonstrates that the ten acids are reliably discerned. In the multivariate analysis of variance approach we are calculating standard deviations σ of the individual RGB values related to a particular compound. This approach allows revealing properties and structure relationships of the cruciform fluorophores **XF1**, **XF2** and **XF3**, solvents and analytes. There are correlations between σ-values of different cruciforms dissolved in the same solvent and the same cruciforms dissolved in different solvents, however the σ-values are

characteristic, making an ambiguous assignment of analytes by using orthogonal fluorophoric sensor arrays possible. This allows us to predict σ-values for unknown analytes.

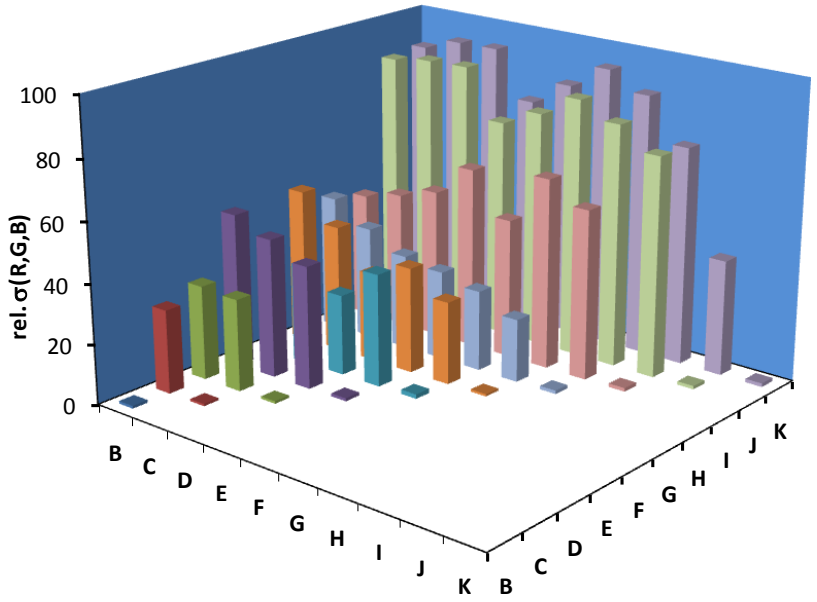

Figure 5.5. Differential correlation plot of the fluorescence response of the different carboxylic acids by the 18-member XF-array. The z-axis represents the relative standard deviation σ of the R,G and B values related to carboxylic acid B.

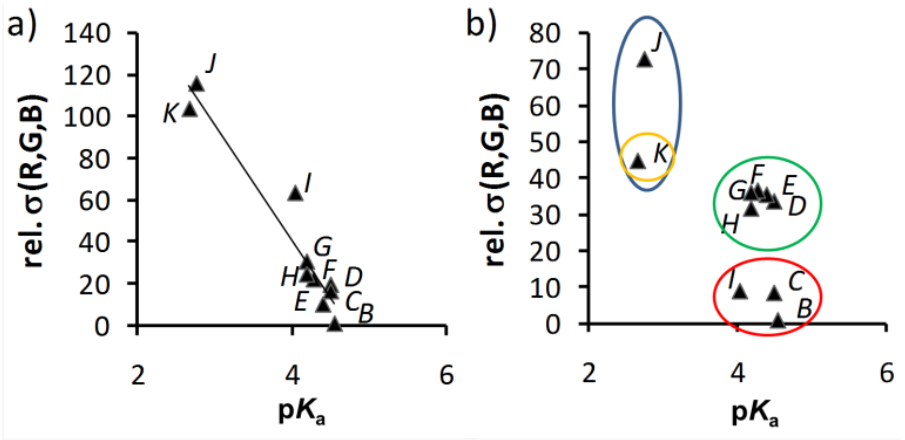

Figure 5.6. Correlation plot of pKa values and the relative standard deviation σ of the RGB values a) **XF2** dissolved in EtOAc, b) **XF3** dissolved in EtOAc; Red circle: acids with a hydroxyl group; blue circle: acids with a halogen substituent; green circle: acids without any functionality, yellow circle: acid with hydroxyl and halogen substituents.

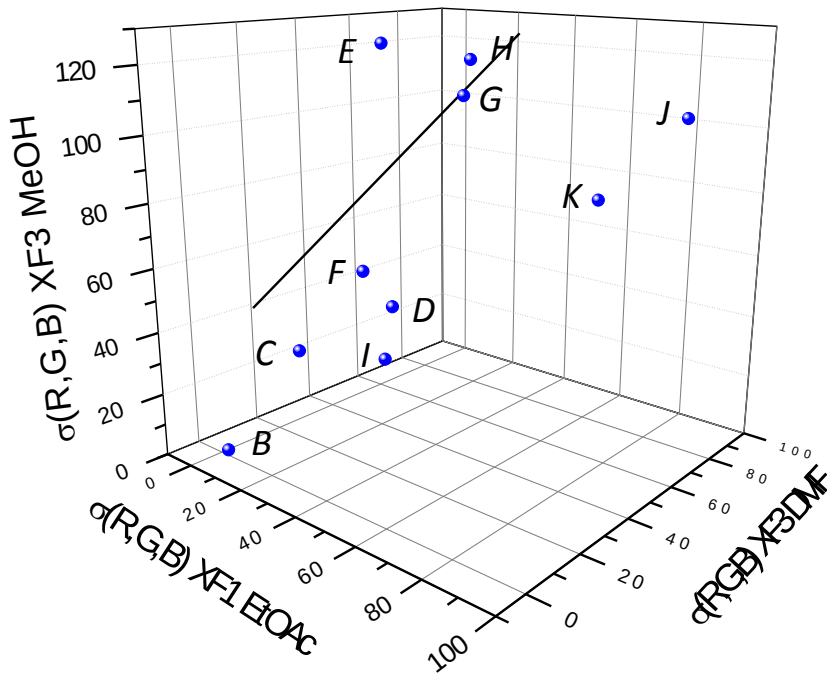

Figure 5.7. 3D plot of two cruciform fluorophores **XF1** and **XF3** in three solvents. The data points represent well separated standard deviations of the individual analytes **B** to **K**.

Interestingly, we found, that **XF2** in EtOAc correlates well with the p*K*a value of the analytes (related to *B* with the highest p*K*a value), while **XF3** results in clustered response that shows a correlation to the chemical structures of the acids (Figure 5.6). All of the nonfunctional acids are clustered (exception: 4-chlorobenzoic acid) in the green region, acids featuring free hydroxyl groups (red circle) are grouped together, while the two most acidic halogenated benzoic acids *J* and *K* show the greatest σ-values. Here too, the presence of the hydroxyl group seems to lower the σ-value for **J** as compared to that of **K**. So interestingly enough, **XF3** appears to recognize functional features, while **XF2** exhibits responses that strictly correlate with the p*K*a values of the acids. Attempts to convert the spectroscopic (as opposed to the photographic) responses (response spectra of **XF2** and **XF3** with **B**-**J**) to RGB values and functionally map the information from the

spectra to those obtained from the photographs is currently not feasible, as there is no simple algorithm that could convert fluorescence spectra directly into RGB values.

In an effort to achieve unambiguous detection of analytes with the smallest number of fluorophores – solvent combinations we analyzed 3D datasets of fluorophoric cruciform sensors in various solvents to find the largest differences in the σ-values. With only three different fluorophore–solvent combinations (Figure 5.7), the minimal set, the analytes **B** to **K** can be identified.

In conclusion, a fluorophore array (three fluorophores, **XF1**-**XF3** in six solvents each) using digital photography discerns ten different carboxylic acids by differential fluorescence response, even though some of the acids have pKa values that are close to each other. The array is considerably more selective than a simple pH-'paper'. Its selectivity should be further tuned up when other more basic or hydrogen-bonding XF are included. The apparent disadvantage that one has to use high concentrations of carboxylic acids to elicit a response is not an issue. Drug formulations (i.e. tablets, gel caps etc.), the final target, can be crushed and used in concentration necessary to elicit a robust fluorescence response. One would then only have to compare the (photographical reproduced) profile of an original tablet with that of the sample at hand or use a statistical algorithm. This concept should be well suited to identify and discern drug formulations that are acidic in nature.

Experimental Procedures

Materials and Instruments

All organic acids and solvents were purchased from commercial sources and were used without further purification. All emission spectra were acquired using a Shimadzu

RF-5301PC spectrofluorophotometer. Photographs were taken with a Canon EOS 30D digital camera equipped with a Canon EFS 18-55mm zoom lens. Photograph exposure times were varied for each solution to produce images reflecting the color of emission (0.25 s – 15 s). All calculations were performed by a program XPattern.exe written in Delphi (Embarcadero Technologies, South San Francisco, USA). Correlation analysis was performed in Microsoft Excel 2007 (Microsoft Corp., Redmond, Washington, USA) and OriginPro 8.5 (Origin Lab Corporation, One Roundhouse Plaza, Northhampton, USA).

Initial Acid Detection Study

To identify working acid concentrations and the ability to distinguish compounds, increasing amounts of phenylacetic acid were dissolved in dichloromethane (Figure 5.8), followed by 10 μL **XF1** stock solution (50 mg/10 mL DCM). Variations in fluorescence were first observed at concentrations of 500 mg/16 mL. This study was also performed with benzoic acid (Figure 5.9), where little change in emission was observed. It was also noted that at high concentrations, solubility issues were encountered as solutions were completely saturated.

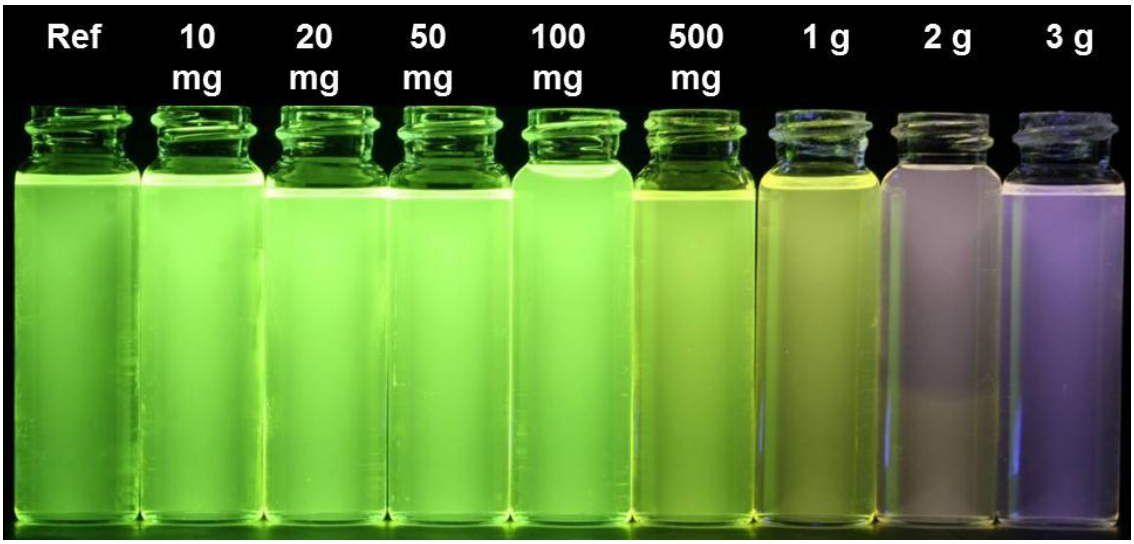

Figure 5.8. Increasing concentrations of phenylacetic acid in DCM/**XF1**.

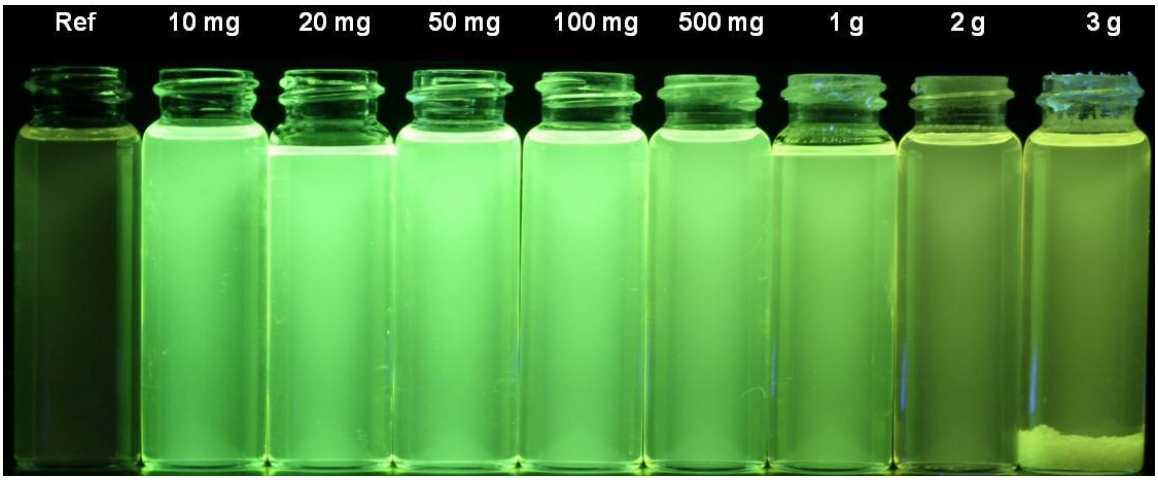

Figure 5.9. Increasing concentrations of benzoic acid in DCM/**XF1**.

Initial Solvent Study

To identify representative solvents for the array, benzoic acid and phenylacetic acid were dissolved at various concentrations in three solvents: non-polar (DCM, figure 5.9), polar-aprotic (CH_3CN, figures 5.10 & 5.11), and polar-protic (MeOH, figures 5.12 & 5.13). Upon observation of fluorescent changes, the ideal concentration for the primary investigation was decided to be 1 g acid/16 mL solvent. Dye concentrations were kept constant at the addition of 10 µL stock solution (50 mg XF/10 mL DCM).

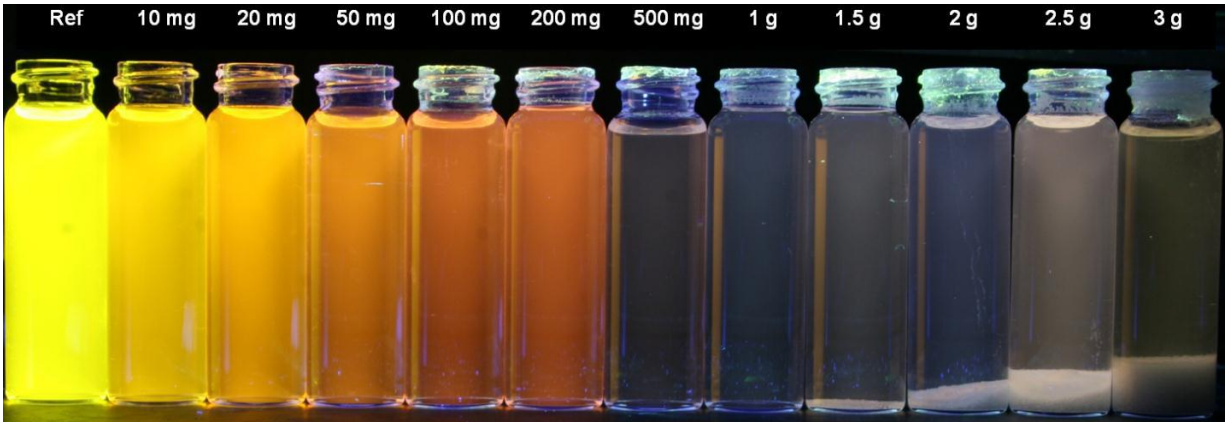

Figure 5.10. Increasing concentrations of benzoic acid in CH_3CN/**XF1**.

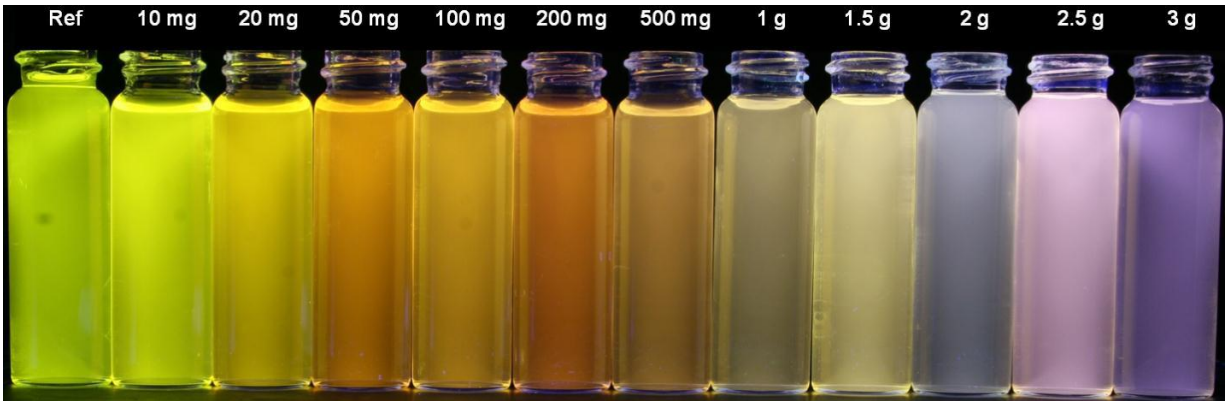

Figure 5.11. Increasing concentrations of phenylacetic acid in CH_3CN/**XF1**.

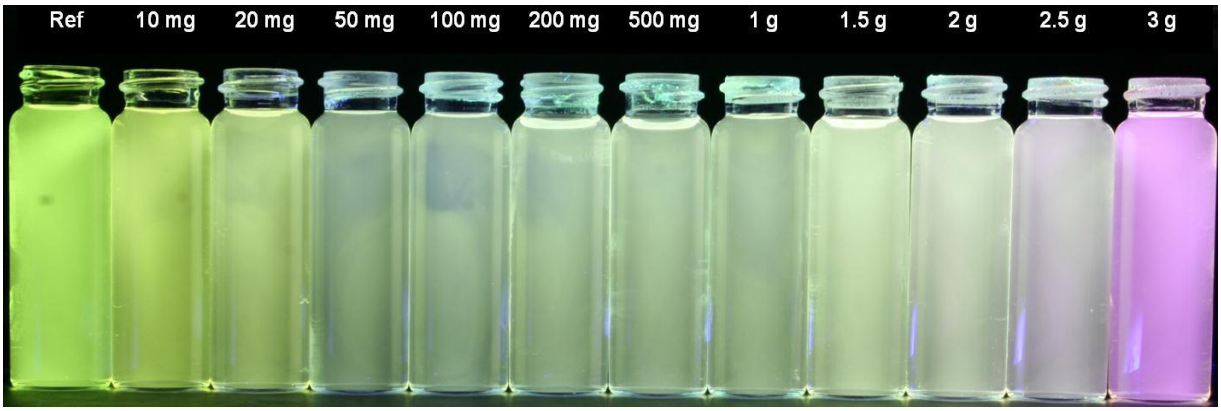

Figure 5.12. Increasing concentrations of benzoic acid in MeOH/**XF1**.

Calculation of RGB Changes

Upon completion of the chemical array, representative colors from each photograph were cut (via Adobe Photoshop) and copied into a table. An identical table was generated where all cells were filled with the corresponding reference XF emission, and the pictures were subtracted using the free downloadable program, ImageJ (Figure 5.13). RGB values were extracted from the generated image for a differential fluorescence correlation plot using multivariate analysis of variance (MANOVA).

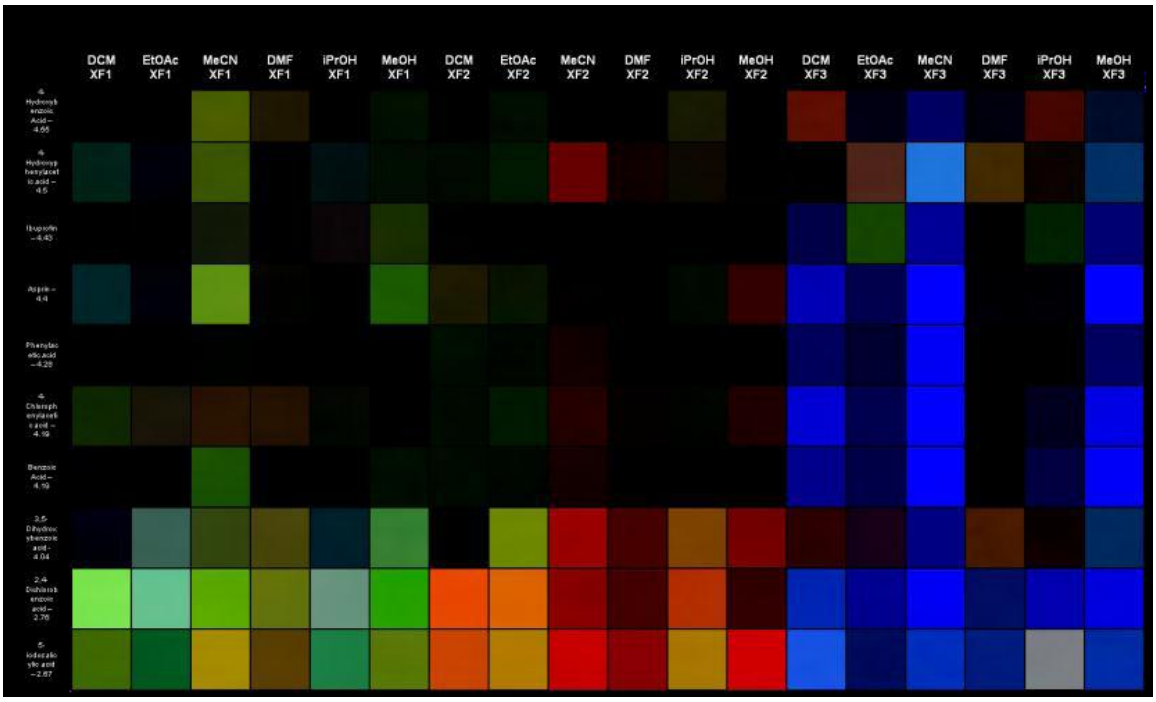

Figure 5.13. Generation of color change map by computer subtraction of observed color changes from reference pictures.

Spectroscopic Analysis

To better visualize the relative intensities of the observable emissions, fluorescence spectra were recorded for all acid/**XF2** and acid/**XF3** combinations in EtOAc; these systems best represented reaction dependence on pKa (Figure 5.14) and structural features (Figure 5.15).

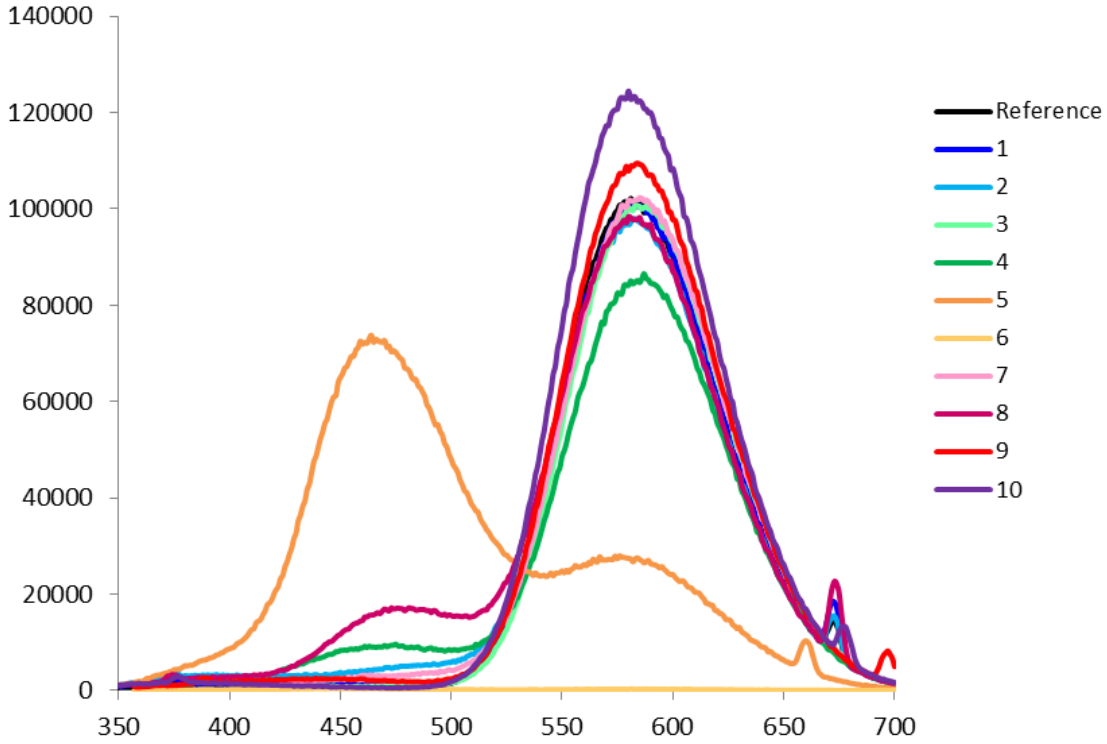

Figure 5.14. Emission spectra of acids **1**-**10**/**XF2** in EtOAc.* Spectra were not normalized to show relative intensities of fluorescence upon reaction. 1. Benzoic Acid, 2. Phenylacetic Acid, 3. 4-OH Benzoic Acid, 4. 3,5-diOH Benzoic Acid, 5. 2,4-diCl Benzoic Acid, 6. 5-Iodosalicylic acid**; 7. 4-OH Phenylacetic Acid, 8. 4-Cl Phenylacetic Acid; 9. Asprin, 10. Ibuprofen; *Fluorimeter slit width constant @ 1.5 mm. The sharp small peaks at 650-700 nm are scattering peaks. **Appears at baseline, quenched relative to others.

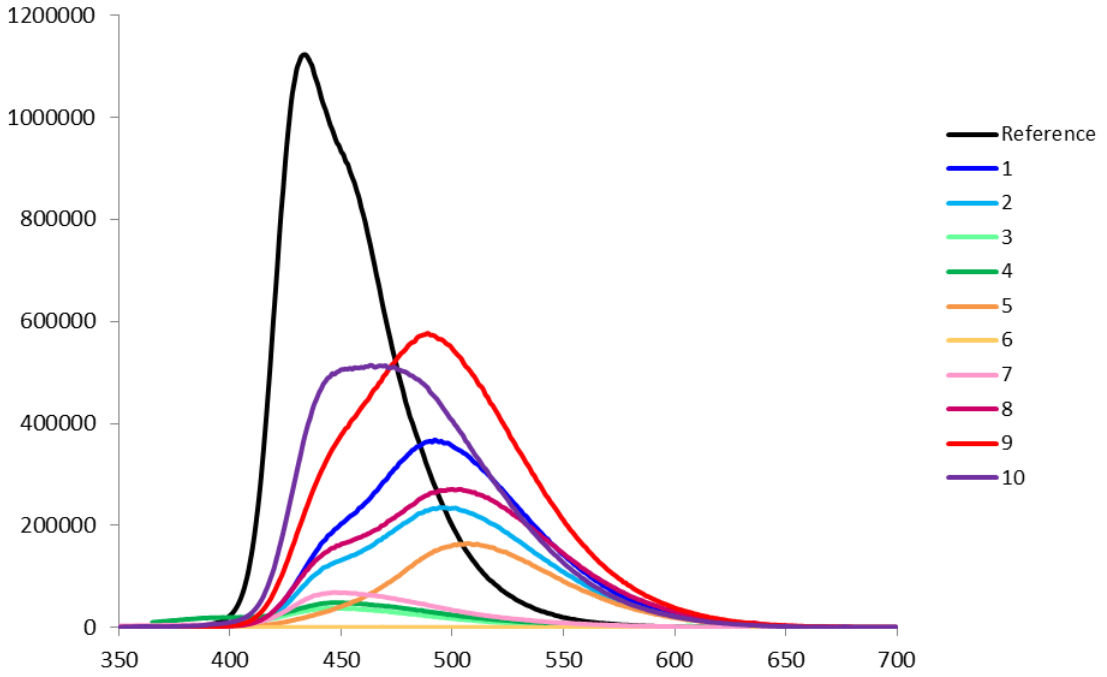

Figure 5.15. Emission spectra of acids 1-10/**XF3** in EtOAc.* Spectra were not normalized to show relative intensities of fluorescence upon reaction. 1. Benzoic Acid, 2. Phenylacetic Acid, 3. 4-OH Benzoic Acid, 4. 3,5-diOH Benzoic Acid, 5. 2,4-diCl Benzoic Acid, 6. 5-Iodosalicylic acid**; 7. 4-OH Phenylacetic Acid, 8. 4-Cl Phenylacetic Acid; 9. Asprin, 10. Ibuprofen; *Fluorimeter slit width constant @ 1.5 mm. **Appears at baseline, quenched relative to others.

Multivariate Analysis of Variance of the Experimentally Obtained RGB Values

The obtained RGB values of individual samples are used as R, G, and B-vectors to calculate standard deviations related to a standard (std). The individual R, G, and B values are treated as independent vectors and are not averaged. The relative standard deviation σ_i gives a single value, which can be correlated with chemical properties to reveal relationships (Figure 5.16).

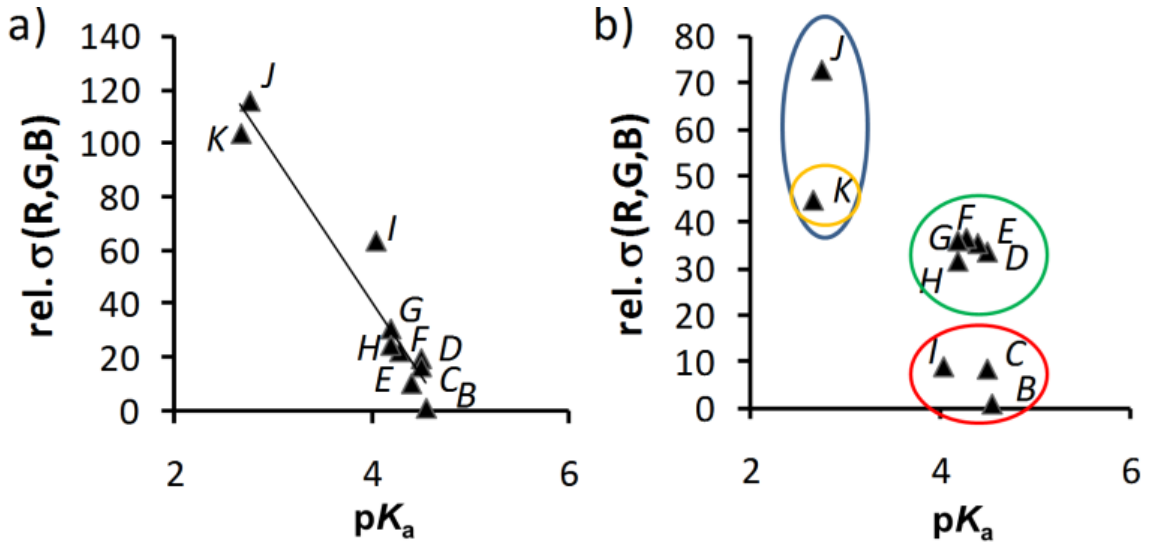

Figure 5.16. Correlation plot of pKa values and the relative standard relative standard deviation σ of the RGB values a) **XF2** dissolved in EtOAc, b) **XF3** dissolved in EtOAc; red circle: acids with a hydroxyl group; blue circle: acids with a halogen substituent; green circle: acids without any functionality, yellow circle: acid with hydroxyl and halogen substituents.

The relative standard deviation σ_i of a single compound can be calculated according to equation 5.1.

$$\sigma_i(R,G,B) = \frac{\sqrt{(R_i - R_{std})^2 + (G_i - G_{std})^2 + (B_i - B_{std})^2}}{3}$$

Equation 5.1. Calculating relative standard deviation σ_i.

These values can be correlated in 2D and 3D plots to find cruciform fluorophores and solvents with large differences in σ_i of the individual analytes (Figure 5.17). Analysis of such plots gives measures of suitable solvent/cruciform fluorophore combinations to unambiguously identify single analytes. The relative σ values were also correlated with the pKa values of the analytes (Figure 5.18).

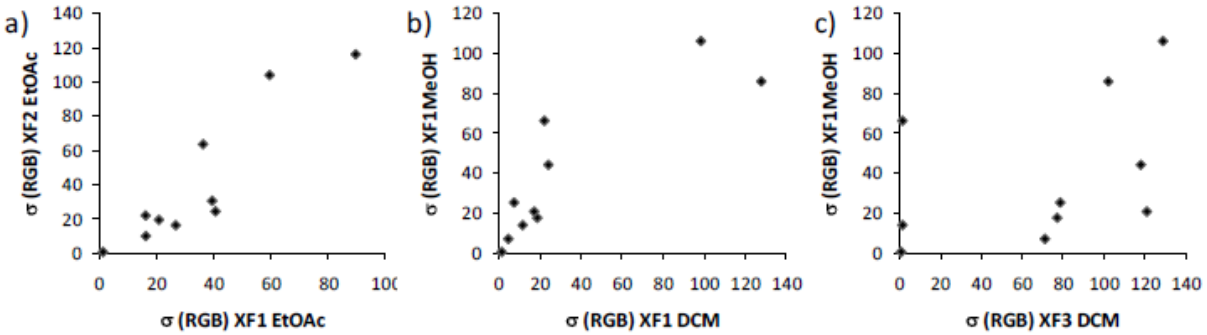

Figure 5.17. Correlation plot of pKa values and the relative standard relative standard deviation σ of the RGB values of samples. a) **XF1** in EtOAc, b) **XF1** in DCM, and c) **XF3** in DCM.

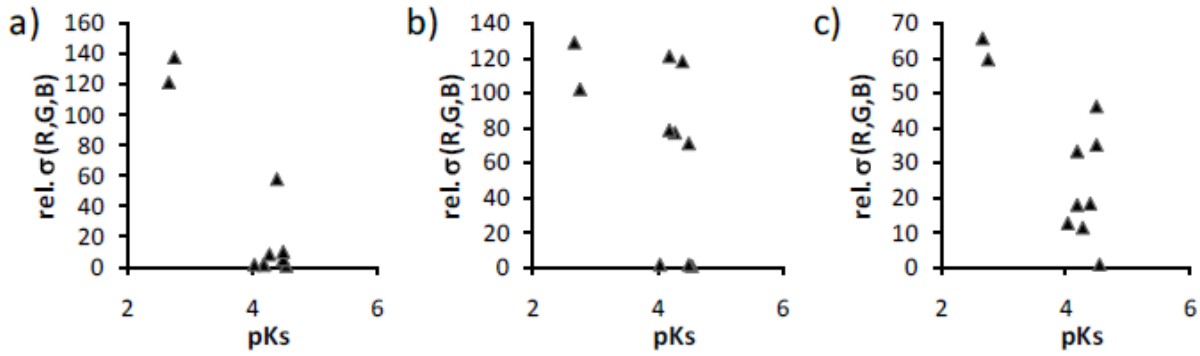

Figure 5.18. Correlation plot of pKa values and the relative standard deviation σ of the RGB values of samples. a) **XF2** in DCM, b) **XF3** in DCM, and c) **XF1** in DMF.

Analysis of cruciform fluorophore – solvent – analyte data is performed in a similar way by extending the equation of the relative standard deviation σ_i to 3D datasets according to equation 5.2.

$$\sigma_i^{3D}(R,G,B) = \frac{\sqrt{\sum_{XF=1}^{n}\sum_{solv=1}^{l}((R_i-R_{std})^2+(G_i-G_{std})^2+(B_i-B_{std})^2)}}{3\times n\times l}$$

Equation 5.2. Calculating relative standard deviation σ_i in three dimensions.

This approach allowed us not only to find out suitable combinations of fluorophoric sensors, but also to discriminate among and identify unknown compounds by statistical analysis of calibration data. Evaluation of an unknown data set yielded 100% accuracy in assignment:

Ibuprofen

Ibuprofen ⟶ Unknown Group 1

Ibuprofen

3,5-Dihydroxybenzoic acid

3,5-Dihydroxybenzoic acid ⟶ Unknown Group 2

3,5-Dihydroxybenzoic acid

Benzoic acid

Benzoic acid ⟶ Unknown Group 3

Benzoic acid

Phenylacetic acid

Phenylacetic acid ⟶ Unknown Group 4

Phenylacetic acid

Darkroom Setup

Fluorescence photographs were recorded in darkroom conditions under UV lamps as illustrated in figure 5.19.

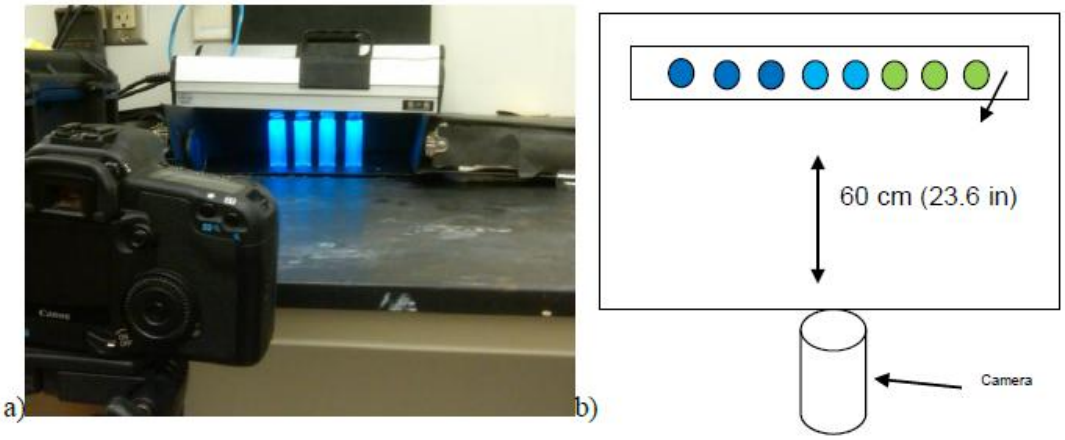

Figure 5.19. Darkroom setup for photographing vials (photo taken under ambient light; all published results were recorded in the dark). b) overhead sketch of darkroom setup. Two hand held UV-lamps with an emission maximum of 365 nm were positioned directly over the uncapped 16 mL vials.

References

[1] (a) Wiskur, S. L.; Ait-Haddou, H.; Lavigne, J. J.; Anslyn, E. V. *Acc. Chem. Res.* **2001**, *34*, 963-972. (b) (c) Zucchero A. J.; McGrier P. L.; Bunz U. H. F. *Acc. Chem. Res.* **2010**, *43*, 397-408. (d) McRae, R.; Bagchi, P.; Sumalekshmy, S.; Fahrni, C. J. *Chem. Rev.* **2009**, *109*, 4780-4827. (e) Shaughnessy, K. H.; Kim, P.; Hartwig, J. F. *J. Am. Chem. Soc.* **1999**, *1213*, 2123-2132. (f) Snowden, T. S.; Anslyn, E. V. *Curr. Opinon Chem. Biol.* **1999**, *3*, 740-746. (g) Thomas, S. W.; Joly, G. D.; Swager T. M. *Chem. Rev.* **2007**, *107*, 1339-1386. (h) Yang, J. S.; Swager, T. M. *J. Am. Chem. Soc.* **1998**, *120*, 5321-5322.3

[2] (a) Rakow, N. A.; Suslick, K. S. *Nature* **2000**, *406*, 710-713. (b) Lin, H. W.; Suslick, K. S.; *J. Am. Chem. Soc.* **2010**, *132*, 15519-15521.

[3] (a) Lavigne, J. J. *Nature Mater.* **2007**, *6*, 548-549. (b) Nelson TL, O'Sullivan C, Greene NT, Maynor MS, Lavigne, J. J. *J. Am. Chem. Soc.* **2006**, *128*, 5640-5641.

[4] Snowden, T. S.; Anslyn, E. V. *Curr. Opinion. Chem. Biol.* **1999**, *3*, 740-746.

[5] Wiskur, S. L.; Anslyn, E. V. *J. Am. Chem. Soc.* **2001**, *123*, 10109-10110.

[6] Suslick, B. A.; Feng, L.; Suslick, K. S. *Anal Chem.* **2010**, *82*, 2067-2073.

[7] (a) Maynor, M. S.; Nelson, T. L.; O'Sullivan, C.; Lavigne J. J. *Org. Lett.* **2007**, *9*, 3217-3220. (b) McGrier, P. L.; Solntsev, K. M.; Miao, S.; Tolbert, L. M.; Miranda, O. R.; Rotello, V. M.; Bunz, U. H. F. *Chemistry Eur. J.* **2008**, *14*, 4503-4510. (c) Bang, J. H.; Lim, S. H.; Park, E.; Suslick, K. S. *Langmuir* **2005** *24*, 13168-13172.

[8] (a) Nyadong, L.; Green, M. D.; De Jesus, V. R.; Newton, P. N.; Fernandez, F. M. *Anal. Chem.* **2007**, *79*, 2150-2157. (b) Newton, P. N.; Green, M. D.; Fernandez, F. M.; Day, N. P. J.; White, N. J. *Lancet Infect. Diseases* **2006**, *6*, 602-613. (c) Newton, P. N.; Fernandez, F. M.; Plancon, A.; Mildenhall, D. C.; Green, M. D.; Ziyong, L.; Christophel, EM.; Phanouvong, S.; Howells, S McIntosh, E.; Laurin, P.; Blum, N.; Hampton, C. Y.; Faure, K.; Nyadong, L.; Soong, C. W. R.; Santoso, B.; Zhiguang, W.; Newton, J.; Palmer, K. *PLOS Medicine* **2008**, *5*, 209-219.

[9] Wilson, J. N.; Bunz U. H. F. *J. Am. Chem. Soc.* **2005**, *127*, 4124-4125.

[10] Zucchero, A. J.; Wilson, J. N.; Bunz, U. H. F. *Am. Chem. Soc.* **2006**, *128*, 11872-11881.

[11] http://www.visionaustralia.org.au/info.aspx?page=628

CHAPTER 6

IDENTIFICATION OF PHARMACEUTICALS: USING CRUCIFORM FLUOROPHORE ARRAYS TO DISCRIMINATE AMONG OVER-THE-COUNTER DRUGS

Introduction

Recent developments in the "chemical tongue" concept have given rise to the use of array-based sensors to discriminate and identify complex mixtures.[1-5] While this technology is limited only to compound identification (i.e., no single components of a mixture can be quantified), such sensors are still quite desirable for applications in quality control and anti-counterfeiting assays. Specifically, array based sensors have been shown to be a quick and easy method of compound identification once an appropriate library of known analytes has been built.[6]

This project seeks to expand on the recent results that are outlined in Chapter 5 of this dissertation where a sensor array based on three cruciform fluorophores were used to discriminate various aromatic organic acids.[6] In our previous investigations, the analytes were chosen based on structural similarities to the active ingredients in many common pharmaceuticals (figures 6.1 and 6.2). In addition to elucidating the ability to discriminate various organic acids, we have shown that our array can successfully identify analytically pure aspirin and ibuprofen, thus setting the precedence for this project.

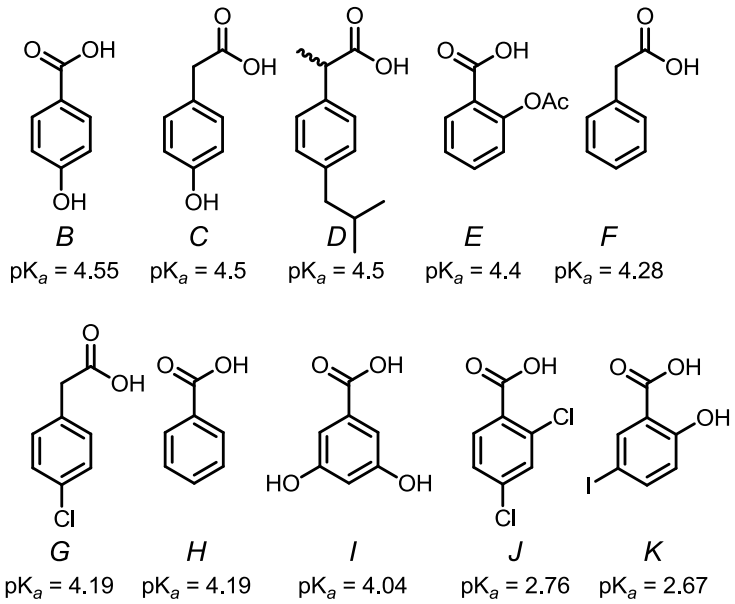

Figure 6.1. Organic acids studied with initial fluorophore array. (*B* = 4-Hydroxybenzoic acid pKa = 4.55; *C* = 4-Hydroxyphenylacetic acid pKa = 4.5; *D* = Ibuprofen pKa = 4.5; *E* = Aspirin pKa = 4.4; *F* = Phenylacetic acid, pKa = 4.28; *G* = 4-Chlorophenylacetic acid pKa = 4.19; *H* = Benzoic acid, pKa = 4.19; *I* = 3,5-Dihydroxybenzoic acid, pKa = 4.04; *J* = 2,4-Dichlorobenzoic acid pKa = 2.76; *K* = 5-Iodosalicylic acid pKa = 2.67).[6]

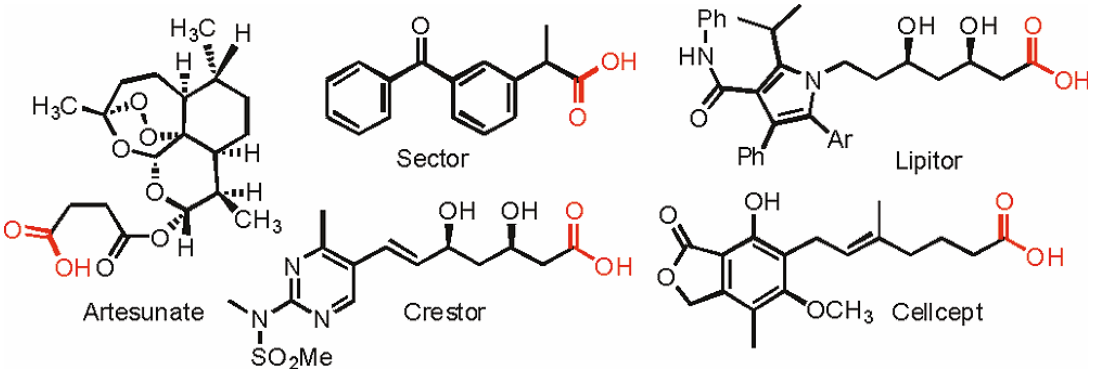

Figure 6.2. Chemical structures of common pharmaceuticals. Initial studies in organic acid discrimination were modeled on structural commonalities between various pharmaceuticals.[6]

Experimental Design, Discussion, and Results

For this study, a large spectrum of samples was required to accurately paint a picture of true pharmaceutical discrimination. To this effect, twenty over-the-counter drugs were purchased from a local pharmacy and organized based on the ailment the drug

was designed to counteract (figure 6.3). In doing this, we hoped to answer an ancillary question in the process of identifying individual drugs: do families of drugs react in a similar fashion, that is to say, do they have similar fluorescent "finger-prints", and if so, can we still distinguish individuals among the family as we were able to do with organic acids that contained similar functionalities.

Pain Relief
1. CVS Arthritis Pain Relief
2. CVS Ibuprofen Liqui-Gel
3. CVS Extra Strength Pain Relief
4. CVS Migraine
5. Excedrin Migraine
6. Advil

Low Dose
7. Bayer Low Dose
8. Junior Strength Ibuprofen
9. CVS Aspirin Low Dose
10. Infant Advil
11. CVS Children's Pain Relief
12. Pedia Cure -- Infant

Mix Symptoms
13. Advil Congestion
14. Advil PM
15. CVS Multisymptom Cold
16. Ex. Strength Pain Relief PM
17. Motrin PM

Allergy
18. CVS Allergy
19. CVS Allergy Relief
20. Claritin

Figure 6.3. List of pharmaceuticals categorized based on the ailment they were designed to counteract.

In addition to choosing a larger analysis set, modifications were made to the design of the fluorophore array (figure 6.4). Based on the results outlined in Chapter 5, the cruciforms (XFs) in the array were changed to include two pyridyl-functionalized

XFs, with **XF1** containing pyridyl units on the electron-rich styryl axis, and **XF2** being substituted with pyridyl units on the electron-poor alkynyl axis. Though both compounds exhibit a reference emission in the blue region of the spectrum, it was thought that the differences in the electronic environments in **XF1** and **XF2** would provide enough differences in reactivity to aid in the discrimination of the analytes.

Finally, **XF3** was selected as a fully functionalized cruciform, containing dibutylamino groups on the distyrylbenzene axis and pyridyl units on the alkynyl axis; we have previously reported that **XF3** exhibits a distinct two-stage response, where the axes will react individually based on the concentration or pH of the analyte being tested.[7] With the inherent ability to provide two discrete changes in emission, **XF3** added another layer of depth to the sensing capability of this fluorophore array.

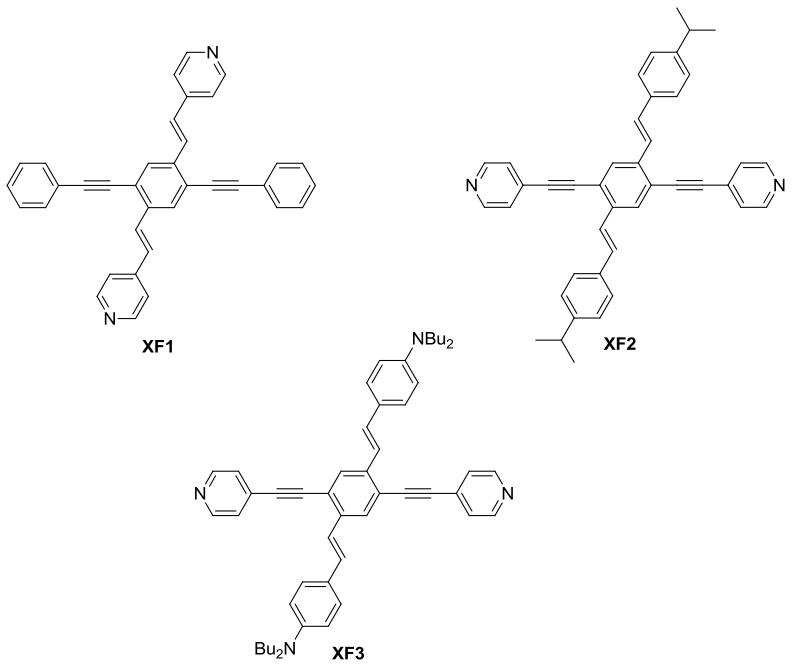

Figure 6.4. Cruciforms chosen for fluorophore array.

Before the initial fluorescence studies began, a problem was encountered regarding our choice of solvent system. Attempts at dissolution into common organic

solvents such as dichloromethane and acetonitrile were unsuccessful, causing us to modify the solvents to reflect highly polar environments, and in two cases, dilute the organic portion with increasing amounts of water. Even still, in all cases tested the solutions were saturated and a significant amount of the pill remained as a solid in the test vial. For the purposes of these experiments, this effect was not treated as a problem, but instead, an advantage in demonstrating the practicality of our experimental design.

For each pharmaceutical tested, the amount used was based on one full dosage of the individual drug. The thought behind this testing process was based on practical applications of a "chemical-tongue" device. If such an apparatus were designed to be used outside of a laboratory for anti-counterfeiting testing, the user would have the ability to test a full dosage of the medication as compared to a predetermined amount that a research lab might investigate for the purposes of research (i.e., a 10 mg sample from a pill as compared to a full tablet).

With the fluorophore array redesigned for the pharmaceutical analytes, solutions were prepared in a manner analogous to those reported in Chapter 5. A single dosage of each drug was prepared and placed in a four dram vial, which was then filled with each of the five solvents and a 10 μL aliquot of dye. Once prepared, digital photographs were taken of each vial under ultra-violet light (λ_{max}= 365 nm) and a portion of each image that most accurately represented the emission as a whole was then inserted into a table (figure 6.5). Once the table was complete, an identical table was prepared, with each cell being filled with a photograph of the corresponding XF reference emission. The colors in these tables were then subtracted, generating the final color difference profiles (figures 6.6 and

6.7). The color profiles (RGB values) of each cell in the color difference profiles were then recorded using a freeware program, ImageJ, for analysis by our collaborators.

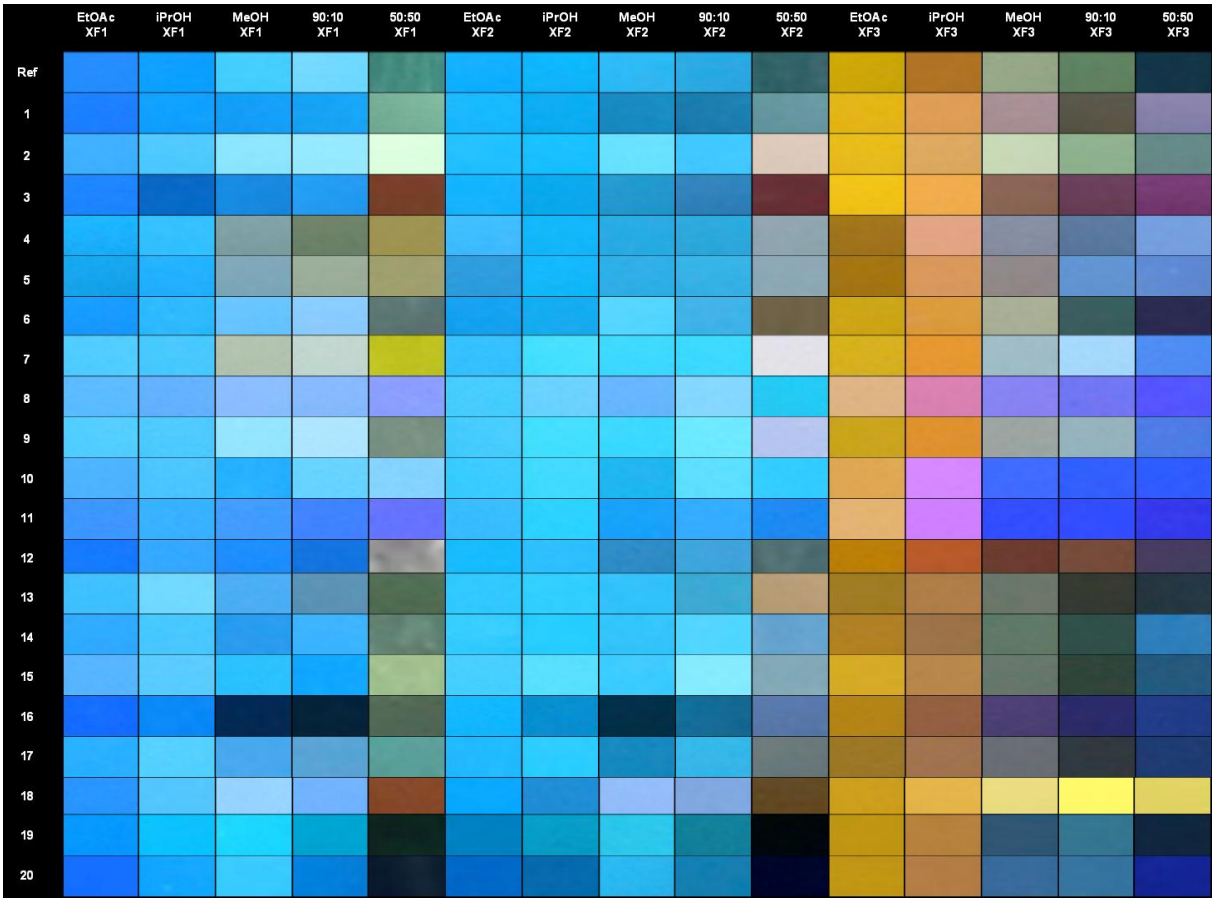

Figure 6.5. Color profiles of pharmaceuticals **1**-**20** upon exposure to **XF1**-**3** in five different solvents. Solvent system: ethyl acetate, isopropanol, methanol, 90:10 methanol:water, and 50:50 methanol:water. Pharmaceuticals: **1**. CVS Arthritis Pain Relief; **2**. CVS Ibuprofen Liqui-Gel; **3**. CVS Extra Strength Pain Relief; **4**. CVS Migraine; **5**. Excedrin™ Migraine; **6**. Advil™; **7**. Bayer Low Dose; **8**. Junior Strength Ibuprofen; **9**. CVS Aspirin Low Dose; **10**. Infant Advil; **11**. CVS Children's Pain Relief; **12**. Pedia Cure - Infant; **13**. Advil Congestion; **14**. Advil™ PM; **15**. CVS Multisymptom Cold; **16**. Extra Strength Pain Relief PM; **17**. Motrin PM; **18**. CVS Allergy; **19**. CVS Allergy Relief; **20**. Claritin™. Vials were photographed under a handheld UV light (λ_{max} ex = 365 nm) using a Canon EOS 30D digital camera equipped with a Canon EFS 18-55mm zoom lens. Photograph exposure times were varied for each solution to produce images reflecting the color of emission.

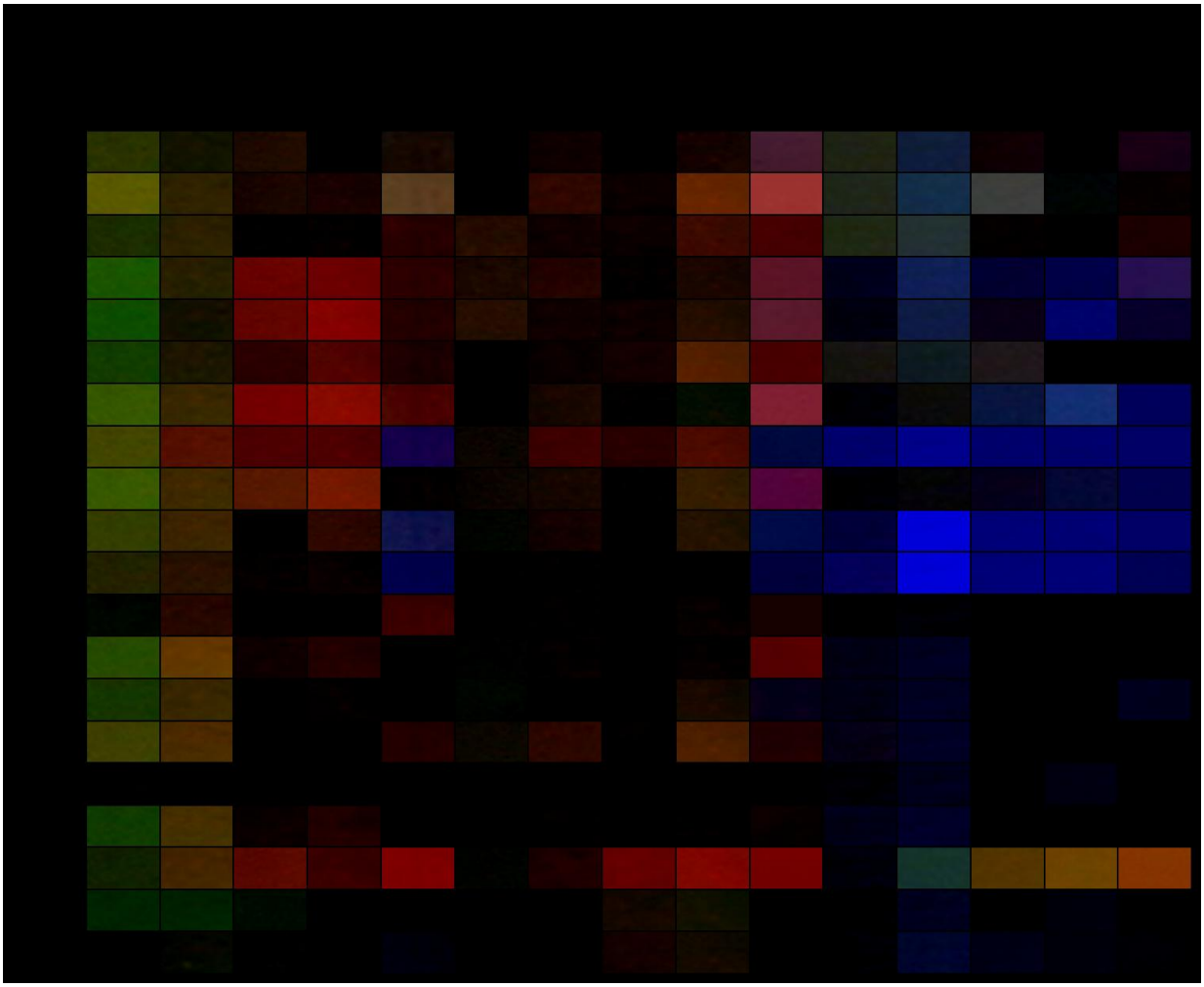

Figure 6.6. Color difference profile of the color changes subtracted from the **XF** reference emissions.

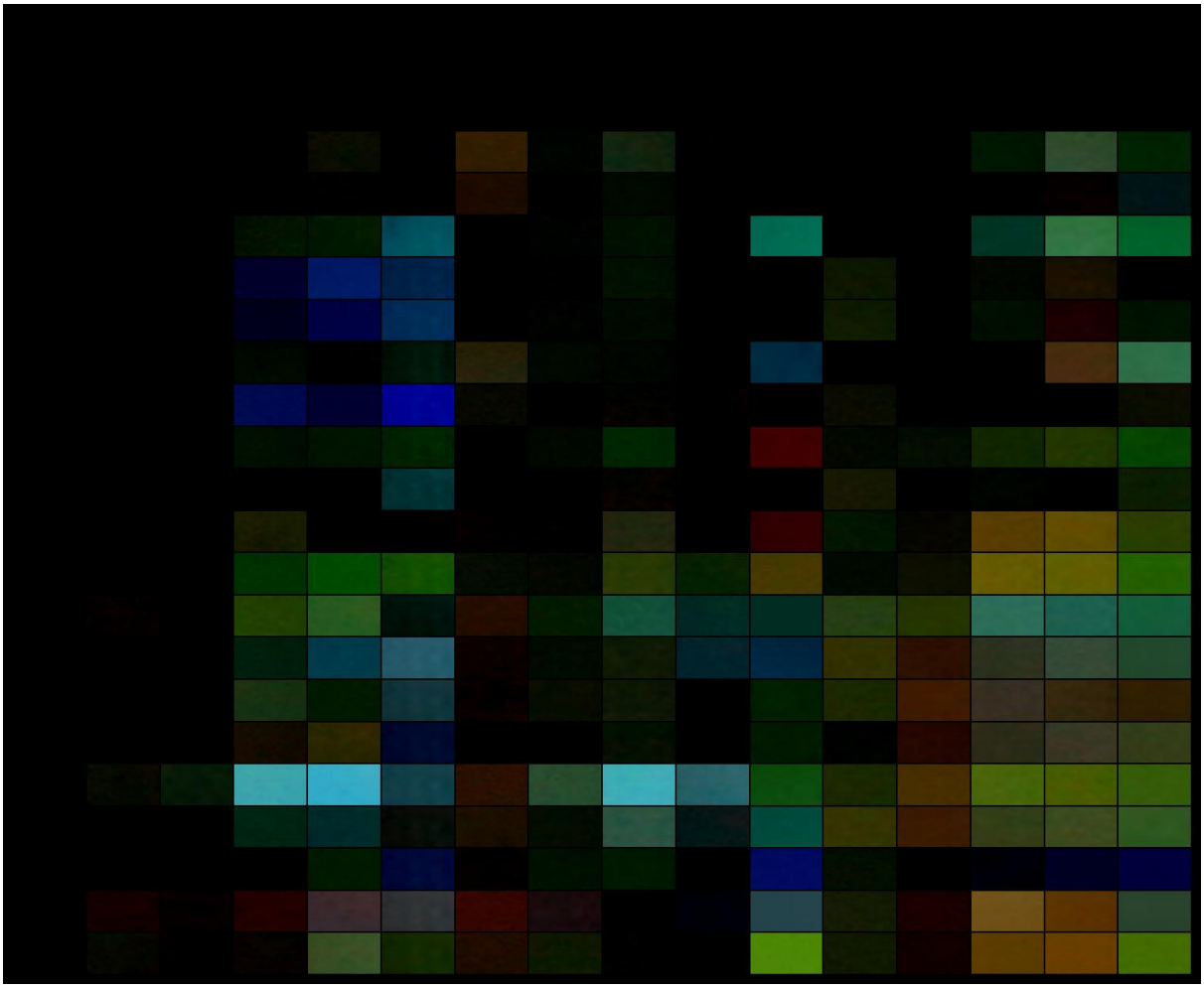

Figure 6.7. Color difference map of the **XF** reference emissions subtracted from the change in color.

After the first analysis, collaborators were unsuccessful in discriminating any of the samples in the library during a blind study of unknown compounds. Subsequent measurements and data collection is planned in the coming months, along with the possible substitution of **XF1** or **XF2** for a fluorophore with a distinctly different reference emission, as we feel as though our analyses were limited by the similar reactivity of the pyridyl cruciforms.

Conclusions

Though this project is not yet complete, it has reached the final stages of analysis; interpretation of the data has started to elucidate some of the answers that we were examining at the beginning of this project. From a qualitative standpoint, we can visually observe different fluorescent "fingerprints" for each pharmaceutical. Unfortunately, this analysis has yet to translate into statistical discrimination between the analytes. It is our hope that through a small modification in the fluorophore system we can achieve 100% accuracy in our efforts to identify unknown samples from the library of known data.

References

[1] a) Rakow, N.A.; Suslick, K.S. *Nature* **2000**, *406*, 710-713. b) Lin, H.W.; Suslick, K.S. *J. Am. Chem. Soc.* **2010**, *132*, 15519-15521.

[2] a) Lavigne, J.J.; *Nat. Mater.* **2007**, *6*, 548-549. b) Nelson, T.L.; O'Sullivan, C.; Greene, N.T.; Maynor, M.S.; Lavigne, J.J. *J. Am Chem. Soc.* **2006**, *128*, 5640-5641.

[3] Snowden, T.S.; Anslyn, E.V. *Curr. Opin. Chem. Biol.* **1999**, *3*, 740-746.

[4] Wiskur, S.L.; Anslyn, E.V. *J. Am. Chem. Soc.* **2001**, *123*, 10109-10110.

[5] Suslick, B.A.; Feng, L.; Suslick, K.S. *Anal. Chem.* **2010**, *82*, 2067-2073.

[6] Davey, E.A.; Zucchero, A.J.; Trapp, O.; Bunz, U.H.F. *J. Am. Chem. Soc.* **2011**, *133*, 7716-7718.

[7] Wilson, J.N.; Bunz, U.H.F. *J. Am. Chem. Soc.* **2005**, *127*, 4124-4125.

CHAPTER 7

DISSERTATION CONCLUSIONS

In summation, this dissertation was designed to provide a precedence for the synthesis and application of advanced cross-conjugated motifs. From the development of "three-armed" cruciforms to the post-functionalization of a poly(*para*-phenyleneethynylene) backbone, the projects described herein have spanned the breadth of chromophore research undertaken in the Bunz group and taken previously successful projects in new directions regarding applications in fluorescence sensing.

While advanced scientific instrumentation can often characterize molecules and provide necessary information for the identification of compounds, these techniques are often impractical when working outside of the laboratory, in an off-site type of setting. For such endeavors, the ability to quickly extract chemical information may be necessary, and users must look to alternative techniques. The idea of a chemical tongue relies on the concept of "finger-printing" molecules via some molecular response based on the addition or removal of a defined analyte. By preparing a number of "finger-prints" into a digital library, one could imagine a mobile chemical identification unit, without any complex scientific instrumentation, merely a hand-held device that could identify and discriminate compounds based on knowledge stored in the library. Chapters five and six in this dissertation outline our initial attempts at designing a fluorescence sensor based on the chemical tongue concept. At the end of my graduate career, I am now of the opinion that chemical sensing and the practical application of the fluorophores discussed herein should dictate the future of research related to these compounds.

When considering research in the Bunz group, there was one key discovery that propagated all of the research serving as the background to this dissertation. In 2003, Bunz and Wilson successfully developed cross-conjugated, small molecule PPE/PPV hybrids, deemed cruciforms (XFs), from which they were able to generate fluorescent responses upon binding of metals and protons to various functionalities in the compounds.[1] Over the past decade, this concept has been expanded into multiple projects and been the primary research focus of three graduate students and multiple post-doctoral students in the Bunz group. This dissertation is only one snippet of a larger body of work in the area of responsive fluorophores. Herein, the principle goal was to exhibit the viability of cross-conjugated materials, be them oligo- or polymeric in nature, in practical sensing techniques. It is my hope that this document will serve as a stepping-stone for a future researcher, one who will see the work accomplished in this document and start anew with different ideas and a novel vision for where this research can proceed.

APPENDIX A

DEVELOPMENT OF GREEN FLUORESCENT PROTEIN ANALOGUES AS FLUORESCENT PROBES FOR PEROXISOME PROLIFERATOR-ACTIVATED RECEPTOR-GAMMA BINDING

Introduction

My involvement in this project originally developed as an extension of my interest in fluorescent conjugated materials and the need for the development of new ligands in the Tolbert/Azizi collaboration. This appendix describes the synthesis (Figure XX1) and characterization of green fluorescent protein (GFP) analogues for use as peroxisome proliferator-activated receptor gamma (PPAR-γ) probes.

One of the primary foci of research in the Tolbert group has been the elucidation of GFP chromophore binding and how it relates to fluorescence.[1] In the past decade it has been revealed that the binding environment, specifically the rigidity of the GFP chromophore itself, is the integral means by which fluorescence is obtained. When discussing the photophysics of the GFP chromophore, it is important to note the two potential means of twisting that lead to a decay of the emission (figure A.1): the single bond aryl twisting, φ, and twisting of the methylene double-bond, τ.[2]

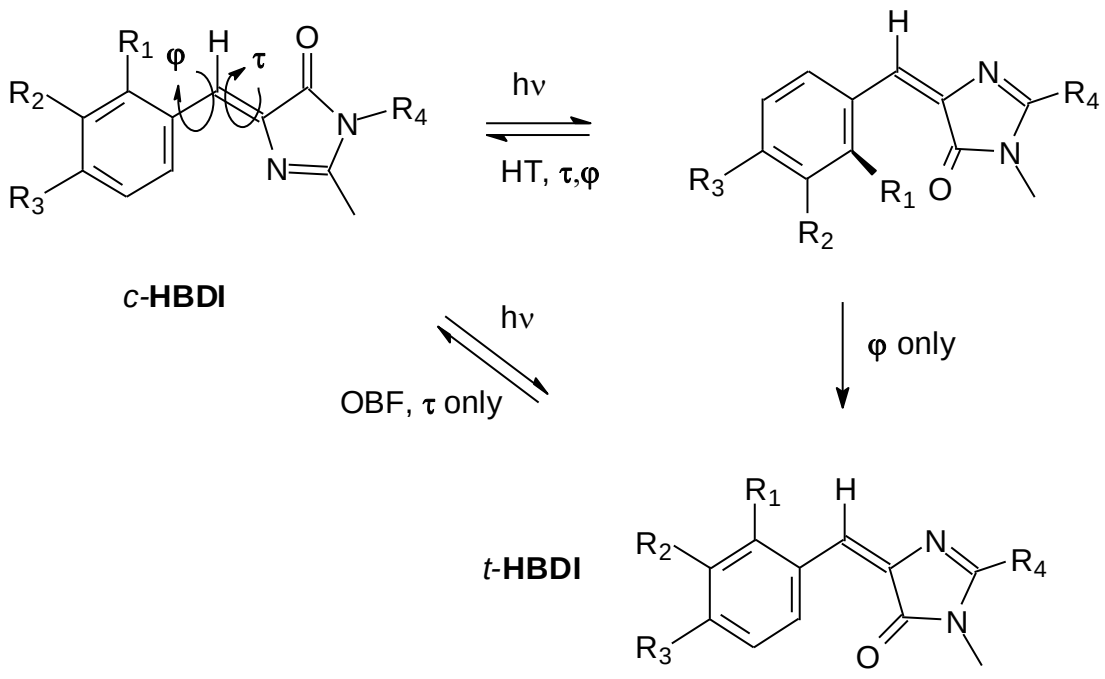

Figure A.1. Modes of twisting for GFP chromophore derivatives.

When these twisting modes are restricted (i.e., the molecule is bound), planarity of the chromophore is maintained in the *trans*- position, generating a fluorescent state. The naturally occurring example of this effect is shown with the wild-type GFP chromophore bound in an 11-strand β-barrel.[3] This effect has been mimicked via binding of the GFP chromophore in a variety of environments, including metal complexation,[4] encapsulation in octa-acids[5], binding to proteins,[6] aggregation with cholate salts,[7] and most recently, via binding to nuclear receptors.[8]

The importance of binding of GFP analogues to nuclear receptors (NRs) lies in the ability to track the fluorogens *in vivo*.[9] The specific focus of this project was to the design ligands to bind proliferator-activated receptor-gamma (PPAR-γ), a nuclear receptor known to regulate fatty acids and the metabolism of glucose.[10] To this effect,

molecules mimicking fatty acids moieties were synthesized to maximize the potential of ligand binding (figure A.2).

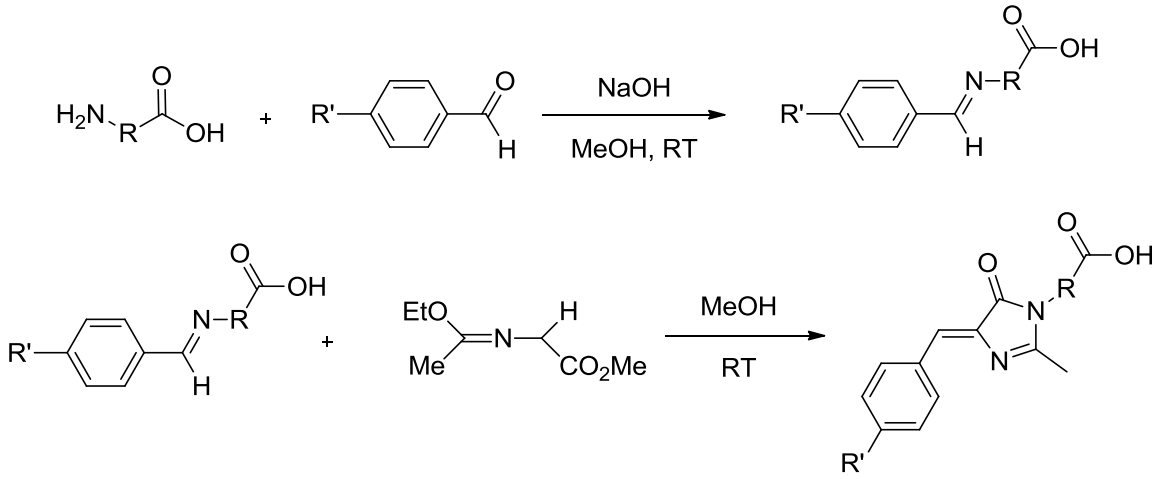

Figure A.2. General synthesis of imidazolidinone ligands.

Current Progress and Future Work

Initially, this project has been aimed at synthesizing a wide range of compounds of varying length using known procedures[11-12] in the effort to determine a relative size of ligand that is able to fit into the binding pocket of PPAR-γ. While this project is only in the initial stages, at present time, eight imidazolidinones have been successfully synthesized, and we are awaiting the results of cell culture binding studies, which is to be undertaken by collaborators.

Experimental Procedures

Materials and Methods

All chemicals and solvents were purchased from commercial sources and were used without further purification unless otherwise specified. ^{1}H NMR spectra were recorded at 298 K on a 300 MHz spectrometer. Chemical shifts are reported in parts per million (ppm), using residual solvent (chloroform-*d*) as an internal standard. The data is

reported as follows: chemical shift, multiplicity (s = singlet, d = doublet, t = triplet, q = quartet, m = multiplet, br = broad), and integration.

Synthesis and Characterization Data

Compound **10** was prepared according to previously reported literature procedures.[1]

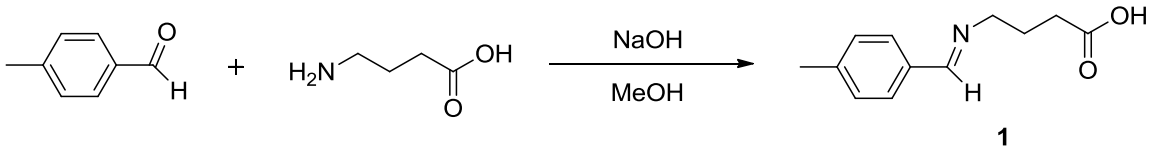

Figure A.3. Synthesis of imine **1**.

Synthesis of **1**

Sodium hydroxide (732 mg, 1.1 mol eq) was dissolved into 2 mL methanol in a four dram vial followed by addition of 4-aminobutanoic acid (1.89 g, 1.1 mol eq.). After the amino-acid had fully dissolved, 4-(1-methylethyl)tolualdehyde (2 g, 0.01665 mol) was added via syringe to the reaction mixture. The reaction vessel was capped with a rubber stopper, vented to the atmosphere with an 18 gauge needle, and allowed to stir for 24 hrs, at which time the solvent was removed under reduced pressure, yielding a white solid. The crude product was washed with diethyl ether (10 mL, 3x) and the solid was collected via vacuum filtration.

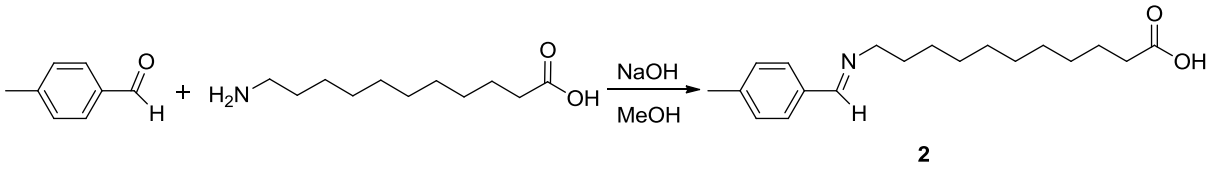

Figure A.4. Synthesis of imine **2**.

Synthesis of **2**

Sodium hydroxide (733 mg, 1.1 mol eq) was dissolved into 5 mL methanol in a four dram vial followed by addition of 11-aminoundecanoic acid (3.69 g, 1.1 mol eq.). After the amino-acid had fully dissolved, 4-tolualdehyde (2 g, 0.01665 mol) was added via syringe to the reaction mixture. The reaction vessel was capped with a rubber stopper, vented to the atmosphere with an 18 gauge needle, and allowed to stir for 24 hrs, at which time the solvent was removed under reduced pressure, yielding a white solid. The crude product was washed with diethyl ether (10 mL, 3x) and the solid was collected via vacuum filtration, yielding the product as a white solid (2.19 g, 44%).

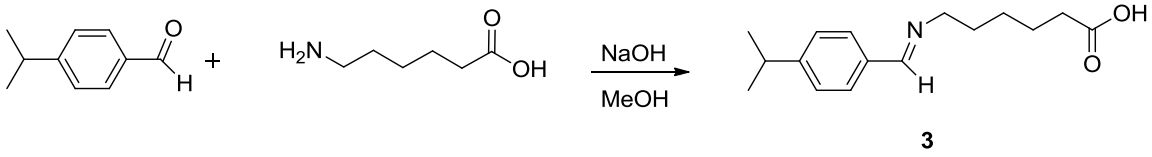

3

Figure A.5. Synthesis of imine **3**.

Synthesis of **3**

Sodium hydroxide (594 mg, 1.1 mol eq) was dissolved into 3 mL methanol in a four dram vial followed by addition of 6-aminohexanoic acid (1.95 g, 1.1 mol eq.). After the amino-acid had fully dissolved, 4-isopropylbenzaldehyde (2 g, 0.0135 mol) was added via syringe to the reaction mixture. The reaction vessel was capped with a rubber stopper, vented to the atmosphere with an 18 gauge needle, and allowed to stir for 24 hrs, at which time the solvent was removed under reduced pressure, yielding a white solid. The crude product was washed with diethyl ether (10 mL, 3x) and the solid was collected via vacuum filtration, yielding the product as a white solid.

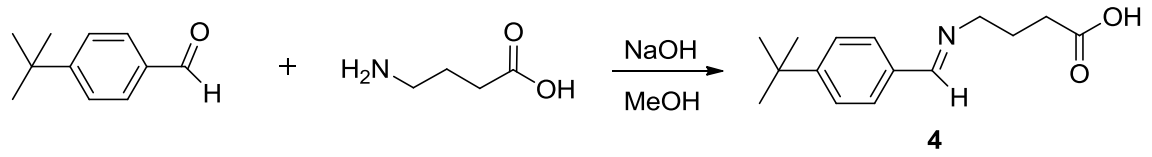

4

Figure A.6. Synthesis of imine **4**.

Synthesis of **4**

Sodium hydroxide (542 mg, 1.1 mol eq) was dissolved into 3 mL methanol in a four dram vial followed by addition of 4-aminobutanoic acid (1.40 g, 1.1 mol eq.). After the amino-acid had fully dissolved, 4-(1,1-dimethylethyl)benzaldehyde (2 g, 0.01233 mol) was added via syringe to the reaction mixture. The reaction vessel was capped with a rubber stopper, vented to the atmosphere with an 18 gauge needle, and allowed to stir for 24 hrs, at which time the solvent was removed under reduced pressure, yielding a white solid. The crude product was washed with diethyl ether (10 mL, 3x) and the solid was collected via vacuum filtration, yielding the product as a white solid.

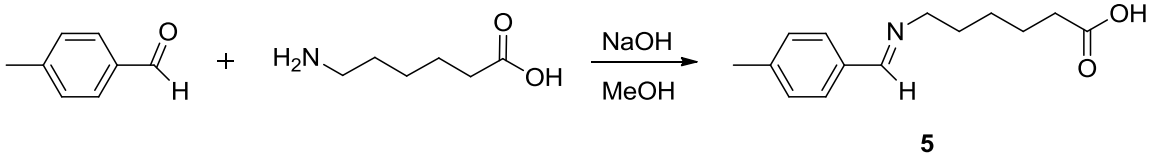

5

Figure A.7. Synthesis of imine **5**.

Synthesis of **5**

Sodium hydroxide (733 mg, 1.1 mol eq) was dissolved into 3 mL methanol in a four dram vial followed by addition of 6-aminohexanoic acid (2.40 g, 1.1 mol eq.). After the amino-acid had fully dissolved, 4-tolualdehyde (2 g, 0.01665 mol) was added via syringe to the reaction mixture. The reaction vessel was capped with a rubber stopper, vented to the atmosphere with an 18 gauge needle, and allowed to stir for 24 hrs, at which time the solvent was removed under reduced pressure, yielding a white solid. The crude product was washed with diethyl ether (10 mL, 3x) and the solid was collected via vacuum filtration, yielding the product as a white solid.

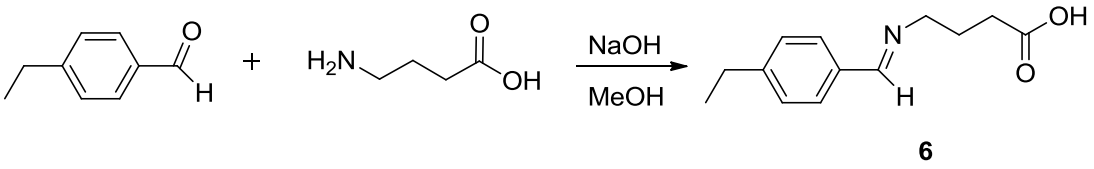

6

Figure A.8. Synthesis of imine **6**.

Synthesis of **6**

Sodium hydroxide (656 mg, 16.4 mmol) was dissolved into 3 mL methanol in a four dram vial followed by addition of 4-aminobutanoic acid (1.69 g, 16.4 mmol). After the amino-acid had fully dissolved, 4-ethylbenzaldehyde (2 g, 14.91 mmol) was added via syringe to the reaction mixture. The reaction vessel was capped with a rubber stopper, vented to the atmosphere with an 18 gauge needle, and allowed to stir for 24 hrs, at which time the solvent was removed under reduced pressure, yielding a white solid. The crude product was washed with diethyl ether (10 mL, 3x) and the solid was collected via vacuum filtration, yielding the product as a white solid.

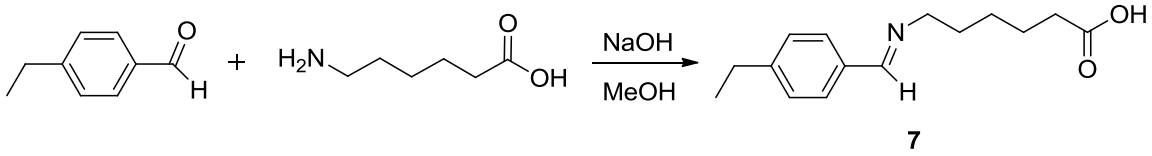

7

Figure A.9. Synthesis of imine **7**.

Synthesis of **7**

Sodium hydroxide (502 mg, 1.1 mol eq) was dissolved into 3 mL methanol in a four dram vial followed by addition of 6-aminohexanoic acid (1.64 g, 1.1 mol eq.). After the amino-acid had fully dissolved, 4-ethylbenzaldehyde (1.53 g, 0.0114 mol) was added via syringe to the reaction mixture. The reaction vessel was capped with a rubber stopper, vented to the atmosphere with an 18 gauge needle, and allowed to stir for 24 hrs, at which time the solvent was removed under reduced pressure, yielding a white solid. The crude

product was washed with diethyl ether (10 mL, 3x) and the solid was collected via vacuum filtration, yielding the product as a white solid.

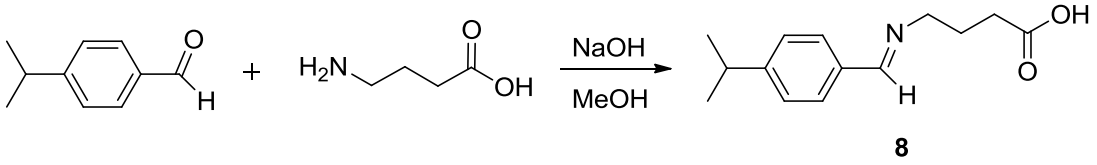

Figure 1.10. Synthesis of imine **8**.

Synthesis of **8**

Sodium hydroxide (594 mg, 1.1 mol eq) was dissolved into 3 mL methanol in a four dram vial followed by addition of 4-aminobutanoic acid (1.53 g, 1.1 mol eq.). After the amino-acid had fully dissolved, 4-isopropylbenzaldehyde (2.0 g, 0.0135 mol) was added via syringe to the reaction mixture. The reaction vessel was capped with a rubber stopper, vented to the atmosphere with an 18 gauge needle, and allowed to stir for 24 hrs, at which time the solvent was removed under reduced pressure, yielding a white solid. The crude product was washed with diethyl ether (10 mL, 3x) and the solid was collected via vacuum filtration, yielding the product as a white solid.

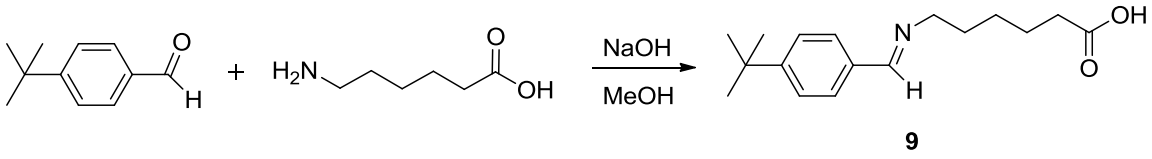

Figure A.11. Synthesis of imine **9**.

Synthesis of **9**

Sodium hydroxide (542 mg, 1.1 mol eq) was dissolved into 3 mL methanol in a four dram vial followed by addition of 6-aminohexanoic acid (2.73 g, 1.1 mol eq.). After the amino-acid had fully dissolved, 4-isopropylbenzaldehyde (2.0 g, 0.0123 mol) was added via syringe to the reaction mixture. The reaction vessel was capped with a rubber

stopper, vented to the atmosphere with an 18 gauge needle, and allowed to stir for 24 hrs, at which time the solvent was removed under reduced pressure, yielding a white solid. The crude product was washed with diethyl ether (10 mL, 3x) and the solid was collected via vacuum filtration, yielding the product as a white solid (2.89 g, 85%).

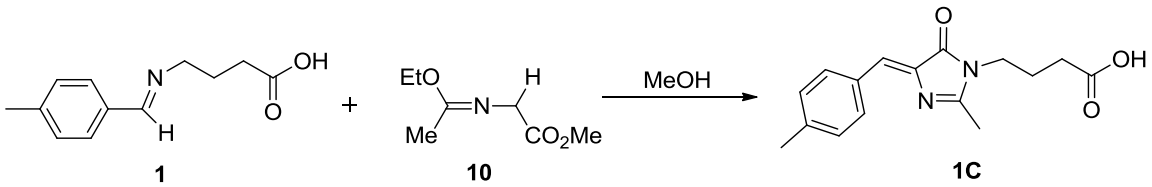

Figure A.12. Synthesis of imidazolidinone **1C**.

Synthesis of **1C**

Compound **1** (500 mg, 0.00243 mol) was dissolved into a minimal amount of methanol (2 mL) in a six dram vial, followed by addition of **10** (427 mg, 1.1 mol eq.) to the reaction vessel via syringe. The mixture was allowed to stir at room temperature for 24 hrs, at which point the solvent was removed under reduced pressure. The resulting yellow solid was then washed with diethyl ether (10 mL, 3x) and collected via vacuum filtration, yielding the final product as a yellow solid (210 mg, 30%).

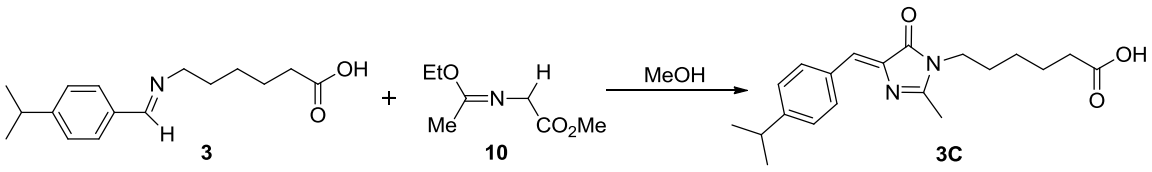

Figure A.13. Synthesis of imidazolidinone **3C**.

Synthesis of **3C**

Compound **3** (500 mg, 0.00191 mol) was dissolved into a minimal amount of methanol (2 mL) in a six dram vial, followed by addition of **10** (335 mg, 1.1 mol eq.) to the reaction vessel via syringe. The mixture was allowed to stir at room temperature for 24 hrs, at which point the solvent was removed under reduced pressure. The resulting

yellow solid was then washed with diethyl ether (10 mL, 3x) and collected via vacuum filtration, yielding the final product as a yellow solid (135 mg, 21%).

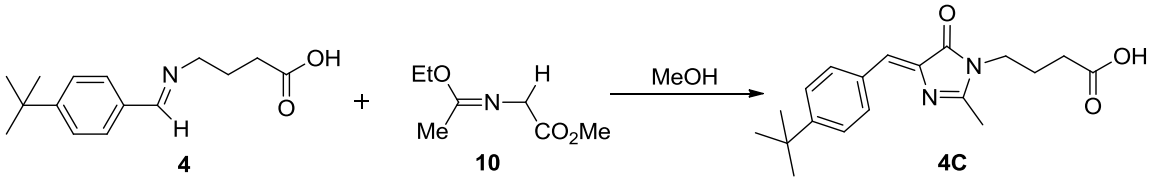

Figure A.14. Synthesis of imidazolidinone **4C**.

Synthesis of **4C**

Compound **4** (500 mg, 2.02 mmol) was dissolved into a minimal amount of methanol (2 mL) in a six dram vial, followed by addition of **10** (354 mg, 2.22 mmol) to the reaction vessel via syringe. The mixture was allowed to stir at room temperature for 24 hrs, at which point the solvent was removed under reduced pressure. The resulting yellow solid was then washed with diethyl ether (10 mL, 3x) and collected via vacuum filtration, yielding the final product as a yellow solid (200 mg, 30%).

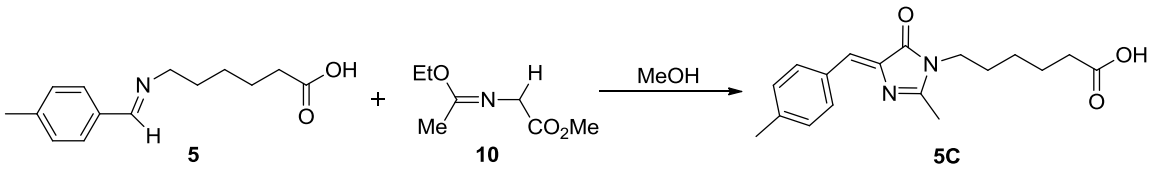

Figure A.15. Synthesis of imidazolidinone **5C**.

Synthesis of **5C**

Compound **5** (500 mg, 2.14 mol) was dissolved into a minimal amount of methanol (2 mL) in a six dram vial, followed by addition of **10** (375 mg, 2.35 mmol) to the reaction vessel via syringe. The mixture was allowed to stir at room temperature for 24 hrs, at which point the solvent was removed under reduced pressure. The resulting

yellow solid was then washed with diethyl ether (10 mL, 3x) and collected via vacuum filtration, yielding the final product as a yellow solid (337 mg, 50%).

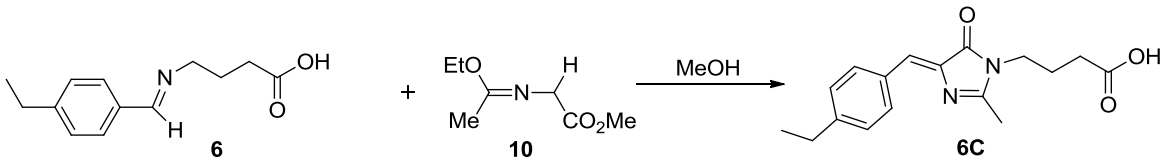

Figure A.16. Synthesis of imidazolidinone **6C**.

Synthesis of **6C**

Compound **6** (500 mg, 2.30 mmol) was dissolved into a minimal amount of methanol (2 mL) in a six dram vial, followed by addition of **10** (400 mg, 2.53 mmol) to the reaction vessel via syringe. The mixture was allowed to stir at room temperature for 24 hrs, at which point the solvent was removed under reduced pressure. The resulting yellow solid was then washed with diethyl ether (10 mL, 3x) and collected via vacuum filtration, yielding the final product as a yellow solid (240 mg, 35%).

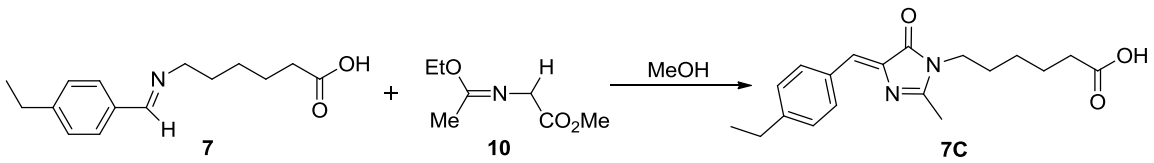

Figure A.17. Synthesis of imidazolidinone **7C**.

Synthesis of **7C**

Compound **7** (500 mg, 2.02 mmol) was dissolved into a minimal amount of methanol (2 mL) in a six dram vial, followed by addition of **10** (354 mg, 2.22 mmol) to the reaction vessel via syringe. The mixture was allowed to stir at room temperature for 24 hrs, at which point the solvent was removed under reduced pressure. The resulting yellow solid was then washed with diethyl ether (10 mL, 3x) and collected via vacuum filtration, yielding the final product as a yellow solid (280 mg, 44%).

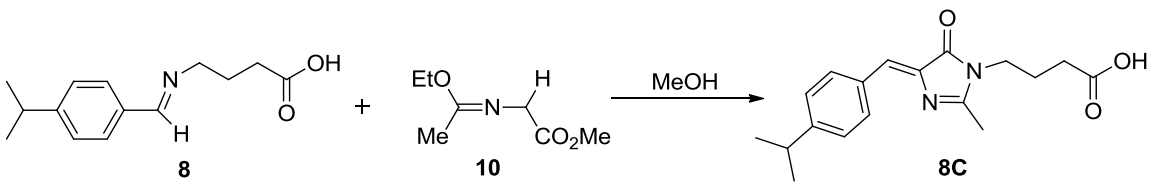

Figure 1.18. Synthesis of imidazolidinone **8C**.

Synthesis of **8C**

Compound **8** (500 mg, 2.14 mmol) was dissolved into a minimal amount of methanol (2 mL) in a six dram vial, followed by addition of **10** (375 mg, 2.35 mmol) to the reaction vessel via syringe. The mixture was allowed to stir at room temperature for 24 hrs, at which point the solvent was removed under reduced pressure. The resulting yellow solid was then washed with diethyl ether (10 mL, 3x) and collected via vacuum filtration, yielding the final product as a yellow solid (208 mg, 31%).

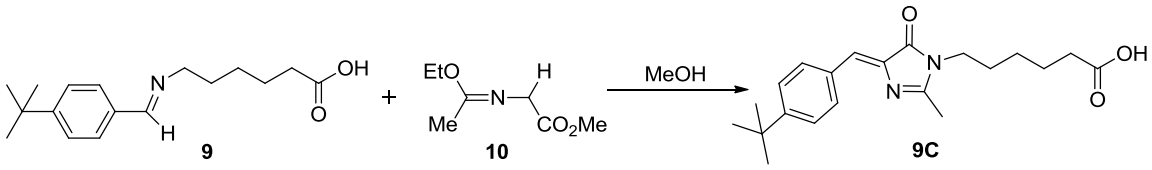

Figure 1.19. Synthesis of imidazolidinone **9C**.

Synthesis of **9C**

Compound **9** (500 mg, 0.00182 mol) was dissolved into a minimal amount of methanol (2 mL) in a six dram vial, followed by addition of **10** (318 mg, 1.1 mol eq.) to the reaction vessel via syringe. The mixture was allowed to stir at room temperature for 24 hrs, at which point the solvent was removed under reduced pressure. The resulting yellow solid was then washed with diethyl ether (10 mL, 3x) and collected via vacuum filtration, yielding the final product as a yellow solid (112 mg, 17%).

References

[1] Tolbert, L. M.; Baldridge, A.; Kowalik, J.; Solntsev, K. M. *Acc.Chem. Res.*, **2011**, *44*, DOI: 10.1021/ar2000925.

[2] (a) Rajbongshi, B.K.; Sen, P.; Ramanathan, G. *Chem. Phys. Lett.* **2010**, *494*, 295-300. (b) Liu, R.S.H. *Acc. Chem. Res.* 2001, *34*, 555-562. (c) Megley, C.M.; Dickson, L.A.; Maddalo, S.L.; Chandler, G.J.; Zimmer, M. *J. Phys. Chem. B.* **2009**, *113*, 302-308.

[3] Ormö, M.; Cubitt, A.; Kallio, K.; Gross, L.; Tsien, R.; Remington, S. *Science* **1996**, *273*, 1392-1395.

[4] Baldridge, A.; Solntsev, K.M.; Tanioka, T.; Kowalik, J.; Hardcastle, K.; Tolbert, L.M. *Chem. Commun.* **2010**, *46*, 5686-5688.

[5] Baldridge, A.; Samanta, S.R.; Jayaraj, N.; Ramamurthy, V.; Tolbert, L.M. *J. Am. Chem. Soc.* **2010**, *132*, 1498-1499.

[6] Baldridge, A.; Feng, S.; Chang, Y.-T.; Tolbert, L.M. *ACS Comb. Sci.* **2011**, *13*, 214-217.

[7] Baldridge, A.; Amador, A.; Tolbert, L.M. *Langmuir* **2011**, *27*, 3271-3274.

[8] (a) Duraj-Thatte, A.M.; Baldridge, A.; Azizi, B.; Tolbert, L.M. *submitted.* (b) Duraj-Thatte, A.M.; Baldridge, A.; Azizi, B.; Tolbert, L.M. *submitted* (c) Duraj-Thatte, A.M.; Baldridge, A.; Azizi, B.; Tolbert, L.M. *in prep.*

[9] a) Htun, H.; Holth, L. T.; Walker, D.; Davie, J. R.; Hager, G. L. *Mol Biol Cell* **1999,** *10*, 471-86. (b) Zhao, H.; Hart, L. L.; Keller, U.; Holth, L. T.; Davie, J. R. *J Cell Biochem.* **2002**, *86*, 365-75.

[10] (a) Greene, M.E.; Blumberg, B.; McBride, O.W.; Yi, H.F.; Kronquist, K.; Kwan, K.; Hsieh, L.; Greene, G.; Nimer, S.D. *Gene Expr.* **1995**, *4*, 281-299. (b) Elbrecht, A.; Chen, Y.; Cullinan, C.A.; Hayes, N.; Leibowitz, M.; Moller, D.E.; Berger, J. *Biochem. Biophys. Res. Commun.* **1996**, *224*, 431-437. (c) Michalik, L.; Auwerx, J.; Berger, J.P.; Chatterjee, V.K.; Glass, C.K.; Gonzalez, F.J.; Grimaldi, P.A.; Kadowaki, T.; Lazar, M.A.; O'Rahilly, S.; Palmer, C.N.; Plutzky, J.; Reddy, J.K.; Spiegelman, B.M.; Staels, B.; Wahli, W. *Phamacol. Rev.* **2006**, *58*, 726-741.

[11] Lerestif, J.M.; Perrocheau, J.; Tonnard, F.; Bazureau, J.P.; Hamelin, J. *Tetrahedron* **1995,** *51*, 6757 – 6774.

[12] Baldridge, A.; Kowalik, J.; Tolbert, L.M. *Synthesis* **2010**, *14*, 2424-2436.

APPENDIX B

RGB RAW DATA FOR MANOVA ANALYSIS OF ORGANIC ACID FLUOROPHORE ARRAY

Table B.1. RGB data taken of **XF1** in DCM.

	DCM XF1 **R**	DCM XF1 **G**	DCM XF1 **B**
4-Hydroxybenzoic acid	0	13	22
4-Hydroxybenzoic acid	0	14	23
4-Hydroxybenzoic acid	4	15	24
4-Hydroxyphenylacetic acid	0	33	25
4-Hydroxyphenylacetic acid	0	35	26
4-Hydroxyphenylacetic acid	0	33	22
Ibuprofen	0	9	21
Ibuprofen	0	8	18
Ibuprofen	0	9	15
Aspirin	0	45	53
Aspirin	0	44	51
Aspirin	0	44	50
Phenylacetic acid	0	27	53
Phenylacetic acid	0	26	49
Phenylacetic acid	0	30	54
4-Chlorophenylacetic acid	0	32	0
4-Chlorophenylacetic acid	0	30	0
4-Chlorophenylacetic acid	1	35	0
Benzoic acid	0	8	39
Benzoic acid	0	6	33
Benzoic acid	0	7	27
3,5-Dihydroxybenzoic acid	0	9	65
3,5-Dihydroxybenzoic acid	0	8	62
3,5-Dihydroxybenzoic acid	0	9	55
2,4-Dichlorobenzoic acid	93	209	71
2,4-Dichlorobenzoic acid	98	209	71
2,4-Dichlorobenzoic acid	97	210	64
5-Iodosalicylic acid	83	162	22
5-Iodosalicylic acid	85	163	21
5-Iodosalicylic acid	87	163	16

Table B.2. RGB data taken of **XF1** in EtOAc.

	EtOAc XF1 **R**	EtOAc XF1 **G**	EtOAc XF1 **B**
4-Hydroxybenzoic acid	34	56	43
4-Hydroxybenzoic acid	31	56	44
4-Hydroxybenzoic acid	36	55	43
4-Hydroxyphenylacetic acid	21	26	28
4-Hydroxyphenylacetic acid	19	28	31
4-Hydroxyphenylacetic acid	17	26	26
Ibuprofen	25	22	13
Ibuprofen	24	22	16
Ibuprofen	22	21	13
Aspirin	28	32	30
Aspirin	22	33	34
Aspirin	23	32	30
Phenylacetic acid	25	28	53
Phenylacetic acid	26	30	36
Phenylacetic acid	25	30	36
4-Chlorophenylacetic acid	3	14	0
4-Chlorophenylacetic acid	3	13	0
4-Chlorophenylacetic acid	2	13	0
Benzoic acid	4	4	7
Benzoic acid	3	4	9
Benzoic acid	3	3	6
3,5-Dihydroxybenzoic acid	57	96	84
3,5-Dihydroxybenzoic acid	55	98	87
3,5-Dihydroxybenzoic acid	54	97	84
2,4-Dichlorobenzoic acid	76	186	117
2,4-Dichlorobenzoic acid	75	185	119
2,4-Dichlorobenzoic acid	75	186	115
5-Iodosalicylic acid	40	147	88
5-Iodosalicylic acid	40	148	93
5-Iodosalicylic acid	39	146	90

Table B.3. RGB data taken of **XF1** in MeCN.

	MeCN XF1 **R**	MeCN XF1 **G**	MeCN XF1 **B**
4-Hydroxybenzoic acid	103	128	0
4-Hydroxybenzoic acid	108	132	0
4-Hydroxybenzoic acid	107	129	0
4-Hydroxyphenylacetic acid	105	102	0
4-Hydroxyphenylacetic acid	106	102	0
4-Hydroxyphenylacetic acid	107	103	0
Ibuprofen	52	51	9
Ibuprofen	54	55	10
Ibuprofen	53	52	12
Aspirin	141	163	32
Aspirin	143	165	35
Aspirin	142	164	33
Phenylacetic acid	25	45	26
Phenylacetic acid	24	44	24
Phenylacetic acid	24	46	25
4-Chlorophenylacetic acid	58	32	0
4-Chlorophenylacetic acid	59	39	0
4-Chlorophenylacetic acid	57	31	0
Benzoic acid	78	129	0
Benzoic acid	75	128	0
Benzoic acid	76	128	0
3,5-Dihydroxybenzoic acid	52	72	17
3,5-Dihydroxybenzoic acid	50	68	12
3,5-Dihydroxybenzoic acid	49	69	13
2,4-Dichlorobenzoic acid	116	170	0
2,4-Dichlorobenzoic acid	115	169	0
2,4-Dichlorobenzoic acid	115	171	0
5-Iodosalicylic acid	222	198	0
5-Iodosalicylic acid	223	197	0
5-Iodosalicylic acid	224	198	0

Table B.4. RGB data taken of **XF1** in DMF.

	DMF XF1 **R**	DMF XF1 **G**	DMF XF1 **B**
4-Hydroxybenzoic acid	59	52	0
4-Hydroxybenzoic acid	59	54	0
4-Hydroxybenzoic acid	60	55	0
4-Hydroxyphenylacetic acid	0	0	0
4-Hydroxyphenylacetic acid	0	0	0
4-Hydroxyphenylacetic acid	0	0	0
Ibuprofen	18	10	0
Ibuprofen	17	9	0
Ibuprofen	17	10	0
Aspirin	39	33	0
Aspirin	35	31	0
Aspirin	35	32	0
Phenylacetic acid	45	44	12
Phenylacetic acid	44	45	7
Phenylacetic acid	43	43	3
4-Chlorophenylacetic acid	28	4	0
4-Chlorophenylacetic acid	29	5	0
4-Chlorophenylacetic acid	30	5	0
Benzoic acid	36	34	11
Benzoic acid	35	35	8
Benzoic acid	38	36	8
3,5-Dihydroxybenzoic acid	74	69	10
3,5-Dihydroxybenzoic acid	74	69	8
3,5-Dihydroxybenzoic acid	71	67	8
2,4-Dichlorobenzoic acid	125	134	8
2,4-Dichlorobenzoic acid	124	133	6
2,4-Dichlorobenzoic acid	124	134	9
5-Iodosalicylic acid	150	123	0
5-Iodosalicylic acid	151	120	0
5-Iodosalicylic acid	151	122	0

Table B.5. RGB data taken of **XF1** in iPrOH.

	iPrOH XF1 **R**	iPrOH XF1 **G**	iPrOH XF1 **B**
4-Hydroxybenzoic acid	28	51	34
4-Hydroxybenzoic acid	26	50	36
4-Hydroxybenzoic acid	26	51	39
4-Hydroxyphenylacetic acid	0	14	1
4-Hydroxyphenylacetic acid	0	10	0
4-Hydroxyphenylacetic acid	0	12	1
Ibuprofen	0	0	0
Ibuprofen	0	0	0
Ibuprofen	0	0	0
Aspirin	12	29	25
Aspirin	13	27	26
Aspirin	11	27	28
Phenylacetic acid	31	58	53
Phenylacetic acid	34	57	57
Phenylacetic acid	35	53	57
4-Chlorophenylacetic acid	0	0	0
4-Chlorophenylacetic acid	0	0	0
4-Chlorophenylacetic acid	0	0	0
Benzoic acid	5	17	18
Benzoic acid	10	16	19
Benzoic acid	13	15	21
3,5-Dihydroxybenzoic acid	0	34	44
3,5-Dihydroxybenzoic acid	0	32	42
3,5-Dihydroxybenzoic acid	0	32	39
2,4-Dichlorobenzoic acid	21	125	58
2,4-Dichlorobenzoic acid	18	124	58
2,4-Dichlorobenzoic acid	22	123	61
5-Iodosalicylic acid	14	127	70
5-Iodosalicylic acid	13	136	70
5-Iodosalicylic acid	15	125	70

Table B.6. RGB data taken of **XF1** in MeOH..

	MeOH XF1 **R**	MeOH XF1 **G**	MeOH XF1 **B**
4-Hydroxybenzoic acid	16	33	0
4-Hydroxybenzoic acid	17	33	0
4-Hydroxybenzoic acid	15	31	0
4-Hydroxyphenylacetic acid	0	15	0
4-Hydroxyphenylacetic acid	0	13	0
4-Hydroxyphenylacetic acid	0	14	0
Ibuprofen	21	44	0
Ibuprofen	23	42	0
Ibuprofen	23	43	0
Aspirin	54	100	0
Aspirin	51	99	0
Aspirin	50	101	0
Phenylacetic acid	0	43	22
Phenylacetic acid	0	41	26
Phenylacetic acid	0	42	25
4-Chlorophenylacetic acid	0	0	0
4-Chlorophenylacetic acid	0	0	0
4-Chlorophenylacetic acid	0	0	0
Benzoic acid	0	40	42
Benzoic acid	0	38	41
Benzoic acid	0	37	38
3,5-Dihydroxybenzoic acid	52	129	50
3,5-Dihydroxybenzoic acid	53	127	51
3,5-Dihydroxybenzoic acid	55	128	52
2,4-Dichlorobenzoic acid	81	167	0
2,4-Dichlorobenzoic acid	82	166	0
2,4-Dichlorobenzoic acid	80	165	0
5-Iodosalicylic acid	141	167	36
5-Iodosalicylic acid	136	164	33
5-Iodosalicylic acid	135	166	35

Table B.7. RGB data taken of **XF2** in DCM.

	DCM XF2 **R**	DCM XF2 **G**	DCM XF2 **B**
4-Hydroxybenzoic acid	0	2	0
4-Hydroxybenzoic acid	0	3	0
4-Hydroxybenzoic acid	0	1	0
4-Hydroxyphenylacetic acid	0	10	0
4-Hydroxyphenylacetic acid	0	11	0
4-Hydroxyphenylacetic acid	0	9	0
Ibuprofen	5	19	0
Ibuprofen	2	18	0
Ibuprofen	4	18	0
Aspirin	61	82	0
Aspirin	58	82	0
Aspirin	56	84	0
Phenylacetic acid	0	18	0
Phenylacetic acid	0	15	0
Phenylacetic acid	0	14	0
4-Chlorophenylacetic acid	0	0	0
4-Chlorophenylacetic acid	0	0	0
4-Chlorophenylacetic acid	0	0	0
Benzoic acid	0	0	0
Benzoic acid	0	0	0
Benzoic acid	0	0	0
3,5-Dihydroxybenzoic acid	0	0	0
3,5-Dihydroxybenzoic acid	0	0	0
3,5-Dihydroxybenzoic acid	0	0	0
2,4-Dichlorobenzoic acid	233	56	0
2,4-Dichlorobenzoic acid	232	55	0
2,4-Dichlorobenzoic acid	230	58	0
5-Iodosalicylic acid	203	56	0
5-Iodosalicylic acid	201	58	0
5-Iodosalicylic acid	202	60	0

Table B.8. RGB data taken of **XF2** in EtOAc.

	EtOAc XF2 **R**	EtOAc XF2 **G**	EtOAc XF2 **B**
4-Hydroxybenzoic acid	18	74	0
4-Hydroxybenzoic acid	20	75	0
4-Hydroxybenzoic acid	18	74	0
4-Hydroxyphenylacetic acid	0	45	0
4-Hydroxyphenylacetic acid	0	46	0
4-Hydroxyphenylacetic acid	0	49	0
Ibuprofen	6	47	0
Ibuprofen	7	50	0
Ibuprofen	9	49	0
Aspirin	32	83	0
Aspirin	32	85	0
Aspirin	31	88	0
Phenylacetic acid	0	41	0
Phenylacetic acid	0	42	0
Phenylacetic acid	0	41	0
4-Chlorophenylacetic acid	0	24	0
4-Chlorophenylacetic acid	0	25	0
4-Chlorophenylacetic acid	0	26	0
Benzoic acid	0	37	0
Benzoic acid	0	38	0
Benzoic acid	0	35	0
3,5-Dihydroxybenzoic acid	111	139	0
3,5-Dihydroxybenzoic acid	108	134	0
3,5-Dihydroxybenzoic acid	109	137	0
2,4-Dichlorobenzoic acid	218	85	0
2,4-Dichlorobenzoic acid	222	82	0
2,4-Dichlorobenzoic acid	219	81	0
5-Iodosalicylic acid	180	155	0
5-Iodosalicylic acid	181	153	0
5-Iodosalicylic acid	179	155	0

Table B.9. RGB data taken of **XF2** in MeCN.

	MeCN XF2 **R**	MeCN XF2 **G**	MeCN XF2 **B**
4-Hydroxybenzoic acid	0	0	0
4-Hydroxybenzoic acid	0	0	0
4-Hydroxybenzoic acid	0	0	0
4-Hydroxyphenylacetic acid	88	0	0
4-Hydroxyphenylacetic acid	86	0	0
4-Hydroxyphenylacetic acid	87	0	0
Ibuprofen	5	0	0
Ibuprofen	3	0	0
Ibuprofen	4	0	0
Aspirin	0	0	0
Aspirin	0	0	0
Aspirin	0	0	0
Phenylacetic acid	47	0	0
Phenylacetic acid	48	0	0
Phenylacetic acid	50	0	0
4-Chlorophenylacetic acid	19	0	0
4-Chlorophenylacetic acid	17	0	0
4-Chlorophenylacetic acid	20	0	0
Benzoic acid	28	0	0
Benzoic acid	22	0	0
Benzoic acid	24	0	0
3,5-Dihydroxybenzoic acid	154	0	0
3,5-Dihydroxybenzoic acid	153	0	0
3,5-Dihydroxybenzoic acid	150	0	0
2,4-Dichlorobenzoic acid	161	0	0
2,4-Dichlorobenzoic acid	155	0	0
2,4-Dichlorobenzoic acid	163	0	0
5-Iodosalicylic acid	184	0	0
5-Iodosalicylic acid	182	0	0
5-Iodosalicylic acid	181	0	0

Table B.10. RGB data taken of **XF2** in DMF.

	DMF XF2 **R**	DMF XF2 **G**	DMF XF2 B
4-Hydroxybenzoic acid	0	0	0
4-Hydroxybenzoic acid	0	0	0
4-Hydroxybenzoic acid	0	0	0
4-Hydroxyphenylacetic acid	0	0	0
4-Hydroxyphenylacetic acid	0	0	0
4-Hydroxyphenylacetic acid	0	0	0
Ibuprofen	0	0	0
Ibuprofen	0	0	0
Ibuprofen	0	0	0
Aspirin	0	0	19
Aspirin	0	0	17
Aspirin	0	0	20
Phenylacetic acid	22	0	0
Phenylacetic acid	21	0	0
Phenylacetic acid	20	0	0
4-Chlorophenylacetic acid	0	0	0
4-Chlorophenylacetic acid	0	0	0
4-Chlorophenylacetic acid	0	0	0
Benzoic acid	5	0	0
Benzoic acid	1	0	0
Benzoic acid	4	0	0
3,5-Dihydroxybenzoic acid	69	0	0
3,5-Dihydroxybenzoic acid	70	0	0
3,5-Dihydroxybenzoic acid	71	0	0
2,4-Dichlorobenzoic acid	86	0	0
2,4-Dichlorobenzoic acid	88	0	0
2,4-Dichlorobenzoic acid	85	0	0
5-Iodosalicylic acid	171	0	0
5-Iodosalicylic acid	170	0	2
5-Iodosalicylic acid	171	0	1

Table B.11. RGB data taken of **XF2** in iPrOH.

	iPrOH XF2 **R**	iPrOH XF2 **G**	iPrOH XF2 **B**
4-Hydroxybenzoic acid	28	59	0
4-Hydroxybenzoic acid	29	60	0
4-Hydroxybenzoic acid	30	60	0
4-Hydroxyphenylacetic acid	17	39	0
4-Hydroxyphenylacetic acid	18	40	0
4-Hydroxyphenylacetic acid	21	41	0
Ibuprofen	0	7	0
Ibuprofen	0	5	0
Ibuprofen	0	6	0
Aspirin	0	55	0
Aspirin	0	54	0
Aspirin	0	53	0
Phenylacetic acid	33	60	0
Phenylacetic acid	32	60	0
Phenylacetic acid	32	58	0
4-Chlorophenylacetic acid	0	1	0
4-Chlorophenylacetic acid	0	0	0
4-Chlorophenylacetic acid	0	0	0
Benzoic acid	0	7	0
Benzoic acid	0	8	0
Benzoic acid	1	9	0
3,5-Dihydroxybenzoic acid	125	66	0
3,5-Dihydroxybenzoic acid	124	67	0
3,5-Dihydroxybenzoic acid	127	65	0
2,4-Dichlorobenzoic acid	177	44	0
2,4-Dichlorobenzoic acid	179	49	0
2,4-Dichlorobenzoic acid	178	47	0
5-Iodosalicylic acid	169	128	0
5-Iodosalicylic acid	170	129	0
5-Iodosalicylic acid	166	131	0

Table B.12. RGB data taken of **XF2** in MeOH.

	MeOH XF2 **R**	MeOH XF2 **G**	MeOH XF2 **B**
4-Hydroxybenzoic acid	0	0	0
4-Hydroxybenzoic acid	0	0	0
4-Hydroxybenzoic acid	0	0	0
4-Hydroxyphenylacetic acid	0	0	0
4-Hydroxyphenylacetic acid	0	0	0
4-Hydroxyphenylacetic acid	0	0	0
Ibuprofen	0	0	0
Ibuprofen	0	0	0
Ibuprofen	0	0	0
Aspirin	0	0	0
Aspirin	1	0	0
Aspirin	2	0	0
Phenylacetic acid	2	0	0
Phenylacetic acid	5	0	0
Phenylacetic acid	4	0	0
4-Chlorophenylacetic acid	0	0	0
4-Chlorophenylacetic acid	0	0	0
4-Chlorophenylacetic acid	0	0	0
Benzoic acid	26	0	0
Benzoic acid	31	0	0
Benzoic acid	28	0	0
3,5-Dihydroxybenzoic acid	115	0	0
3,5-Dihydroxybenzoic acid	118	0	0
3,5-Dihydroxybenzoic acid	116	0	0
2,4-Dichlorobenzoic acid	64	0	0
2,4-Dichlorobenzoic acid	63	0	0
2,4-Dichlorobenzoic acid	66	0	0
5-Iodosalicylic acid	167	0	0
5-Iodosalicylic acid	168	0	0
5-Iodosalicylic acid	166	0	0

Table B.13. RGB data taken of **XF3** in DCM.

	DCM XF3 **R**	DCM XF3 **G**	DCM XF3 **B**
4-Hydroxybenzoic acid	0	0	1
4-Hydroxybenzoic acid	0	0	2
4-Hydroxybenzoic acid	0	0	5
4-Hydroxyphenylacetic acid	0	0	0
4-Hydroxyphenylacetic acid	0	0	0
4-Hydroxyphenylacetic acid	0	0	0
Ibuprofen	0	0	124
Ibuprofen	0	0	125
Ibuprofen	0	0	129
Aspirin	0	8	206
Aspirin	0	10	209
Aspirin	0	9	206
Phenylacetic acid	0	0	138
Phenylacetic acid	0	0	137
Phenylacetic acid	0	0	134
4-Chlorophenylacetic acid	0	0	211
4-Chlorophenylacetic acid	0	0	214
4-Chlorophenylacetic acid	0	0	212
Benzoic acid	0	0	138
Benzoic acid	0	0	140
Benzoic acid	0	0	139
3,5-Dihydroxybenzoic acid	0	0	0
3,5-Dihydroxybenzoic acid	0	0	0
3,5-Dihydroxybenzoic acid	0	0	0
2,4-Dichlorobenzoic acid	0	0	178
2,4-Dichlorobenzoic acid	0	0	179
2,4-Dichlorobenzoic acid	0	0	182
5-Iodosalicylic acid	0	0	227
5-Iodosalicylic acid	0	0	225
5-Iodosalicylic acid	0	0	226

Table B.14. RGB data taken of **XF3** in EtOAc.

	EtOAc XF3 **R**	EtOAc XF3 **G**	EtOAc XF3 **B**
4-Hydroxybenzoic acid	8	0	19
4-Hydroxybenzoic acid	11	0	19
4-Hydroxybenzoic acid	10	0	18
4-Hydroxyphenylacetic acid	22	0	25
4-Hydroxyphenylacetic acid	21	0	23
4-Hydroxyphenylacetic acid	25	0	26
Ibuprofen	0	55	0
Ibuprofen	0	53	0
Ibuprofen	0	54	0
Aspirin	0	0	79
Aspirin	0	0	78
Aspirin	0	0	80
Phenylacetic acid	0	0	82
Phenylacetic acid	0	0	81
Phenylacetic acid	0	0	80
4-Chlorophenylacetic acid	0	0	79
4-Chlorophenylacetic acid	0	0	80
4-Chlorophenylacetic acid	0	0	81
Benzoic acid	0	0	70
Benzoic acid	0	0	74
Benzoic acid	0	0	73
3,5-Dihydroxybenzoic acid	26	0	23
3,5-Dihydroxybenzoic acid	21	0	24
3,5-Dihydroxybenzoic acid	25	0	24
2,4-Dichlorobenzoic acid	0	0	145
2,4-Dichlorobenzoic acid	0	0	144
2,4-Dichlorobenzoic acid	0	0	143
5-Iodosalicylic acid	0	26	92
5-Iodosalicylic acid	0	23	92
5-Iodosalicylic acid	0	24	90

Table B.15. RGB data taken of **XF3** in MeCN.

	MeCN XF3 **R**	MeCN XF3 **G**	MeCN XF3 **B**
4-Hydroxybenzoic acid	0	0	126
4-Hydroxybenzoic acid	0	0	125
4-Hydroxybenzoic acid	0	0	124
4-Hydroxyphenylacetic acid	0	78	221
4-Hydroxyphenylacetic acid	0	80	221
4-Hydroxyphenylacetic acid	0	79	220
Ibuprofen	0	0	152
Ibuprofen	0	0	153
Ibuprofen	0	0	151
Aspirin	0	54	251
Aspirin	0	58	255
Aspirin	0	56	255
Phenylacetic acid	0	0	243
Phenylacetic acid	0	0	246
Phenylacetic acid	0	0	245
4-Chlorophenylacetic acid	0	0	255
4-Chlorophenylacetic acid	0	0	254
4-Chlorophenylacetic acid	0	0	255
Benzoic acid	0	0	255
Benzoic acid	0	0	253
Benzoic acid	0	0	254
3,5-Dihydroxybenzoic acid	0	28	131
3,5-Dihydroxybenzoic acid	0	29	131
3,5-Dihydroxybenzoic acid	0	31	133
2,4-Dichlorobenzoic acid	0	3	245
2,4-Dichlorobenzoic acid	0	4	244
2,4-Dichlorobenzoic acid	0	2	241
5-Iodosalicylic acid	0	18	190
5-Iodosalicylic acid	0	17	187
5-Iodosalicylic acid	0	19	188

Table B.16. RGB data taken of **XF3** in DMF.

	DMF XF3 **R**	DMF XF3 **G**	DMF XF3 **B**
4-Hydroxybenzoic acid	96	57	13
4-Hydroxybenzoic acid	91	60	16
4-Hydroxybenzoic acid	94	59	14
4-Hydroxyphenylacetic acid	92	50	0
4-Hydroxyphenylacetic acid	91	49	0
4-Hydroxyphenylacetic acid	93	48	0
Ibuprofen	50	12	0
Ibuprofen	51	13	0
Ibuprofen	47	12	0
Aspirin	31	8	2
Aspirin	33	11	6
Aspirin	31	10	4
Phenylacetic acid	49	11	0
Phenylacetic acid	47	14	0
Phenylacetic acid	52	14	0
4-Chlorophenylacetic acid	29	2	0
4-Chlorophenylacetic acid	24	0	0
4-Chlorophenylacetic acid	26	0	1
Benzoic acid	23	0	0
Benzoic acid	24	0	0
Benzoic acid	25	0	0
3,5-Dihydroxybenzoic acid	73	26	0
3,5-Dihydroxybenzoic acid	74	25	0
3,5-Dihydroxybenzoic acid	66	23	0
2,4-Dichlorobenzoic acid	0	13	97
2,4-Dichlorobenzoic acid	0	15	99
2,4-Dichlorobenzoic acid	0	16	100
5-Iodosalicylic acid	0	42	128
5-Iodosalicylic acid	0	40	127
5-Iodosalicylic acid	0	42	127

Table B.17. RGB data taken of **XF3** in iPrOH.

	iPrOH XF3 **R**	iPrOH XF3 **G**	iPrOH XF3 **B**
4-Hydroxybenzoic acid	0	0	9
4-Hydroxybenzoic acid	0	0	10
4-Hydroxybenzoic acid	0	0	12
4-Hydroxyphenylacetic acid	0	0	0
4-Hydroxyphenylacetic acid	0	0	0
4-Hydroxyphenylacetic acid	0	0	0
Ibuprofen	0	5	0
Ibuprofen	0	7	0
Ibuprofen	0	3	0
Aspirin	0	0	2
Aspirin	0	0	3
Aspirin	0	0	5
Phenylacetic acid	0	0	23
Phenylacetic acid	0	0	24
Phenylacetic acid	0	0	22
4-Chlorophenylacetic acid	0	0	30
4-Chlorophenylacetic acid	0	0	31
4-Chlorophenylacetic acid	0	0	29
Benzoic acid	0	0	65
Benzoic acid	0	0	64
Benzoic acid	0	0	67
3,5-Dihydroxybenzoic acid	0	0	0
3,5-Dihydroxybenzoic acid	0	0	0
3,5-Dihydroxybenzoic acid	0	0	0
2,4-Dichlorobenzoic acid	0	0	176
2,4-Dichlorobenzoic acid	0	0	177
2,4-Dichlorobenzoic acid	0	0	178
5-Iodosalicylic acid	0	73	131
5-Iodosalicylic acid	0	76	133
5-Iodosalicylic acid	0	74	134

Table B.18. RGB data taken of **XF3** in MeOH.

	MeOH XF3 **R**	MeOH XF3 **G**	MeOH XF3 **B**
4-Hydroxybenzoic acid	0	0	43
4-Hydroxybenzoic acid	0	0	41
4-Hydroxybenzoic acid	0	0	40
4-Hydroxyphenylacetic acid	0	13	102
4-Hydroxyphenylacetic acid	0	14	104
4-Hydroxyphenylacetic acid	0	13	103
Ibuprofen	0	0	117
Ibuprofen	0	0	115
Ibuprofen	0	0	116
Aspirin	0	7	255
Aspirin	0	8	255
Aspirin	0	5	255
Phenylacetic acid	0	0	130
Phenylacetic acid	0	0	132
Phenylacetic acid	0	0	134
4-Chlorophenylacetic acid	0	0	228
4-Chlorophenylacetic acid	0	0	231
4-Chlorophenylacetic acid	0	0	232
Benzoic acid	0	0	249
Benzoic acid	0	0	247
Benzoic acid	0	0	250
3,5-Dihydroxybenzoic acid	0	20	95
3,5-Dihydroxybenzoic acid	0	21	95
3,5-Dihydroxybenzoic acid	0	19	95
2,4-Dichlorobenzoic acid	0	0	222
2,4-Dichlorobenzoic acid	0	0	223
2,4-Dichlorobenzoic acid	0	0	224
5-Iodosalicylic acid	0	32	163
5-Iodosalicylic acid	0	31	164
5-Iodosalicylic acid	0	33	167

APPENDIX C

RGB RAW DATA FOR MANOVA TEST OF UNKNOWN ORGANIC ACIDS

Table C.1. RGB data taken of **XF1** in DCM.

Unknown	DCM XF1 **R**	DCM XF1 **G**	DCM XF1 **B**
1	0	0	0
1	0	0	0
1	0	0	0
2	0	0	0
2	0	0	0
2	0	0	0
3	0	0	0
3	0	0	0
3	0	0	0
4	0	0	0
4	0	0	0
4	0	0	0
5	0	0	0
5	0	0	0
5	0	0	0

Table C.2. RGB data taken of **XF1** in MeCN.

Unknown	MeCN XF1 R	MeCN XF1 G	MeCN XF1 B
1	0	0	0
1	73	98	0
1	75	97	0
2	74	98	0
2	0	0	0
2	0	0	0
3	0	0	0
3	0	0	0
3	0	0	0
4	0	0	0
4	0	0	0
4	0	0	0
5	68	67	0
5	63	61	0
5	68	64	0

Table C.3. RGB data taken of **XF1** in MeOH.

Unknown	MeOH XF1 R	MeOH XF1 G	MeOH XF1 B
1	0	0	0
1	0	0	0
1	0	0	0
2	0	35	4
2	0	38	7
2	0	33	2
3	0	0	0
3	0	0	0
3	0	0	0
4	0	0	0
4	0	0	0
4	0	0	0
5	44	95	14
5	47	96	10
5	45	98	14

Table C.4. RGB data taken of **XF2** in DCM.

Unknown	DCM XF2 R	DCM XF2 G	DCM XF2 B
1	0	14	0
1	2	17	0
1	1	15	0
2	0	6	0
2	0	4	0
2	0	5	0
3	0	16	0
3	0	14	0
3	0	17	0
4	5	11	0
4	6	11	0
4	7	12	0
5	5	26	0
5	6	27	0
5	7	28	0

Table C.5. RGB data taken of **XF1** in MeCN.

Unknown	MeCN XF2 R	MeCN XF2 G	MeCN XF2 B
1	0	0	0
1	0	0	0
1	0	0	0
2	95	0	0
2	94	0	0
2	97	0	0
3	10	0	0
3	11	0	0
3	9	0	0
4	25	0	0
4	27	0	0
4	28	0	0
5	127	0	0
5	128	0	0
5	132	0	0

Table C.6. RGB data taken of **XF2** in MeOH.

Unknown	MeOH XF2 R	MeOH XF2 G	MeOH XF2 B
1	0	0	0
1	0	0	0
1	0	0	0
2	17	0	0
2	19	0	0
2	22	0	0
3	48	0	0
3	46	0	0
3	45	0	0
4	17	0	0
4	18	0	0
4	16	0	0
5	102	0	0
5	104	0	0
5	106	0	0

Table C.7. RGB data taken of **XF3** in DCM.

Unknown	DCM XF3 R	DCM XF3 G	DCM XF3 B
1	0	0	113
1	0	0	112
1	0	0	110
2	0	25	10
2	0	21	7
2	0	22	10
3	0	0	146
3	0	0	147
3	0	0	148
4	0	0	188
4	0	0	191
4	0	0	187
5	13	62	1
5	15	63	2
5	17	67	5

Table C.8. RGB data taken of **XF3** in MeCN.

Unknown	MeCN XF3 R	MeCN XF3 G	MeCN XF3 B
1	0	0	50
1	0	0	49
1	0	0	52
2	0	14	127
2	0	13	126
2	0	16	128
3	0	0	141
3	0	0	137
3	0	0	142
4	0	0	172
4	0	0	174
4	0	0	171
5	0	0	44
5	0	0	52
5	0	0	54

Table C.9. RGB data taken of **XF3** in MeOH.

Unknown	MeOH XF3 R	MeOH XF3 G	MeOH XF3 B
1	0	9	103
1	0	0	101
1	0	0	102
2	0	9	59
2	0	9	60
2	0	10	62
3	0	0	166
3	0	0	162
3	0	0	163
4	0	0	139
4	0	0	135
4	0	0	138
5	0	62	52
5	0	68	55
5	0	68	56

VITA

Evan A. Davey

Evan Andrew Davey was raised in Springfield, Pennsylvania, where he attended Springfield High School before pursuing his B.S. in Chemistry at West Chester University of Pennsylvania. After graduating in 2004, he continued his education at Georgia Institute of Technology, working towards his doctorate in Organic and Polymer Chemistry under the guidance of Prof. Dr. Uwe H.F. Bunz. When he is not working on his research, Dr. Davey passionately follows Philadelphia sports teams and regularly enjoys hunting, fishing, camping, and hiking with his dog, Russe.